Trinity College Dublin
Coláiste na Tríonóide, Baile Átha Cliath
The University of Dublin

Investigating a possible interplay between Hho1p and Hmo1p during stationary phase in *Saccharomyces cerevisiae*

MSc (by Research)

2026

Cian McNulty-Casey

A dissertation presented for the degree of M.Sc. in the Faculty of Science, Technology, Engineering, and Mathematics, Trinity College Dublin

Declaration

I declare that this thesis has not been submitted as an exercise for a degree at this or any other university and it is entirely my own work. I confirm that the work has been completed in full compliance with relevant university policies, including the Academic Integrity policy, the Trinity Policy on Good Research Practice, and the guidance on AI and GenAI in Teaching, Learning, Assessment and Research.

I agree to deposit this thesis in the University's open access institutional repository or allow the Library to do so on my behalf, subject to Irish Copyright Legislation and Trinity College Library conditions of use and acknowledgement.

I consent to the examiner retaining a copy of the thesis beyond the examining period, should they so wish (EU GDPR May 2018).

I have read and I understand the plagiarism provisions in the General Regulations of the University Calendar for the current year, found at: http://www.tcd.ie/calendar.

I have completed the Online Tutorial on avoiding plagiarism 'Ready, Steady, Write', located at http://tcd-ie.libguides.com/plagiarism/ready-steady-write.

Cian McNulty-Casey

Acknowledgements

I would like to express my sincere gratitude to my supervisor Dr Alastair Fleming who supported me through each step of my research masters. Dr Alastair Fleming provided me with constant guidance, feedback and support throughout my research. I would also like to thank all the members of the Fleming Group for their company and support. Thank you to my lab friends, Xuyuan, Zain, Reham, Hadel and Miska. I would also like to thank all the technical staff in the Moyne Institute of Preventive Medicine for their assistance and support.

Table of Contents

Abstract

Chromatin organisation during the stationary phase in *Saccharomyces cerevisiae* plays a vital role in genome stability and transcriptional regulation. The aim of this research was to investigate any potential interaction between Hho1p and Hmo1p during the stationary phase in *Saccharomyces cerevisiae.* The hypothesis was that Hho1p and Hmo1p interact to maintain chromatin structure and regulate transcription during stationary phase in *Saccharomyces cerevisiae*. To test this hypothesis, single and double *HMO1* and *HHO1* gene deletion mutants were constructed, and their phenotypes were compared.

The results show that the single gene deletion mutants of *hho1Δ* mutant and *hmo1Δ* mutant have distinct but partially overlapping phenotypes during the exponential and stationary phase. However, the *hho1Δ hmo1Δ* double mutant exhibited the strongest phenotypic effects compared to the wild type and both single mutants in exponential and stationary phase. ChIP-seq data also revealed an overlap in the sites occupied by both Hmo1p and Hho1p in exponential and stationary phase cells. These data suggest a potential interplay between Hho1p and Hmo1p whereby they may act in a co-ordinated and interactive manner during both exponential and stationary phase, with growth phase specific phenotypic influence and effect. The findings from this research contribute to a greater understanding of the roles of Hho1p and Hmo1p and the interactions between both proteins at different stages of the of the yeast cell growth cycle. This research highlights the importance of Hmo1p and Hho1p in different stages of the yeast cell growth cycle and paves the way for future work comparing the *hho1Δ hmo1Δ* double mutant transcription profile to wt and the single mutants to identify the unique and shared roles of the Hmo1p and Hho1p proteins upon global gene transcription and cell function.

1.Introduction

1.1 Chromatin

Saccharomyces cerevisiae, also known as baker's yeast, has been extensively used for genetic research since the mid decades of the twentieth century. The deep investigation into this organism has hugely helped the understanding of the mechanisms of eukaryotic cell function. *Saccharomyces cerevisiae* has a simple life cycle and short doubling time. It is also easily genetically modified. *Saccharomyces cerevisiae* is widely used as a model organism due to these characteristics. The unicellular organism *Saccharomyces cerevisiae* has a round, oval morphological shape. It appears as single cells or brief chains when viewed under a microscope. *Saccharomyces cerevisiae* multiples in a haploid or diploid state during mitosis. It reproduces by budding, where a smaller daughter cell separates from the mother cell to reproduce asexually. There are approximately 6300 genes in the yeast genome. These genes are tightly packed together along chromosomal arms. A large proportion of yeast genes are in an open chromatin state. This allows for fast induction or active transcription (Grunstein and Gasser 2013). Within the eukaryotic cell, DNA is tightly associated with proteins to form a structure called chromatin. The fundamental subunit of chromatin is the nucleosome. Nucleosomes act as building blocks for chromatin structure and consist of two each of the core histone proteins, H2A, H2B, H3 and H4 (Fig 1.1). Approximately 168 bp of DNA are spooled into two negative super helical coils on top of a core octamer to form the nucleosome (Schäfer et al., 2008). This histone octamer is encircled by the DNA, creating a tightly packed structure that resembles beads on a string. The nucleosomes that contain histone variants display a higher order chromatin structure. It is evident how crucial core histones are to the chromatin mediated control of DNA function. Histone proteins, like other eukaryotic organisms, are essential components of chromatin in *Saccharomyces cerevisiae.* The core histones H2A, H2B, H3 and H4 play a crucial role in packaging DNA into nucleosomes. Histone amino acid sequences and their modifications are highly conserved in eukaryotes. The DNA connecting nucleosomes can be associated with the 'linker' histone H1, which can act to further compact DNA within the nucleus.

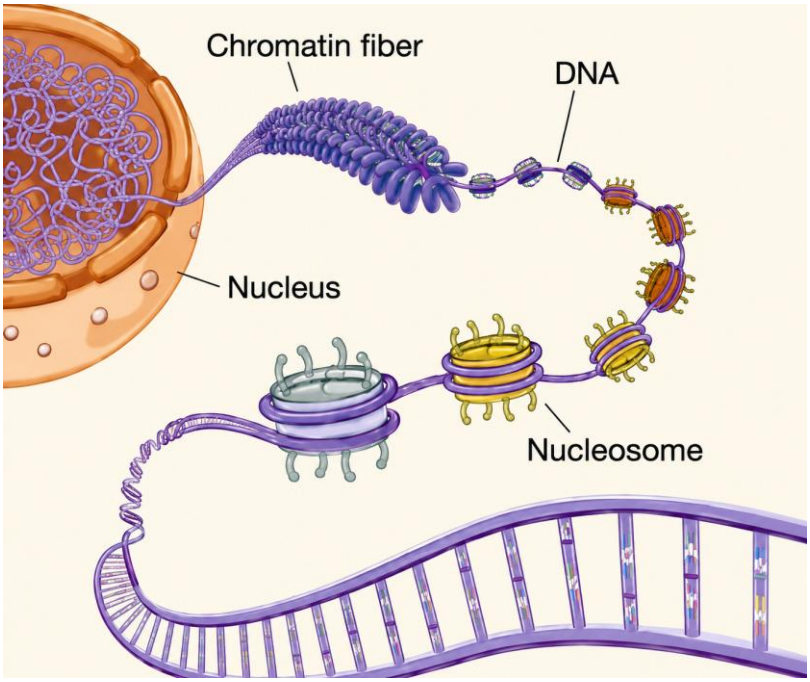

Figure 1.1: Diagram showcasing chromatin-organised DNA. Shows nucleosomes consisting of two copies of the core histone proteins, H2A, H2B, H3 and H4 and DNA. This figure was adapted from (Baker, 2011).

1.2 The core histones

The four core histones making up the octamer are known as H2A, H2B, H3 and H4 (Table 1.1). They all have the same fundamental structure that comprises a structured globular domain and flexible N-terminal tail. The core histones are shown to be highly conserved in eukaryotes (Baxevanis and Landsman, 1998). These small histones combine into an octamer that consists of a single tetramer that contains H3 and H4 and two dimers containing H2A and H2B. This structure gives the nucleosome a very stable DNA-protein complex (Luger et al., 1997). When investigating the genetics of histones and their functions in gene regulation yeast confers a distinct advantage. Indeed, the core histone coding genes that are found in human cells such as H2A, H2B, H3 and H4 are found in quantities of 60-70 copies in human cells, whereas yeast has just two copies of each core histone gene. Thus, *Saccharomyces cerevisiae* is a well-established model organism for the study of histone function.

The core histone proteins

Histone Protein	Size (Mol. weight)/kDa
H2A	**15.3**
H2B	**14**
H3	**15.3**
H4	**11.3**

Table 1.1: The core histone proteins. The table shows the four core proteins, H2A, H2B, H3 and H4 and their sizes.

1.3 The linker histone H1

Histone H1 was first discovered in 1951 in the calf thymus as a lysine rich 'subsidiary' histone (Stedman and Stedman, 1951). It was later discovered that H1 was indeed part of an extended family of histone variants that can be observed in many eukaryotes. Histone H1, which is connected to the exterior of the nucleosome, shields 168 base pairs from MNase cleavage (Noll and Kornberg, 1977). Histone H1 binds to the DNA linker region where the DNA enters and exits the nucleosome (Fig 1.2) (An et al., 1998). Unlike core histones, which are stable components of the nucleosome, linker histones are mobile (Lever et al., 2000). In mammalian cells, H1 has an average stoichiometry of about 0.8 molecules per nucleosome, with variations depending on the type of cell (Woodcock et al., 2006). Histone H1 interacts with approximately 20 bp of DNA to form the chromatosome consisting of approximately 168 bp of DNA, the core histone octamer and one molecule of H1 (Fig 1.2) (Allan et al., 1980). Hydrodynamic studies and electron microscopy have shown that histone H1 is necessary for the full salt dependent condensation of chromatin in vitro (Thoma et al., 1979).

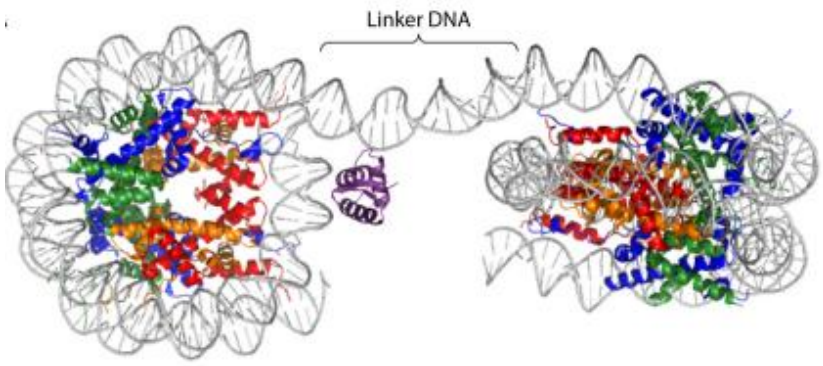

Figure 1.2: Histone H1 is associated with linker DNA. The globular domain of histone H1 (purple) binds the nucleosome at the dyad. This figure is derived from (Panday and Grove 2017).

1.4 Histone H1 in yeast

Although the linker histone H1's structure and function are well defined and characterised in higher eukaryotes, the yeasts' equivalent identity and role remain controversial. Histone H1 plays a role of stabilizing nucleosomes and maintaining higher-order chromatin structures, which control gene expression and cellular responses (Miloshev et al., 2019). It was suggested that the *HHO1* gene encodes the yeast linker histone. *HHO1* encodes the protein Hho1p, and it is similar to mammalian linker H1 histone in molecular weight and charge (Sučhilienė and Gineitis, 1978).

The identification of the *HHO1* gene resulted from an open reading frame (YPL127C) with regions of considerable sequence morphology to the H1 histone of higher eukaryotes being discovered when chromosome XVI in yeast was sequenced (Patterton et al., 1998), which was later shown to be transcribed and translated into a functional protein (Ushinsky et al., 1997). The structure of Hho1p differs from linker histones of other species as Hho1p has two globular domains while the presence of just one globular domain is a common feature for higher eukaryotic linker histones. The structure of Hho1p compared to human H1 can be examined in (Fig 3). It has also been shown that a purified recombinant Hho1p (rHho1p) has electrophoretic and chromatographic properties that are extremely like that of linker histones in mammalian cells (Noll and Kornberg, 1997). However, the deletion of *HHO1* in vegetatively growing yeast shows no striking

phenotype (Patterton et al., 1998). Conversely, it had been proposed to operate during the stationary phase of yeast, where it may promote chromatin compaction and contribute to DNA damage repair (Schäfer et al., 2008). Disrupting *HHO1* leads to a change in chromatin structure in old yeast cells (Uzunova et al., 2013). Linker histones are the most diverse class of histone proteins (Kasinsky et al., 2001). The degree of sequence identity between H1 and Hho1p is only 31 percent.

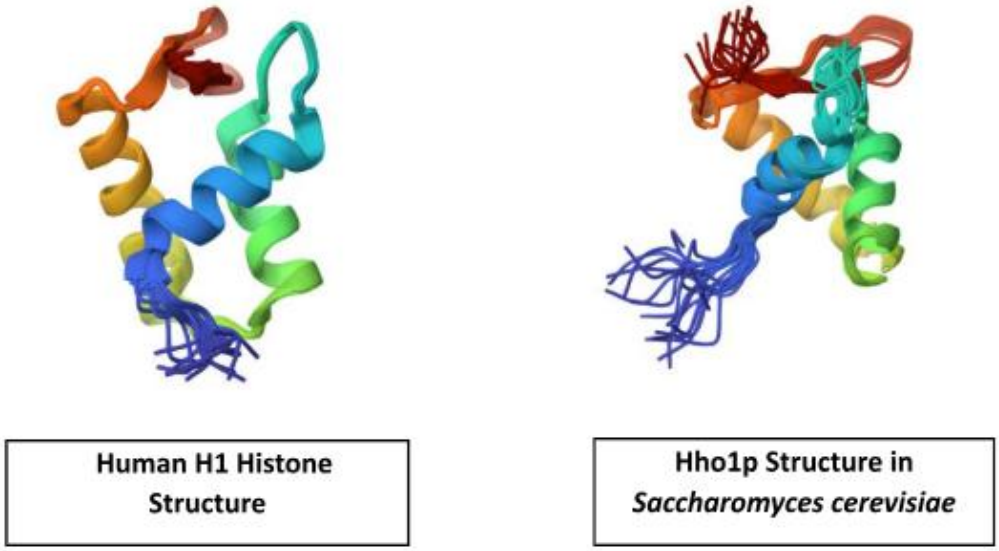

Figure 1.3: Human H1 histone structure (left) and Hho1p structure in *Saccharomyces cerevisiae* (right). H1 consists of a central globular domain with more flexible tail regions at both their N- and C-terminal. Hho1p has a similar structure, except that there is an additional globular domain found at the N terminus.

1.5 High mobility group box protein (HMGB)

Another candidate has been identified that may function as the yeast H1 protein called Hmo1p. Hmo1p is an abundant high mobility group box (HMGB) protein (Ghaemmaghami et al., 2003). Similar to Hho1p, Hmo1p has two globular domains. Hmo1p globular domains are about 80 amino acids each, called box A and box B (Fig 1.4). This makes it more like its H1 mammalian counterpart. Box A has a low DNA binding affinity, meanwhile Box B possesses a higher binding affinity. Box B has a lower structural sensitivity (Kamau et al., 2004). Hmo1p has a C- terminal domain that is distinguished by a stretch of essential amino acids in addition to the A and B domains (Bauerle et al., 2006). *HMO1* gene deletion is not lethal, however deletion results in

significant growth defects and decreased plasmid stability (Ray and Grove, 2009). HMGB proteins like Hmo1p have been shown to have binding sites that overlap with H1, potentially resulting in mutually exclusive association with DNA entry and exit points on the nucleosome (Thomas and Stott, 2012). It has also been noted that the C-terminal extension of HMGB proteins interact specifically with the H3 histone N- terminal tail (Ueda et al., 2004). Also, like H1, HMGB proteins bind DNA (Lee and Thomas, 2000). Whilst there is some indication that Hmo1p could function as a linker histone in yeast, there is little research carried out on the protein to confirm whether Hmo1p could be the yeast functional equivalent of the mammalian H1 protein or whether it interacts with and functions together with Hho1p.

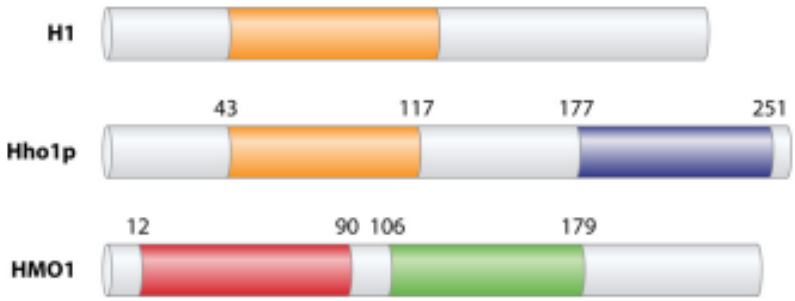

Figure 1.4: Metazoan H1, yeast Hho1p and Hmo1p domain organisation. Metazoan H1 typically contains a N-terminal extension of 40 amino acids followed by a globular domain of 80 amino acids (orange) and a long CTD characterised by S / TPXK-like repetitions. Yeast Hho1p contains a lysine-rich N-terminal segment followed by a globular domain similar to that of H1 (orange). Another lysine-rich section links this planetary domain to the second (purple) globular domain. Yeast Hmo1p consists of box A (red), which has little resemblance to HMG consensual domains, followed by a lysine-rich linker, box B (green) domain and a lysine-rich CTD. This figure was adapted from (Panday and Grove, 2017).

1.6 Yeast growth cycle

The growth of *Saccharomyces cerevisiae* cells follows the yeast growth cycle (Fig 1.5). The yeast growth cycle is divided into several different stages and these stages include the lag phase, the exponential phase, the stationary phase and death phase. The growth

phase of *Saccharomyces cerevisiae* begins with the lag phase. In this phase, the yeast cells are adapting to its environment and not actively dividing but are often synthesising crucial enzymes for growth. The duration of this phase varies depending on several factors including temperature and nutrients available. When the yeast cells have adapted to their environment and conditions are favourable the exponential phase begins. The exponential phase is also known as the log phase. This is a period of exponential growth of yeast cells. Yeast cells rapidly divide in this stage and a doubling time can be obtained with a consistent rate of growth. In the exponential phase, *Saccharomyces cerevisiae* metabolizes glucose through fermentation. Once glucose is depleted, the cells temporarily cease growth and switch to respiration to derive energy from the previously produced ethanol. This transition from fermentation to respiration is known as the diauxic shift. As all the carbon sources are depleted, yeast cells reach true stationary phase. Live yeast cells level remains constant during this stage in the yeast growth cycle. Some of these yeast cells enter a state of dormancy to adapt to the limited nutrient resources. The stationary phase of microbial growth has been established as a crucial point in molecular biology and cellular physiology field. Starvation is one of the most common stresses encountered by living organisms. (Herman, 2002). This stage in *Saccharomyces cerevisiae* features a steady population of living but non dividing cells. Stationary phase is the stage of the yeast growth cycle where cells move from active proliferation to a quiescent state. Quiescence is a survival strategy during which transcription and translation are reduced to save energy. Importantly, quiescence is a reversible state as these cells can re-enter the cell cycle when nutrients become available. Not much is known about the fate of chromatin during stationary phase except the long-established observation that chromosomes become condensed and there is an overall shutdown in transcription (Choder, 1991). Stationary phase cells also showcase the ability to accumulate storage carbohydrates glycogen and trehalose and have an increased resistance to a variety of environmental stresses. These characteristics increase the ability of *Saccharomyces cerevisiae* cells to survive extended periods of starvation (Herman, 2002). To complete the yeast growth cycle, the last stage of the cycle is the death phase. In this stage there are very limited nutrients available and yeast cells death rate exceeds the rate of cell division. This leads to a constant decrease in the population of viable yeast cells.

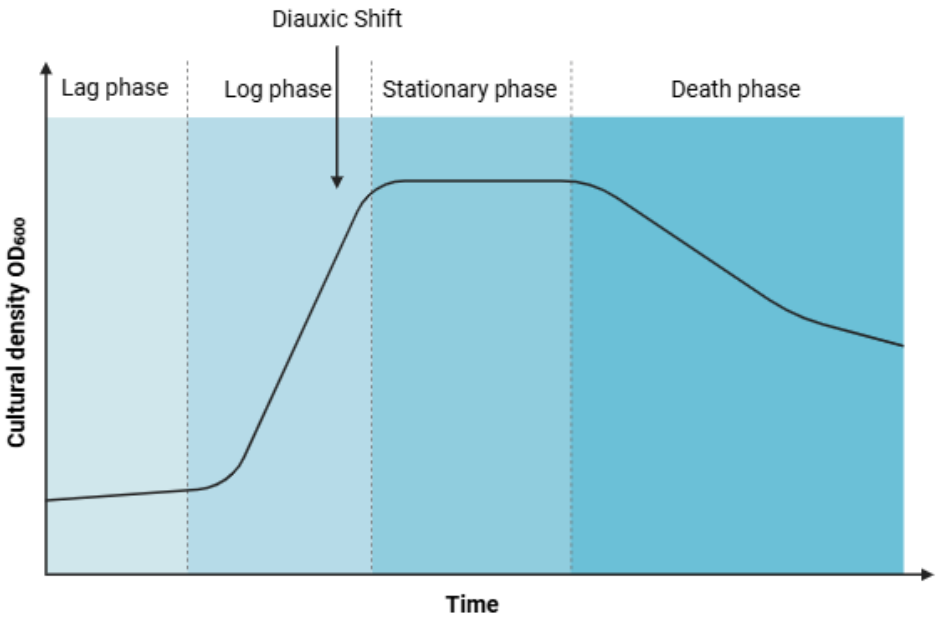

Figure 1.5: The yeast growth cycle in batch culture. Schematic representation of the growth cycle of *Saccharomyces cerevisiae* in batch culture. Following inoculation, cells undergo a lag phase during which they adapt to the growth environment. This is followed by the logarithmic (exponential) growth phase, characterised by rapid cell division and high metabolic activity. As preferred carbon sources such as glucose become depleted, cells undergo the diauxic shift, transitioning from fermentative to respiratory metabolism. Continued nutrient limitation leads to entry into the stationary phase, where cell division ceases and cells activate stress response and survival pathways. Prolonged stationary phase ultimately results in the death phase, marked by a decline in viable cell numbers. This figure was created using BioRender.

1.7 Yeast stationary phase cultures form two cell populations

It has been previously established that *Saccharomyces cerevisiae* stationary phase cultures contain a mixture of two cell populations (Allen et al., 2006). During the stationary phase, the younger daughter cells form a quiescent cell population. The older mother cells form a non-quiescent population of cells that undergo apoptosis and necrosis. Quiescent cells are cells that are in a state of dormancy and are not proliferating. The definition of quiescence is that quiescence is a form of temporary and reversible growth arrested state

that cells can enter in response to unfavourable environmental conditions (De Virgilio, 2012). Quiescence in *Saccharomyces cerevisiae* is therefore a biological state of reversible growth where cells stop growing and reduce metabolic activity, but with stimulation from appropriate signals can re-enter the cell cycle and renew division. Quiescence plays a vital role in maintaining cellular integrity. Quiescence is the most prevalent nature state of *Saccharomyces cerevisiae* and is also essential for long-term survival in an unfavourable environment (Kasinsky et al., 2001). It is the quiescent cell population that will remain viable during SP. Quiescence is important in complex eukaryotes for the survival of stem cells and plays an important role in diseases such as cancer (Suda et al., 2005).

A mixture of both quiescent and non-quiescent cells can be observed in the stationary phase due to the growth rate of the population equalling the death rate in the stationary phase. This leads to a steady population size. In *Saccharomyces cerevisiae,* with a stationary phase population of quiescent and non-quiescent cells, the proportions of both cells can change depending on several variables. These factors include the growth environment, the cell type and the existence of outside stimuli. A vital thing to note also is that not all non-proliferating cells present in the stationary phase are quiescent. A method published by the Margaret Werner-Washburnes group, described an experiment in which you isolate two subpopulations from stationary phase using density centrifugation (Allen et al., 2006). This experiment is used in this thesis and separates the less dense upper fraction, which is non-quiescent, from the denser lower fraction, which is quiescent. Evidence suggests that the difference in cell density is due to the accumulation of trehalose in the quiescent cells which is used as a storage carbohydrate (Svenkrtova et al., 2016). The entry into quiescence can take several days and the entry process is not the same for all cells. Leaving quiescence can also differ for cells due to the longer a cell remains in quiescence can affect the duration it takes for it to re-enter the cycle (Laporte et al., 2018).

1.8 The transition to quiescence is highly regulated

The paper by (Allen et al., 2006) described the isolation of two distinct populations from yeast SP cultures after separation by density centrifugation. The less dense upper population of cells was heterogeneous and mostly made up of non-quiescent (NQ),

budded mother cells. These NQ cells rapidly lost their ability to re-enter the cell cycle. After 14 days, many of these cells showed characteristic markers of apoptosis and necrotic cell death. The denser, lower population of cells was comprised of mostly unbudded daughter cells that retained viability and had the ability to re-enter the cell cycle upon glucose replenishment. The quiescent (Q) daughter cells and the NQ mother cells were morphologically and physiologically different from each other. One example was that the Q population had increased thermo-tolerance when compared to the NQ population (Allen et al., 2006). Several different events have been implicated in controlling the development of the Q population of cells. It is believed that during the post-diauxic cell division, that the cells undergo asymmetric divisions and build protective cell walls around the daughter cells that become quiescent. These Q cells accumulate storage carbohydrates and contain abundant highly functional mitochondria that allow for long-term viability (Davidson et al., 2011). Overall, a tightly regulated programme of events that is not fully understood plays a role in the formation of the long-lived Q cells.

1.9 Potential interplay between Hho1p and Hmo1p during stationary phase

The potential interplay between both Hho1p and Hmo1p in the stationary phase in *Saccharomyces cerevisiae* is the main focus of this research thesis. In the stationary phase of *Saccharomyces cerevisiae* cells undergo increased chromatin compaction and have reduced transcriptional activity. It is possible that Hho1p and Hmo1p cooperate with each other to stabilise chromatin structure during the stationary phase, or conversely that one protein compensates for the loss of the other. These interactions are functionally relevant under conditions of nutrient limitation and cellular stress. One of the main questions is whether Hho1p and Hmo1p act redundantly, synergistically, or antagonistically of each other. This information will give us a better understanding on how yeast cells adapt to nutrient deprivation.

1.10 The aim of this research

The aim of this research was to study the roles of Hho1p and Hmo1p in yeast cells and to analyse any potential functional interactions between both Hho1p and Hmo1p in *Saccharomyces cerevisiae* during the stationary phase. I will investigate the role of these two histone H1 candidates in both exponential and stationary phase cells. I constructed

and analysed the double *hho1Δ hmo1Δ* gene deletion mutant and compared the characteristics of this mutant against the two single gene deletion mutants, *hho1Δ* and *hmo1Δ* and the wild-type strain. The overall aim was to test the hypothesis that Hho1p and Hmo1p exhibit functional interplay during the stationary phase in *Saccharomyces cerevisiae,* such that combined loss of both proteins in the double *hho1Δ hmo1Δ* mutant results in phenotypes that are more severe or distinct than those observed in either single gene deletion mutant.

2. Materials and Methods

2.1 Yeast strains and growth conditions

Materials used for the preparation of growth media were sourced from Formedium. Cells were cultivated using yeast extract peptone dextrose (YPD) broth and agar. YPD broth was composed of 1% (w/v) yeast extract, 2% (w/v) peptone and 2% (w/v) dextrose (glucose). YPD agar was prepared by supplementing YPD broth with 2% (w/v) agar. Cells were grown at 30 °C with a shaking speed of 200 x g, unless otherwise specified. Overnight starter cultures were created by inoculating 5 mL of YPD with a single yeast colony. The following day, this culture was used to inoculate a larger volume of YPD. The culture was allowed to grow until it reached the desired OD_{600} was reached, which was measured using a spectrophotometer. A volume of this starter culture was sub-inoculated in a larger volume of YPD broth and grown under the same conditions until the log phase was attained, which was an optical density reading between 0.6 and 0.8 on the spectrophotometer. The experiment showed the presence of diauxic shift and stationary phase specific quiescent cells.

The strains that contain autotrophic markers were cultured in a synthetic complete (SC) medium. The SC medium was made by combining 0.19% yeast nitrogen base, 0.059% complete supplement medium and 0.5% $(NH_4)_2SO_4$. In the case of solid media, 2% agar was added to the solution which was then autoclaved. Glucose was added later to the medium to achieve a final concentration of 2%. Finally, amino acids were included or excluded depending on the experiment.

Saccharomyces cerevisiae strains were in the BY4741 background and were obtained from the gene deletion library (Table 2.1).

Yeast strains used in this research

Strain	Genotype	Source	Comment
BY4741 (wt)	*Mata; his3Δ1; leu2Δ0; met15Δ0; ura3Δ0*	ResGen library	Background strain for deletion mutants used in this study
hho1Δ	*Mata; his3Δ1; leu2Δ0; met15Δ0; ura3Δ0, hho1Δ::KAN*	ResGen library	Background strain for *hho1Δ*
hmo1Δ	*Mata; his3Δ1; leu2Δ0; met15Δ0; ura3Δ0, hmo1Δ::KAN*	ResGen library	Background strain for *hmo1Δ*
hho1Δ hmo1Δ	*MATa; his3Δ1; leu2Δ0; met15Δ0; ura3Δ0; hho1Δ::KAN; hmo1Δ::URA3*	This study	Double deletion mutant generated in this study.

Table 2.1: Yeast strains used in this research.

2.2 Growth curve and final cell density

The YPD liquid medium was used for growing cells, and ThermoSpectronic (Genesys 10 UV) was used to measure OD_{600}. The measurements were taken hourly by measuring a 100 µL sample. The final cell density was determined after 24 hours of growth in YPD using a haemocytometer.

2.3 Microscope images of the yeast cells

Cells were grown in YPD overnight at 30 °C to the mid-log and day 7 of the stationary phase. The cells were then washed with distilled water, and 10 µL was spotted onto a glass slide. They were viewed under a Leica DM500 microscope at 100x magnification with an oil immersion lens. Photographs were taken using the Leica Application Suite (LAS) software to capture the image.

2.4 Growth “Spot” tests

Cultures were grown to the mid-exponential phase and day 7 of the stationary phase and equal cell densities ($1x10^7$ cells/mL) were resuspended in YPD. The cultures were spotted in serial 10-fold dilutions and grown at 30 °C unless otherwise stated. The cultures were grown at different temperatures, 15 °C, 20 °C, 30 °C, 37 °C and 42 °C to verify sensitivity to temperatures. Cell sensitivity to cell wall damaging agents was verified by spot tests on YPD media containing the indicated concentrations of caffeine.

2.5 Cell transformation (High-efficiency LiAc transformation)

Gene disruption and gene tagging were performed using PCR-mediated approaches with modified protocols (Wach et al., 1997). The transformation protocol was based on a high efficiency protocol from (Gietz and Schiestl, 2007). The cells were cultured overnight in a 10 mL culture and counted using a haemocytometer. A pre-warmed 50 mL culture of YPD was inoculated to a final cell density of $5x10^6$/mL. The cells were grown until a cell density of $2x10^7$/mL (approximately 2 doublings) was reached. The cells were centrifuged for 5 minutes at 1500 g, and the supernatant was discarded. The cells were resuspended in 25 mL of sterile water and centrifuged again for 5 minutes at 1500 g. The supernatant was once again discarded, and the cells were resuspended in 1 mL of sterile 100 mM LiAc. This suspension was then transferred to a 1.5 mL microcentrifuge tube, and the cells were pelleted at top speed for 30 seconds before removing the LiAc.

The cells were then resuspended in 400 µL of 100 mM LiAc, giving it a final density of approximately $2x10^9$ cells/mL. This suspension was vortexed and divided into 50 µL aliquots. The cells were pelleted, and a transformation mix was added to each cell pellet. The vital transformation mix contained 240 µL PEG (50% w/v PEG 3350), 36 µL 1 M LiAc and 25 µL of 10 mg/mL single stranded DNA from salmon testes (Sigma), which had been boiled previously for 5 minutes at 95 °C and then placed on ice, and approximately 1 µg DNA. The mixture was made up to 360 µL with sterile water and vortexed vigorously for 1 minute. The mixture was incubated in a water bath at 42 °C for 40 minutes. Cells were then centrifuged at 7000 g for 30 seconds and the transformation mix was gently removed with a micropipette. The pellet was gently resuspended in 1 mL of sterile water. The cells were plated directly onto the relevant selective media for

transformants using auxotrophic markers. The transformation was confirmed by PCR and western blot analysis where appropriate.

Primers used in strain construction and confirmation in this research

Name	Sequence	Comment
ACT1-F	CTGAATTAACAATGGATTCTGG	Strain confirmation
ACT1-R	AGATACCTCTCTTGGATTGAGC	Strain confirmation
Kan-B-F	CTGCAGCGAGGAGCCGTAAT	Strain confirmation
Kan-B-R	TGATTTTGATGACGAGCGTAAT	Strain confirmation
HMO1-F	AGTACCAATTAGTCCCAGCG	Strain confirmation
HMO1-R	ACACTATGGGCAAAGCAAGC	Strain confirmation
URA3-F	TCGGTAATCTCCGAGTGG	Strain confirmation
URA3-R	GCTTCGTTGTCGTTGACTG	Strain confirmation

Table 2.2: Primers used in strain construction and confirmation in this research.

Plasmid used in this study

Name	Selectable marker	Source	Comment
pRS406	URA3	Fleming lab	Integrative plasmid carrying URA3 used for gene deletion

Table 2.3: Plasmid used in this study.

2.6 DNA extraction

The DNA extraction procedure started with centrifuging an overnight 10 mL cell culture at 1500 g for 5 minutes. After discarding the supernatant, the cells were resuspended in 1 mL of water and transferred to a 1.5 mL microcentrifuge tube. Further pelleting was done by centrifugation at 6000 g for 5 minutes. The supernatant was then discarded. Following this, the pellets were resuspended in 200 µL of breaking buffer (containing 2% Trixton X-100, 1% SDS, 100 mM NaCl, 10 mM Tris-Cl (pH 8.0), 1 mM EDTA (pH 8.0) and approximately 500 µL of glass beads were added. To the suspension, 200 µL of phenol/chloroform/isoamyl alcohol was added and mixed by vortexing for 5 minutes. After that, 200 µL of TE (pH 7.5) was added and briefly vortexed, following by centrifugation at 13,400 g for 5 minutes. The upper aqueous layer was transferred to a new 1.5 mL microcentrifuge tube and 400 µL of chloroform was added. This was centrifuged at 14,600 g for 5 minutes and the upper aqueous layer was transferred to a new 1.5 mL microcentrifuge tube. For precipitation, 1 mL of 100% ethanol was added, and DNA was pelleted by centrifugation at 13,400 g for 5 minutes. After discarding the supernatant, the pellet was resuspended in 500 µL of 70% ethanol. The DNA was again pelleted by centrifugation and the resulting pellet was dried and resuspended in 400 µL of TE (pH 7.5) and 25 µg of RNase A was added. The mixture was incubated at 37 °C for 1 hour and then the DNA was ethanol precipitated.

2.7 Ethanol precipitation

To precipitate DNA, 30 µL of 4 M Lithium Chloride, 30 µL of molecular water (nuclease-free) and 200 µL of 100% ethanol was added. The mixture was stored at -20 °C. The precipitated DNA was pelleted by centrifugation at 14,600 g for 10 minutes, followed by resuspension in 1 mL 70% ethanol. After further centrifugation at 14,600 g for 10 minutes, the pellet was dried in a heat block at 37 °C. The dried pellet was then resuspended in either nuclease-free water. Then the tube was added to the heat block for 2 minutes at 37 °C before being stored at -20 °C until the next experiment.

2.8 End point polymerase chain reaction (PCR)

PCR was carried out using the MyTag HS DNA polymerase mix as per the manufacturer's instructions. The PCR reaction conditions included an initial denaturation step at 95 °C for 1 minute, followed by 30 cycles of denaturation at 95 °C for 15 seconds, annealing for 15 seconds and extension at 72 °C for 10 seconds. A final extension step was carried out at 72 °C for 2 minutes. The annealing temperature was determined based on the primers used.

2.9 Fractionation of day 7 stationary phase cultures

2.9.1 Preparation of Percoll density gradient

As described in (Allen et al., 2006) fractionation of stationary phase cultures have been performed with minor modifications. To prepare a solution with a final NaCl concentration of 167 mM, Percoll (GE Healthcare) was diluted 9:1 (v/v) with 1.5 M NaCl. To create density gradients, 15 mL of glass Cortex tubes were filled of Percoll solution and centrifuged in a Sorvall centrifuge using a SS-34 rotor at 10,500 g for 15 mins at 20 °C. The density gradients were created beforehand and kept at 4 °C for up to 24 hours until needed.

2.9.2 Density gradient separation of yeast cultures

To fractionate the cultures, 6.5 mL of cells was centrifuged at 1500 g for 5 minutes and the supernatant was removed. The cells were resuspended in 650 µL of Tris buffer (50 mM Tris-Cl, pH 7.5) and carefully layered on to pre-made gradients drop by drop with the entire 650 µL of resuspended cells. The gradients were centrifuged at 2000 g for 60 minutes at 20 °C, resulting in two distinct bands. Then, the upper fraction (non-quiescent

cells) was collected by gently pipetting some of the band, approximately 50% of the gradient, and added to a 15 mL centrifuge tube. The cells were washed once in 5x volume Tris buffer and pelleted by centrifugation at 1500 g for 5 minutes at 18 °C. The number of cells recovered was measured by spectrophotometry, and 10 OD_{600} unit samples for protein extraction, which was washed in 1 mL of 20% trichloroacetic acid and stored at -80 °C until required.

The lower fraction (quiescent cells) was collected and washed in 5x volume Tris buffer and pelleted by centrifugation at 1500 g for 5 minutes at 18 °C. The pellet was resuspended in 350 µL Tris buffer, loaded onto another gradient and centrifuged as before to purify the lower band. After centrifugation, the lower band was harvested and washed with 5x volume Tris buffer. Then resuspended the cell pellet in 10 mL of Tris buffer and measured the optical density of the purified cells. 10 OD_{600} unit samples were taken for RNA extraction.

2.10 Western blot analysis

2.10.1 Protein extraction

The 20% TCA protocol (Szymanski and Kerscher, 2013), was adapted to extract protein. Cells were grown overnight in a 50 mL culture to mid-log phase (OD_{600} 0.6 - 0.8). A volume of equivalent to 10 OD_{600} units was removed and centrifuged at 1500 g for 5 minutes. After removing the supernatant, the cell pellet was resuspended in 1 mL of 20% trichloroacetic acid (TCA) and transferred to a 1.5 mL microcentrifuge tube. It was then centrifuged at 13,200 g for 1 minute and the supernatant was removed. The pellet was resuspended in 250 µL 20% TCA, and approximately 500 µL of glass beads were added. The samples were vortexed for 30 seconds using a high-speed benchtop homogenizer and kept on ice for 1 minute, repeated three times. The cell lysate was transferred to a 1.5 mL microcentrifuge tube. The glass beads were washed using 500 µL 5% TCA and the wash was added to the cell lysate and kept on ice for 3 minutes. The cell lysate was centrifuged at 13,200 g for 1 minute and the supernatant was discarded. The pellet was resuspended in 300 µL 1x Laemmli (0.1% 2-mercaptoethanol, 10% glycerol, 2% SDS and 63 mM unbuffed Tris-Cl) and incubated at 95 °C for 5 minutes. After centrifuging for 1 minute at 13,200 g, the supernatant was transferred to a new 1.5 mL microcentrifuge tube and stored at -20 °C.

2.10.2 Bradford assay

This method was used for protein quantification of cell lysates and was performed according to instructions by Sigma. Bovine Serum Albumin (BSA) standards, ranging from 1 to 10 µg/mL, and diluted protein samples in H_2O. Next, the Bradford Reagent (Sigma) was added and measured the absorbance (A_{595}) with a spectrophotometer. By comparing the absorbance values to a standard curve, were able to calculate the protein concentration accurately. To ensure consistency, adjusted the protein sample concentration to 2 mg/mL using 1x Laemmli buffer and stored them at -20 °C.

2.10.3 SDS-Polyacrylamide gel electrophoresis (PAGE)

To prepare for protein examination, it is necessary to first clean the glass plates. Depending on the specific protein being analysed, 10 mL of either 10% or 15% (v/v) acrylamide-resolving gel solution should be made per gel. Assemble 1 mm thick plates and clamp them tightly, then pour the gel solution between the plates until 1 cm below the comb top when inserted. Immediately, overlay the gel with 1 mL of isopropanol to allow for polymerisation and let it set for 20 minutes. Remove the isopropanol layer and prepare 10 mL of 5% (v/v) acrylamide stacking gel to be layered on top of the resolving gel. Immerse plastic combs containing 15 wells into the stacking gel and allow the gels to set before using them for SDS-PAGE. See the recipes below for details on both the resolving and stacking gels.

15% resolving gel (10 mL): 2.3 mL H_2O, 2.5 mL 1.5 M Tris-HCl (pH 8.8), 5 mL 30% acrylamide, 100 µL 10% (w/v) SDS, 100 µL 10% (w/v) ammonium persulfate (APS), 4 µL TEMED.

10% resolving gel (10 mL): 3.8 mL H_2O, 2.6 mL 1.5 M Tris-HCl (pH 8.8), 3.4 mL 30% acrylamide, 100 µL 10% (w/v) SDS, 100 µL 10% (w/v) ammonium persulfate (APS), 2 µL TEMED.

Stacking gel (10 mL): 6.4 mL H_2O, 1.65 mL 1 M Tris-HCl (pH 6.8), 1.65 mL 30% acrylamide, 100 µL 10% (w/v) SDS, 100 µL 10% (w/v) ammonium persulfate (APS), 10 µL TEMED.

For precise protein analysis, it is highly recommended to heat the protein for 5 minutes at 95 °C before loading 40 µg into each well. Also, to include the EZ-Run Prestained *Rec* Protein Ladder (Fisher) was loaded as a size reference sample. The gels were run for 3 hours at 100 V in running buffer (25 mM Tris, 190 mM glycine, 0.1% w/v SDS) to ensure optimal results.

2.10.4 Western blot

In this research, the western blotting protocol was adapted from Current Protocols in Molecular Biology (Gallagher et al., 2011). To transfer the protein to a polyvinylidene (PDVF) membrane, a transfer buffer consisting of (25 mM Tris, 190 mM glycine and 20% v/v methanol) was used. The transfer process was carried out at 300 mA for 90 minutes using Bio-Rad equipment (Mini trans-blot 153BR) surrounded by ice. Before using the PDVF membrane, it was activated by soaking it in 100% methanol for 20 seconds, followed by water for 2 minutes. Also, two sponges and four pieces of blotting paper were soaked in a transfer buffer. After the transfer, the membrane was incubated in 20 mL of blocking buffer at room temperature for 1 hour to prevent non-specific binding of the primary antibody. The primary antibody was then added and incubated overnight at 4 °C to allow for specific binding to the target protein. The following day, the membrane was washed four times with TBST (Tris-buffered saline, 0.05% Tween 20) for 5 minutes to remove any unbound primary antibody. The secondary antibody was then added and incubated in 20 mL of blocking buffer at room temperature for 2 hours to bind to the primary antibody. The membrane was washed once for 10 minutes in TBST and three times in TBS to remove any unbound secondary antibodies. Lastly, the bound antigens were visualized using image quant (LAS4000) imager after preparing the Enhanced chemiluminescent (ECL). Western blotting substrate according to the manufacturer's instructions.

The table below (Table 2.4) provides information on the antibodies used in the western blot analysis, including their dilution in the blocking buffer.

Marvel blocking buffer: 5% (w/v) Marvel non-fat dry milk in TBS with 0.05% Tween 20 (v/v).

BSA blocking buffer: 5% bovine serum albumin (w/v) in TBS with 0.01% Tween 20 (v/v).

Antibodies used in western immunoblotting

Protein	Concentration	Species	Source	Blocking buffer
Hho1	1:1000	Rabbit	Abcam (71833)	5% Milk/TBST

Table 2.4: Antibodies used in western immunoblotting.

2.11 RNA protocols

2.11.1 RNA extraction

RNA was extracted using the hot phenol method adapted from Current Protocols (Collart and Oliviero 1993). Firstly, 50 mL of cultures were grown to the mid-exponential (OD_{600} 0.6 - 0.8) phase and day 7 stationary phase specific quiescent cells. A 50 mL sample was centrifuged for 5 minutes at 1500 g. The pellet was resuspended into 1 mL of sterile water and transferred to a 1.5 mL tube. The cells were then pelleted by centrifugation. At this stage, the cell pellets were either stored frozen at -80 °C or RNA was immediately extracted. The cell pellet was resuspended in 400 µL TES (10 mM Tris-Cl pH 7.5, 10 mM EDTA pH 8.0 and 0.5% w/v SDS) and 400 µL saturated phenol to extract RNA. This was incubated at 65 °C for 1 hour with occasional vortexing for 10-15 seconds. The sample was then placed on ice for 5 minutes and centrifuged for 5 minutes at 13,500 g. The upper layer was transferred to a new 1.5 mL microcentrifuge tube and 400 µL of saturated phenol was added. The sample was vortexed and kept on ice for 5 minutes. The sample was then centrifuged for 5 minutes at 14,600 g. The upper aqueous layer was transferred to a new 1.5 mL microcentrifuge tube and 400 µL chloroform was added, followed by centrifugation for 5 minutes at 14,600 g. The upper aqueous layer was transferred to a new 1.5 mL microcentrifuge tube and 40 µL sodium acetate (4 M, pH 5.3) was added and followed by 1 mL of ice cold 100% v/v ethanol. This was kept at -20 °C for one hour and then centrifuged for 10 minutes at 14,600 g at 4 °C. Lastly, the pellet was completely dried and then resuspended in nuclease-free water. The RNA concentration was quantified

utilizing a Nano-drop ND-100 spectrophotometer (Thermo Scientific). Measurements were taken at an absorbance wavelength of 260 nm.

2.11.2 RNA sequencing

To perform RNA sequencing, the total RNA was extracted as per the standard protocol. Next, DNase treatment and purification of the extracted RNA was carried out using the RNeasy Minielute Cleanup Kit from Qiagen, following the manufacturer guidelines. The quality of the RNA was assessed using the 2100 Bioanalyzer system before sequencing (Fig 2.1).

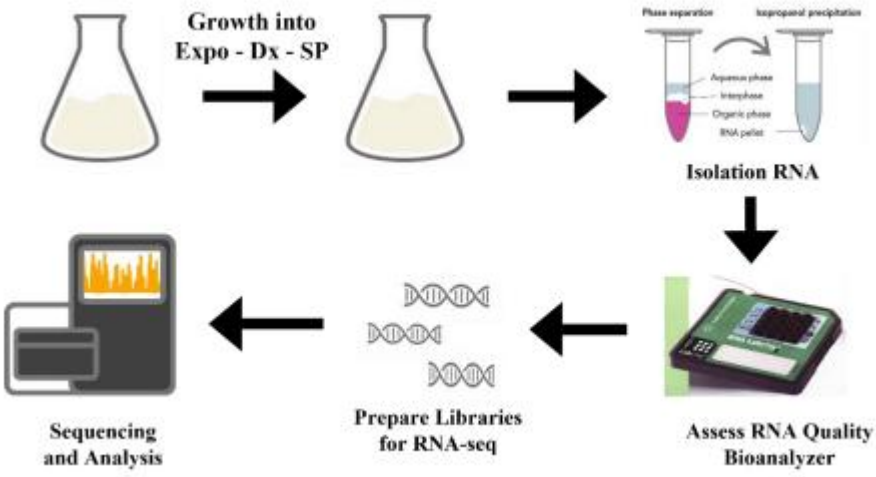

Figure 2.1: Schematic to illustrate the major steps in RNA sequencing. Yeast cells were grown to mid-exponential phase of growth and to day 7 of the stationary phase and purified for lower quiescent cells and total RNA was isolated, DNase treated and purified before sent for sequencing. Figure adapted from (Carsten Kröger and Ali Bakheet, 2023).

2.12 Statistical analysis

Statistical analysis was conducted using Microsoft Excel and GraphPad Prism 11. To determine the statistical significance of the results, a T-test was performed as appropriate. Results were deemed to be statistically significant if the p-value was less than (0.05). BioVenn was utilised to generate all Venn diagrams.

3. Results

3.1 Double *hho1Δ hmo1Δ* mutant construction

3.1.1 Introduction

The linker histone H1 protein binds to the DNA linker region where the DNA enters and exits the nucleosome (An et al., 1998). The linker histone H1 structure and function are well characterized in higher eukaryotes such as mice and humans. However, the yeast equivalent's identity and role remain controversial. It is commonly accepted that the *HHO1* gene encodes the yeast-linker histone H1 (Brush, 2015). The *HHO1* gene was identified by a scan of the yeast genome sequence for homologs of the conserved histone H1 globular domain (Landsman, 1996). However, the deletion of the *HHO1* gene in vegetatively growing yeast shows no striking phenotypes (Bryant et al., 2012). Intriguingly, Hho1p has been proposed to operate during the stationary phase of yeast to promote chromatin compaction and contribute to DNA repair (Patterton et al., 1998). However, whether Hho1p is the actual linker histone H1 equivalent remains a controversial topic.

Lately, another candidate has been identified that may function as the yeast H1 protein called Hmo1p. *HMO1* gene deletion is not lethal but deletion results in significant growth defects and decreased plasmid stability (Ray and Grove, 2009). *In vivo,* Hmo1p has shown to maintain a novel chromatin structure at the rDNA site within the nucleolus and facilitates ribosomal RNA transcription (Gadal et al., 2002).

To investigate if there is any interplay between Hho1p and Hmo1p in the stationary phase of *Saccharomyces* cerevisiae, I analysed the phenotypes of *hho1Δ* and *hmo1Δ* gene deletion mutants and a double *hho1Δ hmo1Δ* gene deletion mutant. The first steps in my project were to confirm the single gene deletion mutations in the *hho1Δ* and *hmo1Δ* mutants and subsequently construct and confirm the double *hho1Δ hmo1Δ* mutant.

3.1.2 Confirmation of the *HHO1* and *HMO1* gene deletions

The first set of experiments were to confirm that the deletion of the *HHO1* and *HMO1* genes in each of the mutant strains obtained by the yeast gene deletion library (ResGen) were correct. This confirmation was vital to begin characterising the mutant strains. Both mutants were constructed by replacing their gene coding regions with the *KAN* gene

(Baker et al., 1998). Western blotting was performed to confirm the *hho1Δ* deletion mutant, since there was an anti-Hho1p antibody available, whilst PCR was performed to confirm the *hmo1Δ* mutant in the absence of an antibody against this protein.

3.1.3 Confirming the *HMO1* single gene deletion by PCR analysis

The *hmo1Δ* mutant was constructed by replacing the *HMO1* gene coding region with the *KanMX* gene. PCR was used to confirm the *HMO1* gene deletion using primers up and downstream of the expected gene deletion region in the *hmo1Δ* mutant together with primers internal to the *KAN* selectable marker used in the gene deletion attempt to confirm the *hmo1Δ* mutant (Fig 3.1). Two different areas were amplified to confirm the presence of the *KanMX* gene. The first area was amplified using the upstream *hmo1Δ* con-F and Kan-B primers, which should give a 457 bp product in the mutant and be negative in the wt. The second PCR used downstream primers, *hmo1Δ* con-R and Kan-C, which should give an 821 bp product in the mutant and be negative in wt (Fig 3.2).

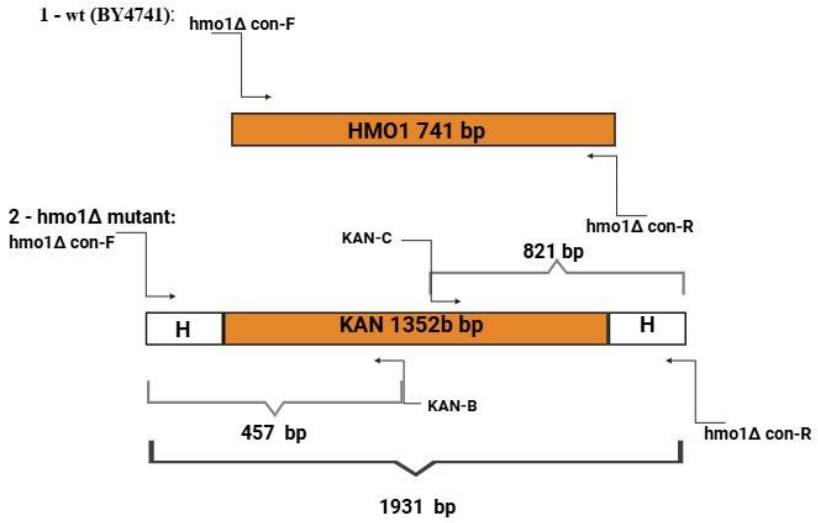

Figure 3.1: Schematic to show PCR design for gene deletion confirmation. Two different areas were amplified to confirm the presence of the *KanMX* gene. The first area was upstream *hmo1Δ* con-F and Kan-B primers which are positive in the mutant and negative in the wt lane. The positive confirmation is 457 bp in size. The second was downstream *hmo1Δ* con-R and Kan-C primers which are positive in the mutant and negative in wt. The positive confirmation is 821 bp in size.

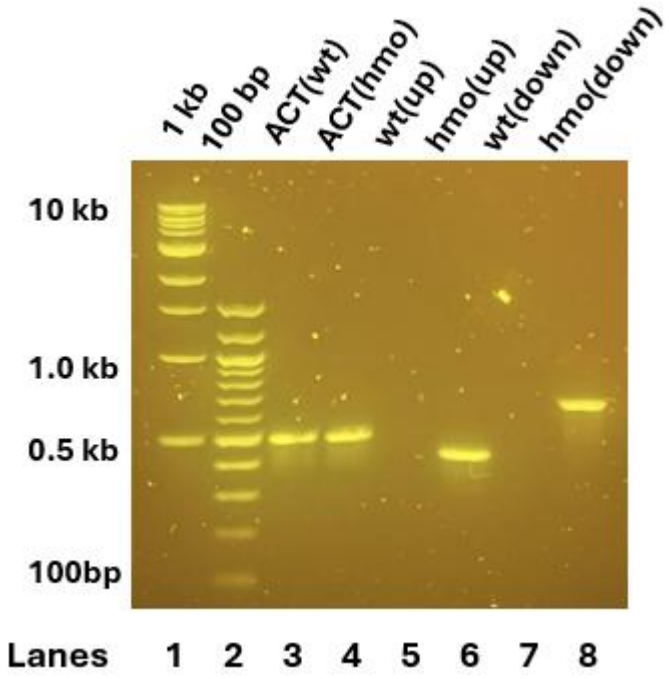

Figure 3.2: PCR confirmation of the *hmo1Δ* mutant. Result of the PCR confirmation reactions. Two different areas were amplified to confirm the presence of the *KanMX* gene: upstream *hmo1Δ* con-F and Kan-B primers which are positive in the mutant (lane 6) and negative in the wt (lane 5), and downstream *hmo1Δ* con-R and Kan-C primers which are positive in the mutant (lane 8) and negative in wt (lane 7). ACT was used as a positive control for the PCR reactions in lanes 3 and 4.

The results of the *HMO1* gene deletion confirmation PCR reactions are shown in (Fig 3.2). The 500 bp products in lanes 3 and 4 represent control PCRs of the *ACT1* gene which was used as a positive control to confirm the DNA preparations from wt and the potential hmo1 mutant could both support PCR amplification. In lane 6, the expected 457 bp product was evident following the upstream amplification of the hmo1 mutant, whilst no product was formed following the same amplification of wt DNA (lane 5). When the downstream amplification was performed on the hmo1 mutant, the expected 821 bp product was present (lane 8), which was absent following amplification of wt DNA (lane 7). Together, this confirms the *hmo1Δ* mutant is correct.

3.1.4 Confirming the *HHO1* single gene deletion by western blot analysis

I next carried out Western blot analysis using an anti-Hho1 antibody to confirm the deletion of *HHO1* gene (Fig 3.3). Total protein was extracted from wt, the potential

hho1Δ mutant and the previously confirmed *hmo1Δ* mutant, and a Western blot was performed. The data showed the presence of the Hho1p protein, of the expected size of 35 kDa, was detected in the wild-type strain and *hmo1Δ* mutant but was absent in the *hho1Δ* mutant strain (Fig 3.3). Ponceau S staining of the membrane verified equal protein loading across all samples (Fig 3.3). Together, this confirms the *HHO1* gene deletion mutant is correct, and shows that, as the Hho1p levels are similar to wt in the *hmo1Δ* mutant, *HMO1* does not influence Hho1p expression.

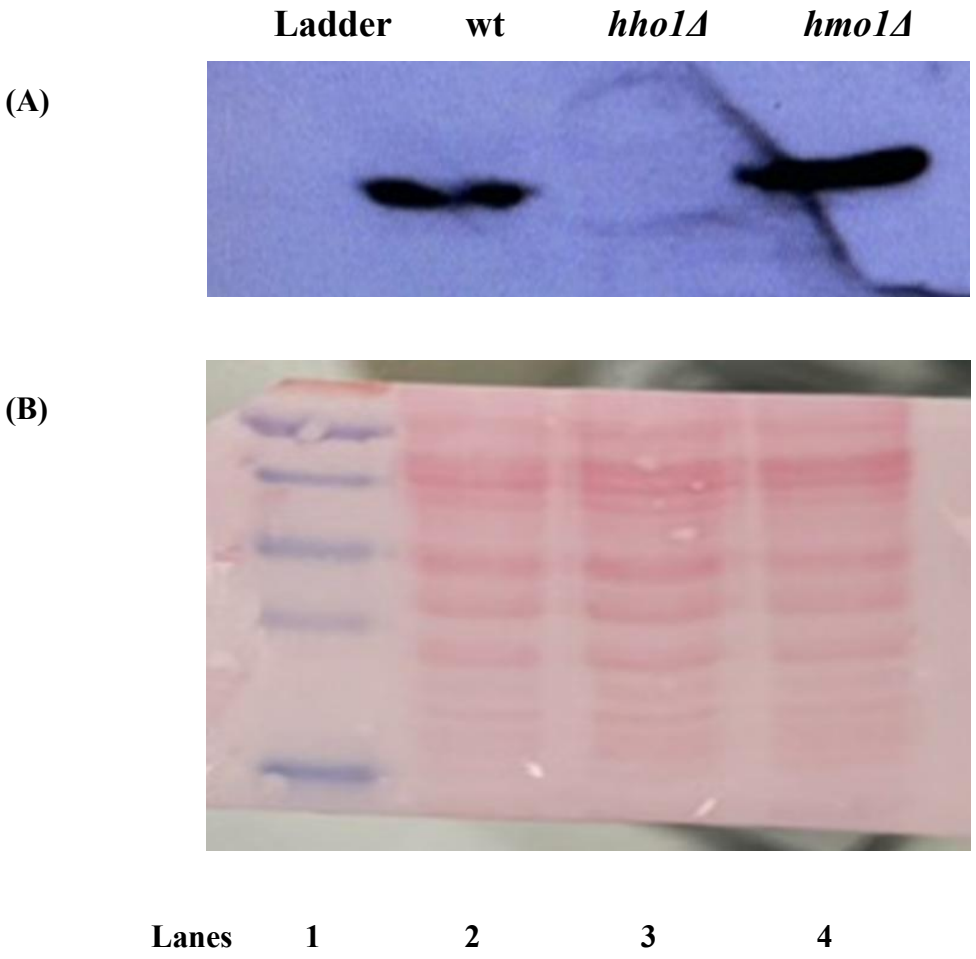

Figure 3.3: Western blot confirmation of the *hho1*Δ mutant. Total protein extracts from wild type (wt), *hho1Δ* and *hmo1Δ* strains were probed with anti-Hho1 and anti-rabbit secondary antibodies. **(A)** Hho1p was detected in both wt and *hmo1Δ* mutant strains but absent in the *hho1Δ* mutant strain. **(B)** Ponceau S staining of the membrane demonstrates equal protein loading.

3.1.5 Constructing the *hho1Δ hmo1Δ* double mutant

Since I had now confirmed both the *HMO1* and *HHO1* single gene deletions in their respective *hmo1Δ* and *hho1Δ* mutant strains, I next wanted to construct a double *hmo1Δ hho1Δ* gene deletion mutant strain. This would enable examination of any possible combined effects of losing both genes to investigate whether they might function together function in related pathways, or not. For example, the double mutant strain will clarify if Hmo1p and Hho1p act redundantly or additively of each other, or whether the loss of both genes produces a phenotype that is more severe or fundamentally different from each single mutant.

To construct this double mutant, I first attempted introducing the *hho1Δ* deletion into the previously confirmed *hmo1Δ* mutant strain. However, after multiple attempts and optimisation of the gene deletion protocol, I was unable to confirm the deletion. Indeed, 50 candidate transformants from multiple independent deletion attempts were screened for the deletion of *HHO1* in the *hmo1Δ* mutant strain without success. I therefore hypothesised that this could be due to a potential duplication of the *HHO1* gene in the *hmo1Δ* mutant strain meaning my attempts may have only deleted one copy of the *HHO1* gene and leaving the other copy to be expressed.

I therefore switched my approach to introducing the *hmo1Δ* deletion into the previously confirmed *hho1Δ* mutant strain. This approach was carried out using a URA3 cassette amplified from a pRS406 plasmid template (Fig 3.4). A simplified overview of the construction strategy is shown in (Fig 3.5), outlining the integration events and expected genomic rearrangement following successful recombination event to ultimately replace the *HMO1* gene with the URA3 selectable marker in the *hho1Δ* mutant background. Following transformation and selection on uracil-drop out medium potential candidate *hho1Δ hmo1Δ* mutants were isolated and screened by a PCR strategy described in (Fig 3.5).

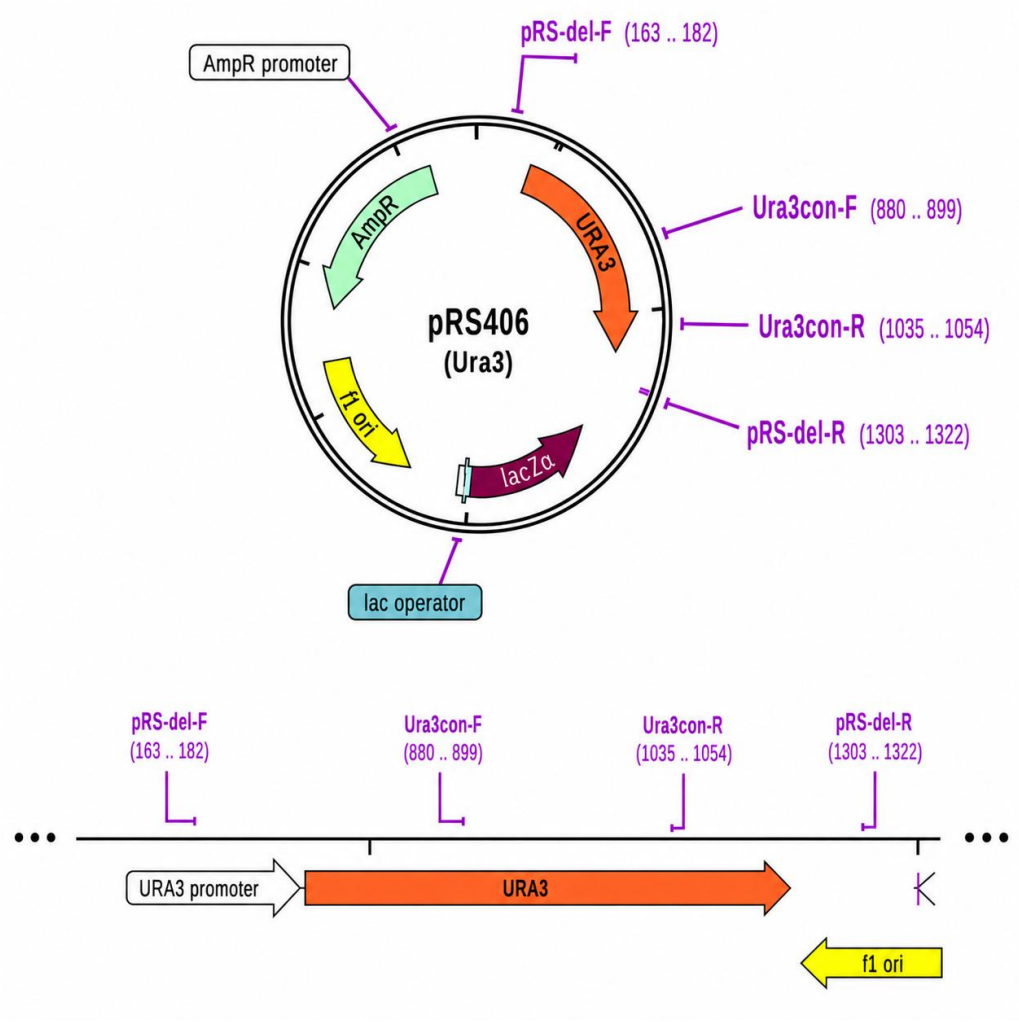

Figure 3.4: Schematic representation of the pRS406–URA3 cassette used to delete *HMO1* in the *hho1Δ* mutant strain. The plasmid pRS406 contains the URA3 selection marker flanked by sequences homologous to regions upstream and downstream of *HMO1*. Homologous recombination replaces the endogenous *HMO1* ORF with URA3, generating the *hho1Δ hmo1Δ* double mutant. Confirmation primers (Ura3con-F and Ura3con-R) amplify diagnostic fragments distinguishing deletion alleles.

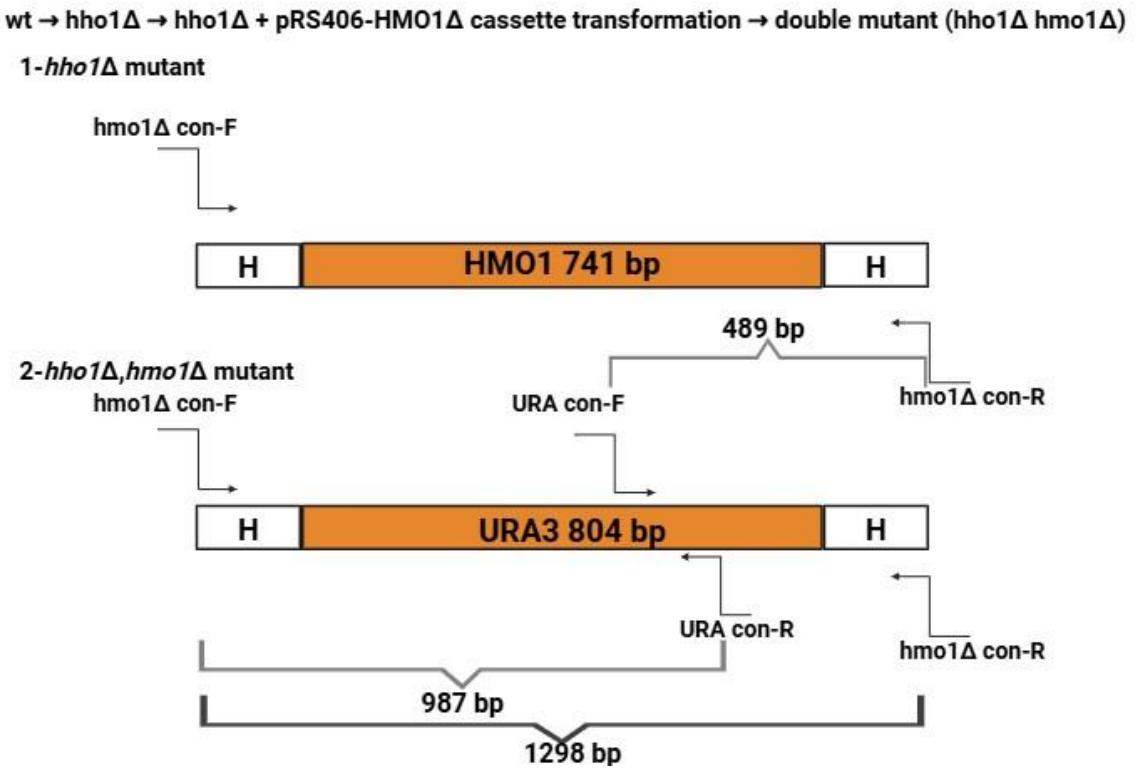

Figure 3.5: *hho1Δ hmo1Δ* double mutant construction schematic and PCR design. Schematic used to illustrate the PCR design to confirm the double mutant construction. The *HMO1* gene was replaced in the *hho1Δ* mutant strain using a URA3 disruption cassette on the pRS406 plasmid. Primer positions used for PCR confirmation are indicated, including external genomic primers flanking the deletion site and internal primers specific to URA3. Successful integration of URA3 produces PCR products confirming the construction of the double *hho1Δ hmo1Δ* mutant strain.

3.1.6 Confirming the *HMO1* gene deletion in *hho1Δ* mutant and therefore confirming the double *hho1Δ hmo1Δ* mutant.

Six potential HMO1 gene deletion mutants in the *hho1Δ* mutant background were initially screened by PCR using a primer flanking the *HMO1* locus and a primer internal to *URA3* (Fig 3.6). The area that was amplified to confirm the presence of URA3 gene was from primer *hmo1Δ* con-F to Ura3 con-R. Successful amplification of the expected 987 bp product was seen in two of the candidates, T4 and T6, which indicates these strains have had *HMO1* replaced by *URA3* (Fig 3.5).

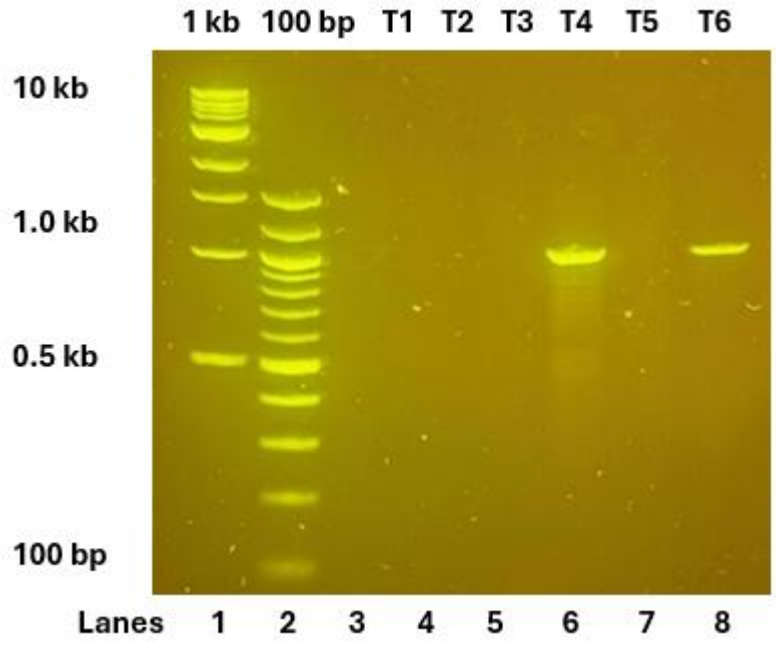

Figure 3.6. PCR-based screening of *HMO1* gene deletion in the *hho1Δ* mutant strain. Six transformants were screened, Transformant 1 (T1) to Transformant 6 (T6) by PCR to verify correct integration of the URA3 disruption cassette at the *HMO1* locus in the *hho1Δ* mutant strain. An upstream primer flanking the *HMO1* locus and an internal primer specific to URA3 were used to confirm the correct cassette insertion. The area that was amplified to confirm the presence of URA3 gene was from primer *hmo1Δ* con-F to Ura3 con-R (Fig 3.5).

Further verification by PCR was performed on the two *hho1Δ hmo1Δ* double mutant candidates (T4 and T6) using primers up and downstream of the expected *HMO1* gene deletion along with primers internal to the selectable marker as depicted in (Fig 3.5). In this case, all three separate reactions as depicted in (Fig 3.5) were amplified to confirm the presence of the URA3 gene at the HMO1 locus. The amplified areas were generated using, (i) *hmo1Δ* con-F to *hmo1Δ* con-R, which amplifies across the *HMO1* gene region and yields a 1235 bp sized band in wt (lane 3), and a 1298 bp band in the two possible double mutants (lanes 6 and 9). I also performed a PCR using primers, *hmo1Δ* con-F and Ura3 con-R, to yield the expected 987 bp size fragment in the two mutant candidates (lanes 7 and 10), and no product in wt (lane 4). Finally, I performed a PCR using primers Ura3 con-F to *hmo1Δ* con-R which gave the expected 489 bp sized bands in the two double mutant candidates (lanes 8 and 11), and no product in wt (lane 5). A PCR for a region of

the *ACT1* gene was performed as a positive PCR control for each amplification (panel B). Together, the data confirms that the *hho1Δ hmo1Δ* double mutant has been correctly constructed.

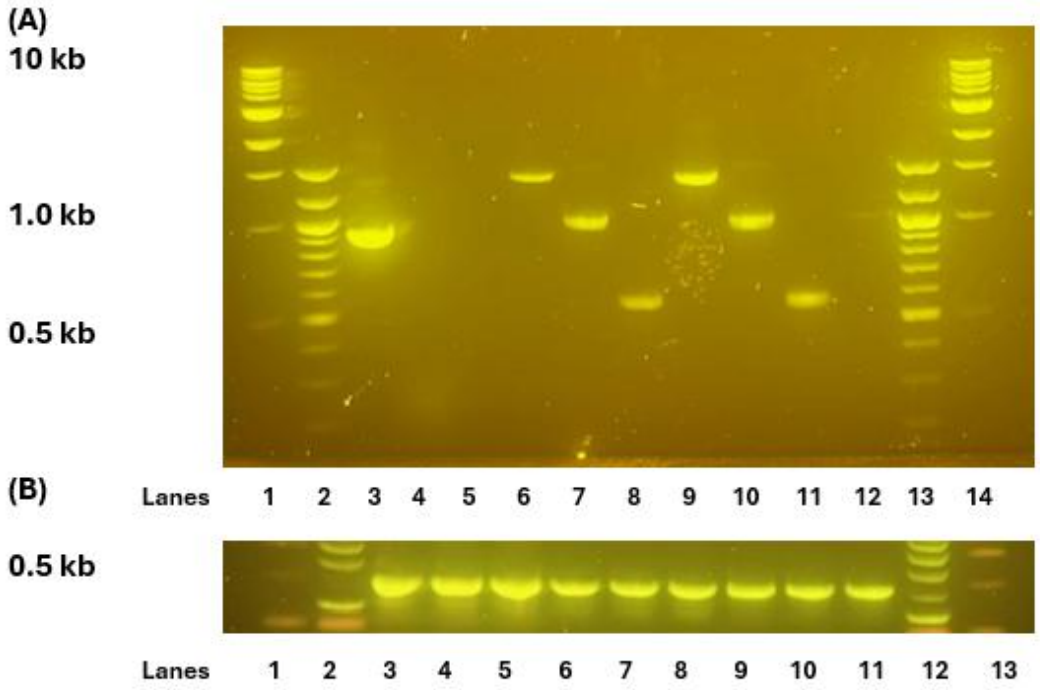

Figure 3.7: PCR confirmation of the double *hho1Δ hmo1Δ* mutant. **(A)** Result of the PCR confirmation reactions. Three separate areas were amplified to confirm the presence of the URA3 gene. The amplified areas were, *hmo1Δ* con-F to *hmo1Δ* con-R, which is positive in wt (lane 3) and also positive in the candidate double *hho1Δ hmo1Δ* mutant (lane 6 and 9), *hmo1Δ* con-F to Ura3 con-R, which is negative in wt (lane 4) and positive in the double *hho1Δ hmo1Δ* mutant (lane 7 and 10) and Ura3 con-F to *hmo1Δ* con-R, which is negative in wt (lane 5) and positive in the double *hho1Δ hmo1Δ* mutant (lane 8 and 11). The expected sizes of the PCR products produced to confirm the double *hho1Δ hmo1Δ* mutant as depicted in the schematic in Figure 3.5 (Fig 3.5) were, lane 3 = 1235 bp, lane 4 and 5 = 0 bp, lane 6 = 1298 bp, lane 7 = 987 bp, lane 8 = 489 bp, lane 9 = 1298 bp, lane 10 = 987 bp and lane 11 = 489 bp.

(B) ACT was used as a positive control for the PCR reaction.

3.2 Characterisation of mutants deficient for *hho1Δ* and *hmo1Δ*

3.2.1 Introduction

Although the linker histone H1's structure and function are well characterized in higher eukaryotes, the yeast's equivalent identity and role remain controversial. It is commonly accepted that the *HHO1* gene encodes the yeast linker histone (Brush, 2015). Hho1p has been proposed to operate during the stationary phase of yeast where it may promote chromatin compaction and contribute to DNA damage repair (Patterton et al., 1998). However, whether Hho1p is the actual yeast linker histone H1 equivalent remains controversial.

Only recently another candidate has been identified that may function as the yeast H1 protein and it is called Hmo1p. *HMO1* gene deletion is not lethal. However, deletion results in significant growth defect and plasmid instability (Ray and Grove, 2009). Hmo1p is also associated with DNA entry and exit points on the nucleosome (Bermejo et al., 2009). To investigate the role of Hho1p and Hmo1p and examine which might be the most likely candidate for linker histone H1 function in *Saccharomyces cerevisiae*, I analysed the phenotypes of *hho1Δ* and *hmo1Δ* single gene deletion mutants and the double *hho1Δ hmo1Δ* double mutant I constructed in the previous chapter. The first steps in this chapter were to determine if *hho1Δ* and *hmo1Δ* deletion mutants displayed similar or different phenotypes in the exponential phase and then see if these similarities or differences continued into the stationary phase. If yeast linker histone H1 is functioning in stationary phase, it would be predicted that the best candidate for yeast linker histone H1 would have the greatest severity of phenotypes during stationary phase in the appropriate mutant.

3.2.2 Mutants deleted for *HHO1* and *HMO1* show distinct phenotypes

I analysed the phenotypes of the *HHO1* and *HMO1* single gene deletion mutants, along with the double *hho1Δ hmo1Δ* mutant to try and determine which mutant has the greatest severity of phenotypes during both exponential and stationary phase and therefore determine which protein, Hho1p or Hmo1p is the best candidate for fulfilling the H1 function in yeast. The analysis also showcased how the double *hho1Δ hmo1Δ* mutant performed, which gives us an insight into whether the Hho1p and Hmo1p proteins function independently or cooperatively.

3.2.3 Analysis of growth in liquid media containing glucose

To investigate the growth of the mutants in exponential phase, the separate strains were individually inoculated into a liquid culture containing glucose (YPD), and the increase in optical density (OD $_{600\ nm}$) was monitored hourly using a spectrophotometer (Fig 3.8).

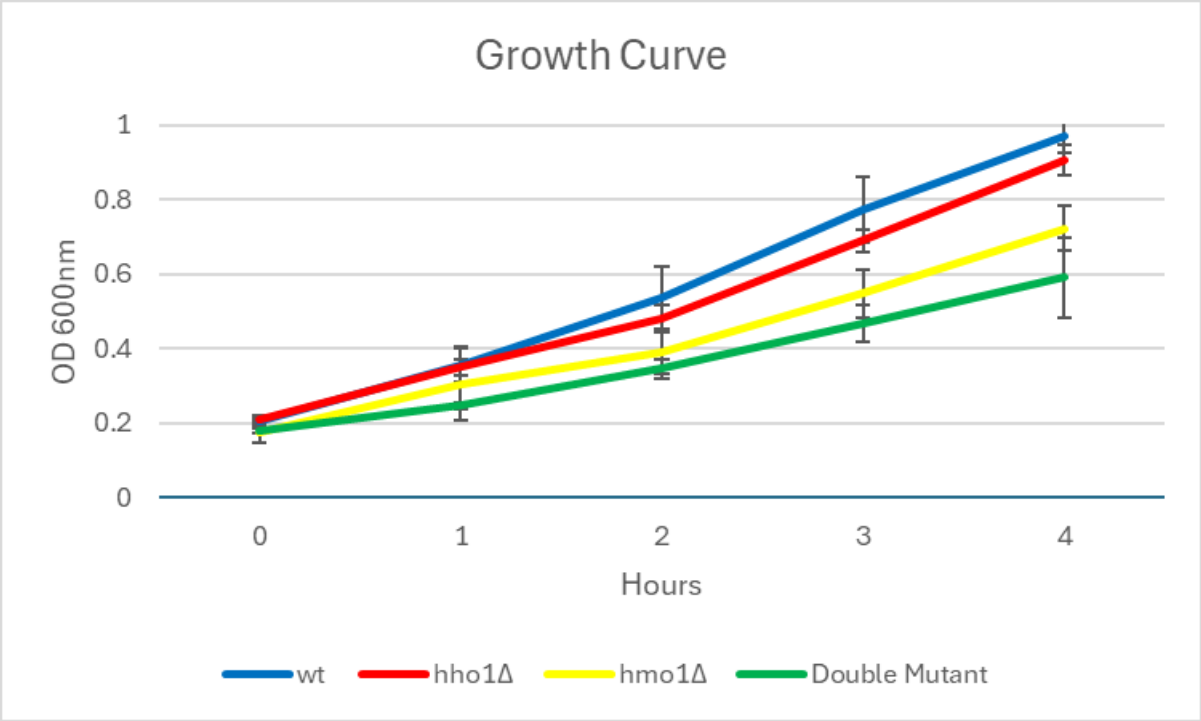

Figure 3.8: Analysing exponential growth of *hho1Δ* mutant *hmo1Δ* mutant and double *hho1Δ hmo1Δ* mutant compared to wild type. wild type (wt), single and double mutants were grown at 30 °C in YPD and OD $_{600\ nm}$ readings were taken at hourly intervals indicated. This experiment was performed in triplicate and error bars represent standard deviation (SD).

From (Fig 3.8), it is evident that all the cultures were in the exponential phase. In this glucose containing media, the hho*1Δ* mutant showed no significant growth defect in exponential phase compared to wt, but the *hmo1Δ* mutant and double *hho1Δ hmo1Δ* mutant showed a slower growth rate compared to wt.

To quantify the growth rates, I calculated the doubling time of each mutant and wt (Fig 3.9).

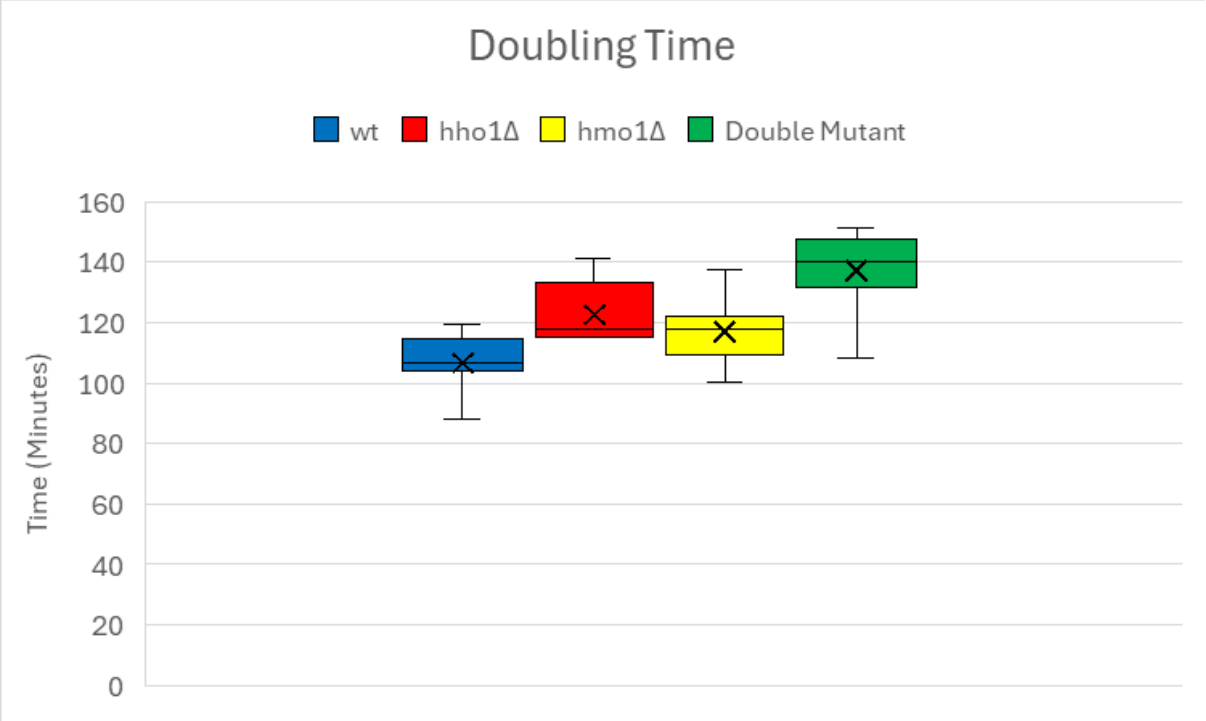

Figure 3.9: Doubling times of wt, *hho1Δ* mutant, *hmo1Δ* mutant and double *hho1Δ hmo1Δ* mutant. Doubling time of each strain indicated following growth in YPD media. The experiment was performed in triplicate and error bars represent standard deviation (SD). The double *hho1Δ hmo1Δ* mutant had a statistically significantly slower doubling time compared to wt, with a p-value of less than (0.05). The double *hho1Δ hmo1Δ* mutant had a p-value of (0.000135).

The doubling time of the strains as seen above (Fig 3.9) showcases that the double *hho1Δ hmo1Δ* mutant has a slower doubling time compared to wt. Overall, both the *hho1Δ* mutant and the *hmo1Δ* mutant showed no significant difference to wt and each other when comparing their doubling times. A t test showed the double mutants doubling time was a significant result with a p-value less than (0.05).

3.2.4 Analysis of cell density during entry into stationary phase

I next calculated the final cell density of each strain after 24 hours of growth in YPD, by counting cells using a haemocytometer (Fig 3.10).

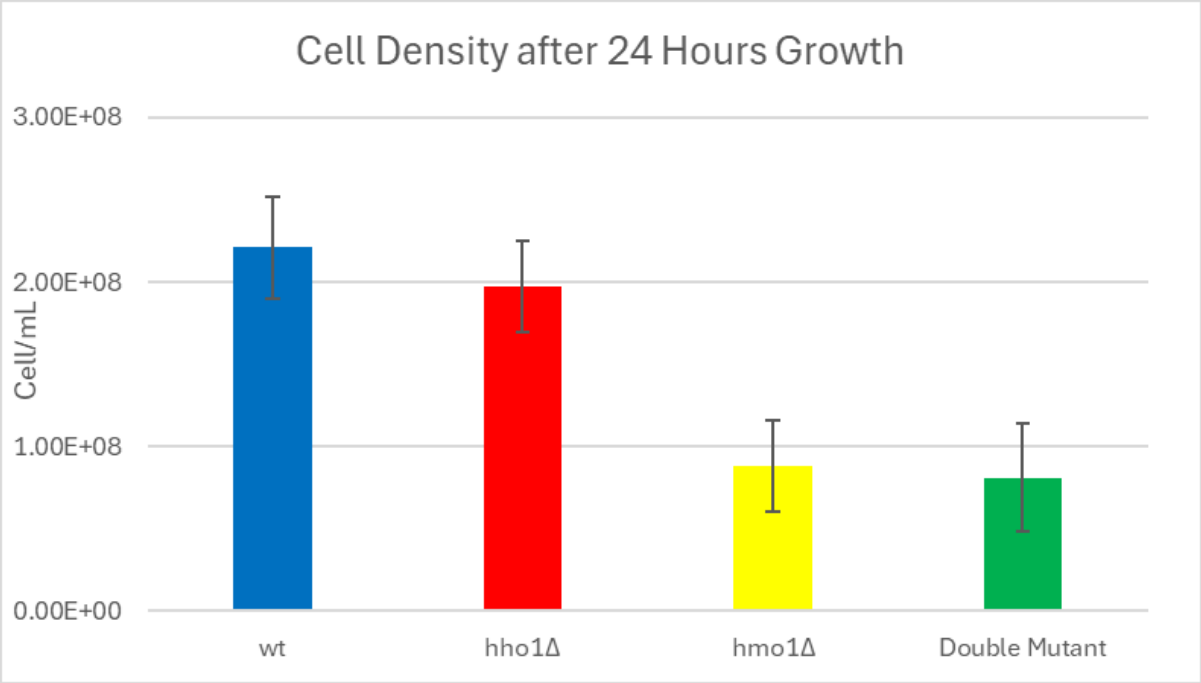

Figure 3.10: Analysis of growth into stationary phase, cell density after 24 hours growth in YPD. All strains were measured for cell density using a haemocytometer. The experiment was performed in triplicate and error bars represent standard deviation (SD). All three mutant strains produced a statistically significant result with p-values less than (0.05), compared to wt. *hho1Δ* mutant had a p value of (0.00182), meanwhile both *hmo1Δ* mutant and the *hho1Δ hmo1Δ* double mutant had extremely statistically significant p-values with p values less than (0.001).

The cell density at 24 hours of both wt and the three mutant strains yielded a statistically significant result. A t-test was performed on all three mutant strains, and it confirmed that all three mutant strains are statistically significantly different to wt, with p-values of ($p<0.05$). The *hmo1Δ* mutant and the *hho1Δ hmo1Δ* double mutant had extremely significant p-values where p = ($p< 0.001$). This revealed strong evidence that these mutant strains had significantly lower cell density after 24 hours of growth compared to that of wt. The most significant difference in cell density was between wt and the double mutant. The double *hho1Δ hmo1Δ* mutant at 24 hours of growth cell density was 37% of that achieved by wt. This indicates that the double *hho1Δ hmo1Δ* mutant has both a significantly different doubling time and lower 24-hour cell density compared to wt. This would suggest that the double mutant grows slowly in exponential phase compared to wt and is unable to attain wt levels before it enters stationary phase. It also suggests that both

single gene mutants *hho1Δ* and *hmo1Δ,* enter stationary phase at a lower cell density compared to wt.

3.2.5 Analysis of cell viability after 24 hours of growth in YPD

I next analysed the cell viability after 24 hours of growth in YPD. This was measured by spreading the diluted cultures of each strain onto YEPD agar plates and counting the colonies formed (Fig 3.11).

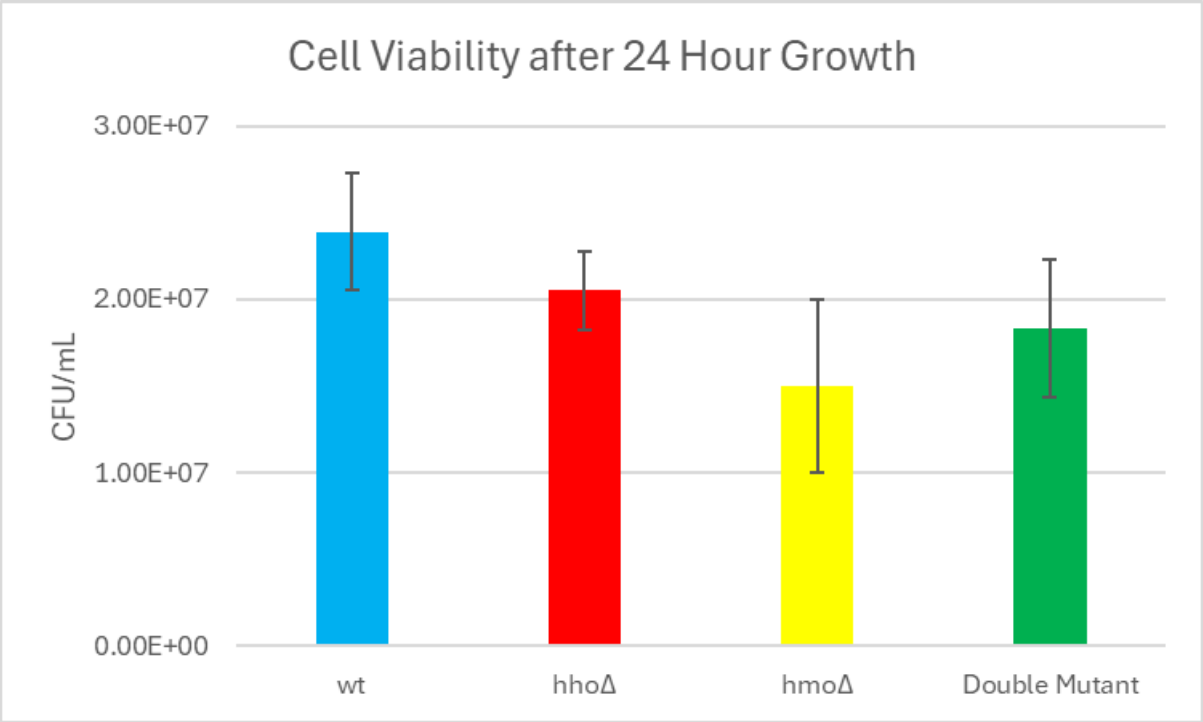

Figure 3.11: Analysis of viability of wt, *hho1Δ* mutant, *hmo1Δ* mutant and double *hho1Δ hmo1Δ* mutant after 24 hours of growth in YPD. Cell viability as measured by colony forming unit (CFU) capacity after 24 hours of growth. The experiment was performed in triplicate and error bars represent standard deviation (SD).

The data revealed that after 24 hours of growth, none of the mutant's lost viability compared to wt, as confirmed by a t-test. This is contrast to the statistically significant results of the cell density of the mutants compared to wt after 24 hours growth. Next, I monitored the cell viability of all four strains during day 7 in the stationary phase to see if the mutant's lost viability during their time in the stationary phase.

3.2.6 Analysis of cell viability during the stationary phase on day 7

The cell viability of wt, *hho1Δ* mutant, *hmo1Δ* mutant and the double *hho1Δ hmo1Δ* mutant in the stationary phase was investigated by measuring the colony forming unit (CFU) capacity of cells at day 7 in their respective growth cycles (Fig 3.12). This was to help us to determine if there was any difference in viability between the mutant strains compared to wt, which was previously not noted in the 24-hour cell viability experiment.

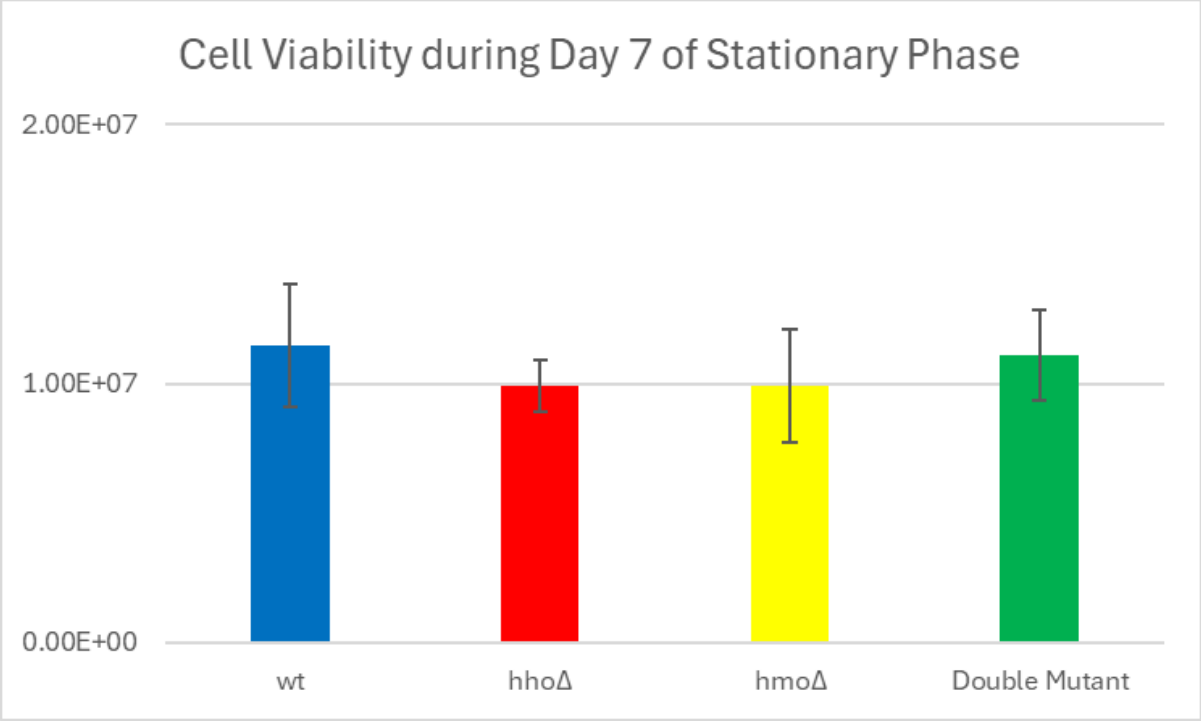

Figure 3.12: Analysis of viability of wt, *hho1Δ* mutant, *hmo1Δ* mutant and double *hho1Δ hmo1Δ* mutant during day 7 stationary phase. The experiment was performed in triplicate and error bars represent standard deviation (SD).

The data revealed, following t-tests, that the mutant strains did not have statistically significant differences in cell viability at day 7 in the stationary phase compared to wt. Therefore, we can conclude that none of the mutants lost viability over a 7-day period compared to wt.

3.2.7 Analysing *hho1Δ mutant*, *hmo1Δ* mutant and double *hho1Δ hmo1Δ* mutant cell morphology

I next analysed the cell morphology of each mutant strain. Cells were grown to the exponential phase and, separately to day 7 of the stationary phase before being viewed using a light microscope (Fig 3.13). Images were captured using a Leica ICC50 microscope camera with the LAS EZ software to compare any potential morphological differences between the strains.

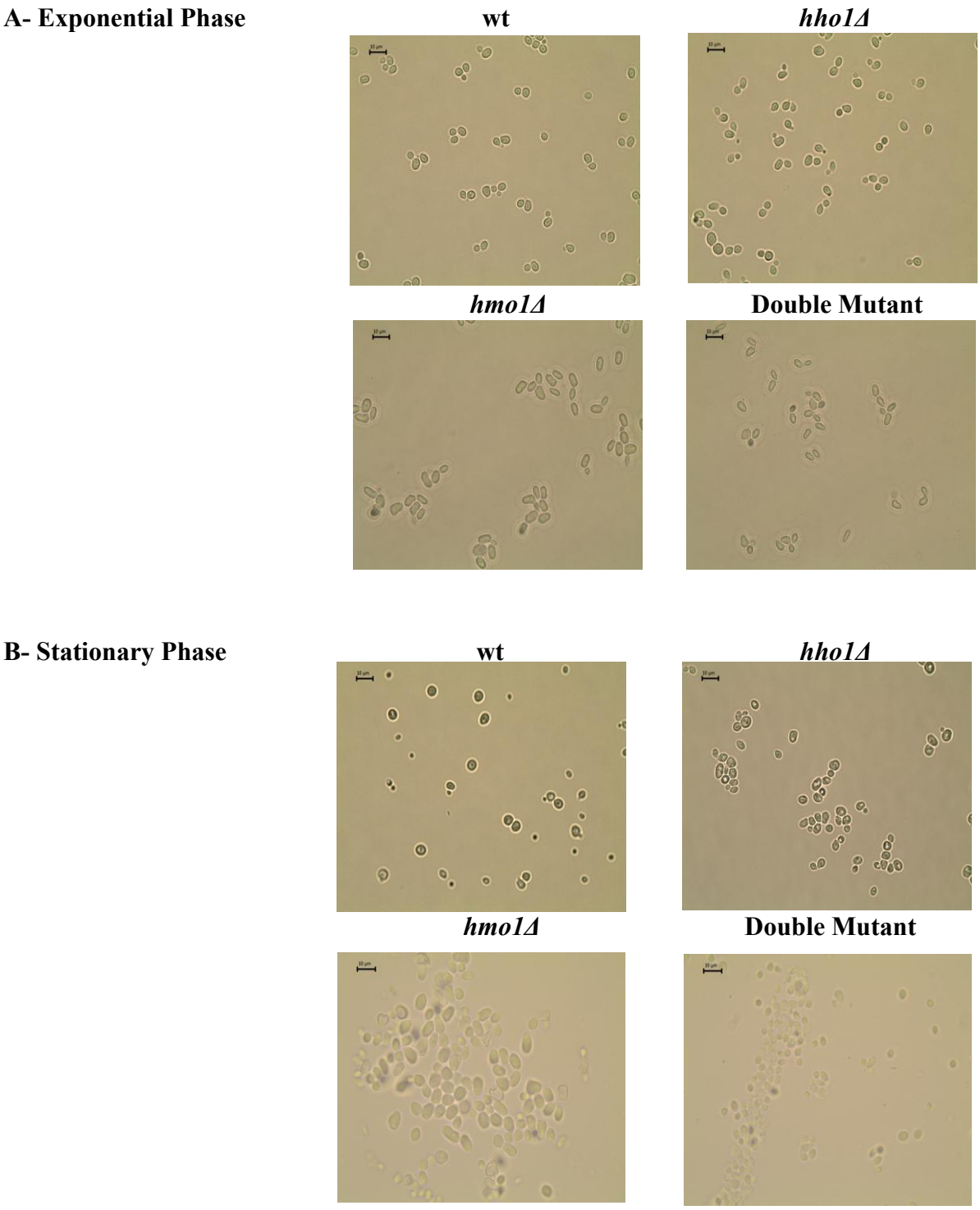

Figure 3.13: Cell images of wt, *hho1Δ* mutant, *hmo1Δ* mutant and the double *hho1Δ hmo1Δ* mutant cells. The different mutant strains shown in the cell images were grown in YPD media and were examined in both the exponential (A) and stationary phase (day 7) (B). Images were acquired using a 100x oil immersion objective (1000× total magnification).

There were no notable differences observed between the cell morphology of both wt and the *hho1Δ* mutant cells in both the exponential and the stationary phase. Both strains had cells of similar size and shape. Meanwhile, the *hmo1Δ* mutant strain and the double *hho1Δ hmo1Δ* mutant strain displayed an elongated rod-like morphology in the exponential phase compared to the wt. The elongated shape was not as distinct in the double *hho1Δ hmo1Δ* mutant strain in the stationary phase but was noticeable in the *hmo1Δ* mutant strain during the stationary phase. Also, the *hmo1Δ* mutant strain cells appeared larger in the stationary phase compared to wt stationary phase cells.

3.2.8 Testing for phenotypes by challenging cells in various 'Spot Tests'

Next, I carried out a series of experiments to challenge exponential phase and day 7 stationary phase cells with various stress conditions by so-called 'spot tests'. The cells were serially diluted and spotted onto plates containing caffeine or placed under specific growth conditions. This analysis offers a quick way to rapidly screen for any phenotypes that any of the mutant strains might display. This can offer an insight into the roles of *HHO1* and *HMO1* and indicate whether the role is specific to the exponential or stationary phase.

3.2.9 Analysis of temperature sensitivity

Cells from the exponential phase (Fig 3.14A) and day 7 stationary phase cultures (Fig 3.14B) were spotted onto YPD media and incubated at temperatures ranging from 15 °C to 42 °C (Fig 3.14).

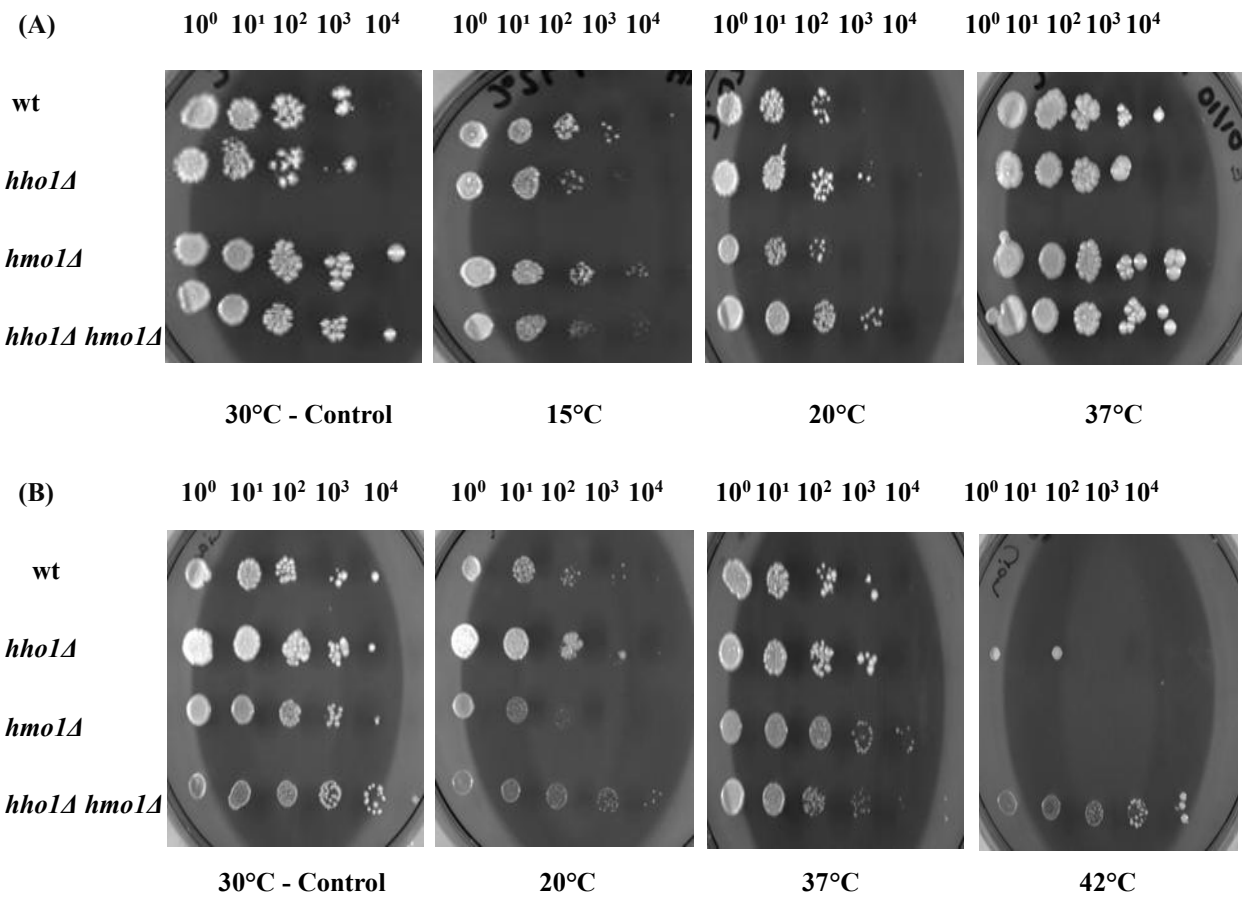

Figure 3.14: Temperature sensitivity growth tests of exponential and stationary phase growth cultures on YPD plates. (A) Exponential phase cells were serially diluted, spotted onto YPD plates and the plates were incubated at the indicated temperatures. **(B)** Stationary phase cells were serially diluted, spotted onto YPD plates and the plates were incubated at the indicated temperatures. YPD - control plates. 5 µL of culture was spotted on YPD plates. The images were taken after three days of incubation.

Following the incubation for three days, the plates were removed from their respective incubators and photographs were taken. In the exponential phase plates, none of the mutant strains showed a growth defect compared to the wt strain at the high or low temperatures tested. In the day 7 stationary phase plates, the *hmo1Δ* mutant strain appears to have a slight growth defect in the low temperature 20 °C plate, compared to the wt strain. Also, in the stationary phase plates, at the higher temperatures, the double *hho1Δ hmo1Δ* mutant appears to show resilience to the higher temperatures compared to wt. This can be seen slightly in the 37 °C plate and more prevalent in the 42 °C. This is an interesting result that showcases the double *hho1Δ hmo1Δ* mutant having unexpected resistance to higher temperatures in day 7 stationary phase.

3.2.10 Analysis of sensitivity to caffeine

I next tested the mutant strain cell's ability to grow in the presence of caffeine which causes a cell-wall stress response. Cells from the exponential phase cultures were spotted onto YPD-Caffeine plates (Fig 3.15A) and likewise with the day 7 stationary phase cultures being spotted onto YPD-Caffeine plates (Fig 3.15B).

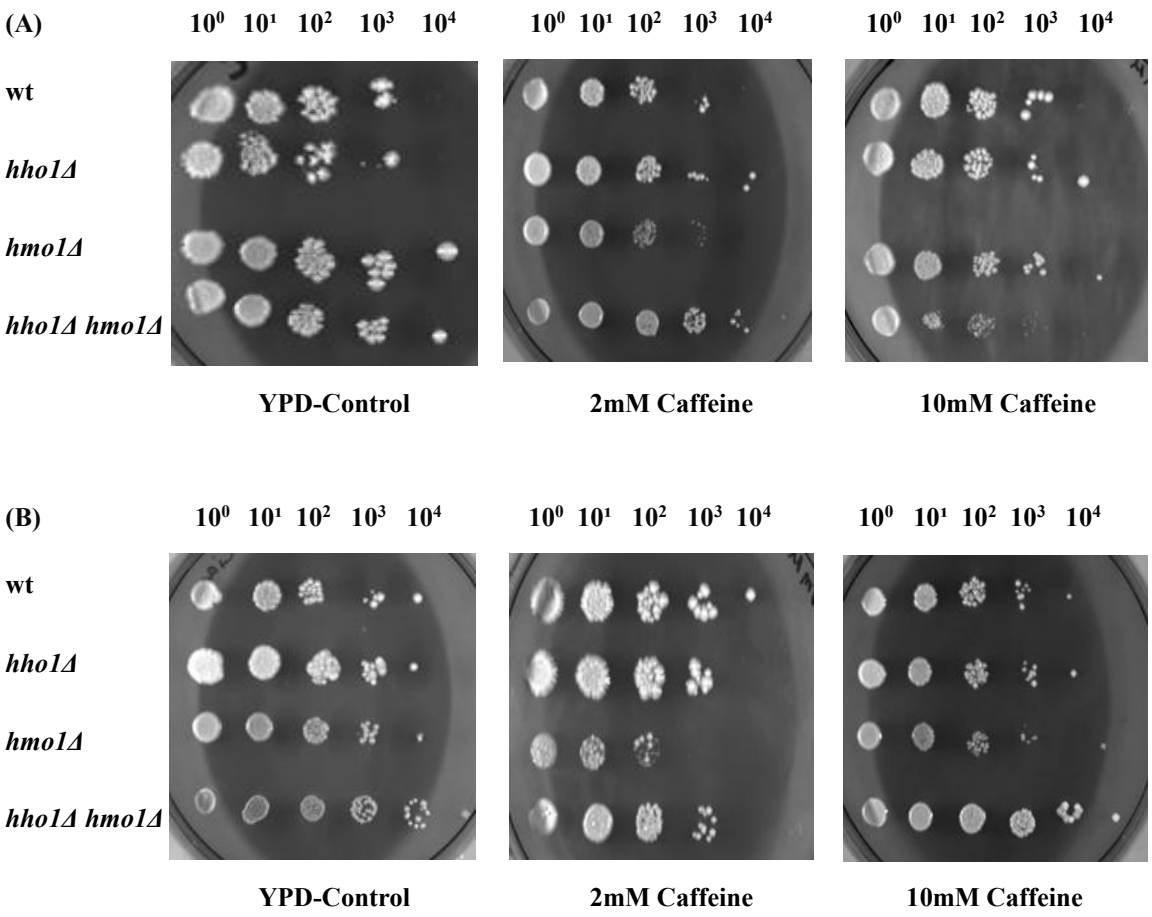

Figure 3.15: Testing cell sensitivity to caffeine of exponential and stationary growing cultures. (A) Exponential phase cells were serially diluted and plated as a 10-fold dilution series starting at $1x10^7$ cells/mL. **(B)** Stationary phase cells were serially diluted and plated as a 10-fold dilution series starting at $1x10^7$ cells/mL. The dilutions were spotted onto YPD-Caffeine (YP-Caff 2%). 5 µL of culture was spotted onto the plates. The images were taken after two days of incubation at 30 °C.

Following the incubation for two days, the plates were removed from the 30 °C incubator and photographs were taken. Interestingly, the exponentially growing or stationary phase mutant strains showed no extra resistance to the caffeine compared to wt, apart from a slight

growth defect in the double *hho1Δ hmo1Δ* mutant in the exponential phase on the 10 mM Caffeine plate.

3.3 Separation of stationary phase cultures into quiescent and non-quiescent cell populations

3.3.1 Introduction

When *Saccharomyces cerevisiae* is grown in glucose-based rich nutrient media, it goes through several different growth stages. These stages begin with a rapid logarithmic growth phase, driven by fermentation. When glucose is depleted at the diauxic shift, there are global reprogramming events that occur that contribute to a slower growth phase where fermentation products are used as a secondary carbon source via respiration. As soon as all available carbon sources are depleted, *Saccharomyces cerevisiae* cells enter the true stationary phase (SP), where cell growth and proliferation has ceased (Herman, 2002).

Until recently it was thought that all cells in SP cultures were non-proliferative. However, recent studies have revealed that *Saccharomyces cerevisiae* SP cultures consist of two populations. One population is quiescent, and the other population is non-quiescent (Allen et al., 2006). The quiescent population is comprised of young daughter cells that retain viability for long periods of time, while the non-quiescent population is mostly composed of mother cells that are older and undergo cell death. Only the quiescent population can re-enter the cell cycle once nutrients are replenished (Allen et al., 2006).

The understanding of SP has grown in recent years due to the ability to separate the distinct quiescent and non-quiescent populations. Nevertheless, the function of chromatin and the linker histone H1 in regulating quiescent and non-quiescent formation and function is not well understood. In this chapter, I monitored the quiescent and non-quiescent populations in the *hho1Δ hmo1Δ* double mutant strain compared to wt during SP to investigate if Hho1p or Hmo1p play a role in quiescent and non-quiescent development in stationary phase.

3.3.2 Percoll gradient centrifugation to separate quiescent (Q) and non-quiescent (NQ) cells

Previous studies have shown that stationary phase quiescent and non-quiescent cell populations can be separated by a Percoll gradient centrifugation procedure since the two cell populations, quiescent (Q) and non-quiescent (NQ) cells have different cell densities (Allen et al., 2006). The Q cells are most dense and form a band at the bottom of the gradient following centrifugation. In contrast, the less dense NQ cells form an upper band following centrifugation. I grew wt and double *hho1Δ hmo1Δ* mutant strain cells to day 7 of stationary phase and then performed the Percoll density gradient centrifugation to examine Q and NQ cell development during SP in the double mutant strain compared to wt.

I loaded the separate density gradients with an equal number of cells (Fig 3.16A). Following Percoll gradient centrifugation, the wt formed two distinct bands consistent with the formation of NQ (upper band) and Q (lower band) (Fig 3.16B). In wt, more lower Q cells formed compared to the upper NQ cells. Following the Percoll gradient centrifugation of the double *hho1Δ hmo1Δ* mutant strain, although the two bands were visible after centrifugation, there were more upper NQ cells and fewer lower Q cells visible compared to wt (Fig 3.16B).

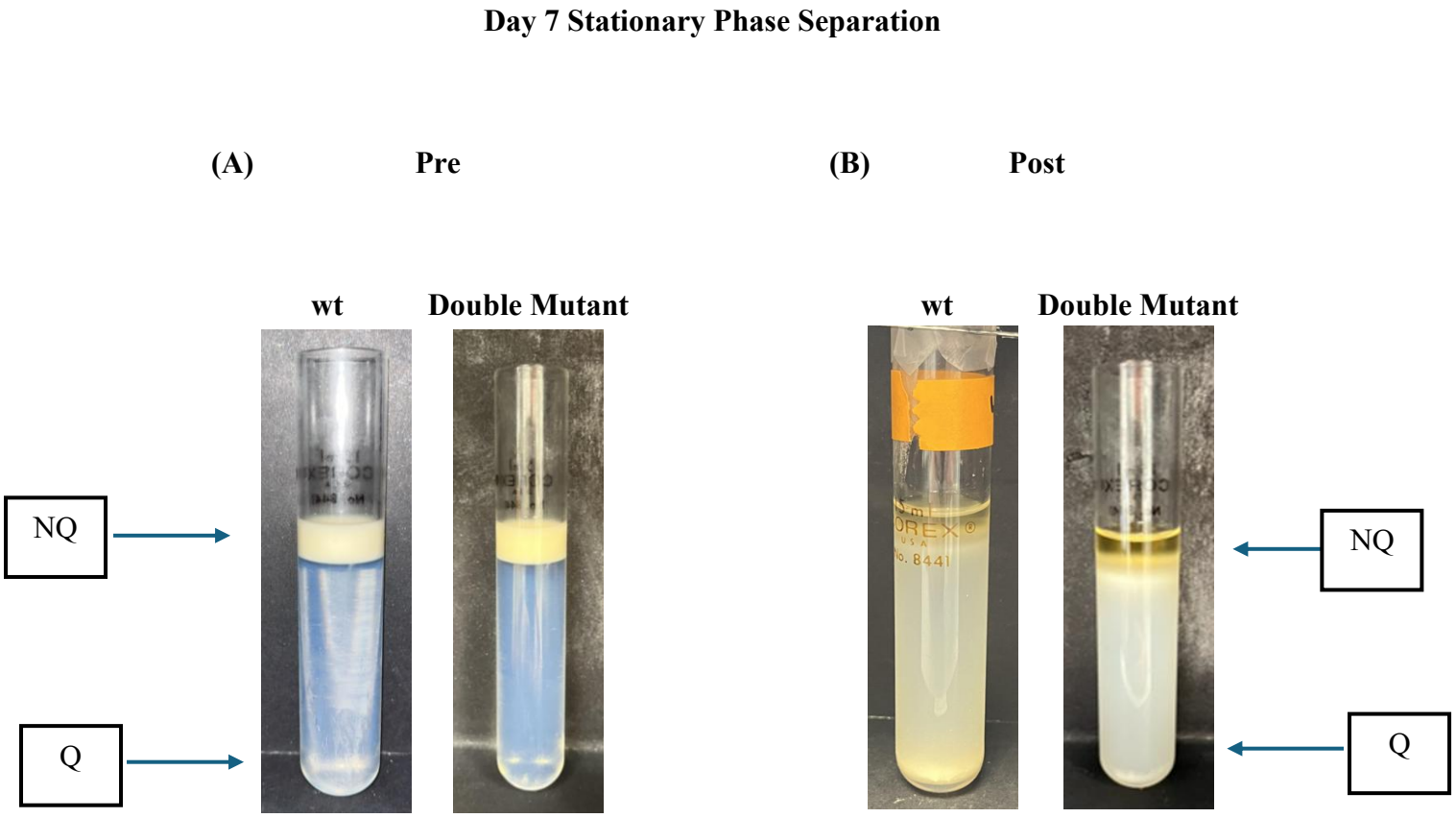

Figure 3.16: Separation of Day 7 stationary phase cultures into quiescent (Q) and non-quiescent cell (NQ) populations. Images of day 7 stationary phase wt and double *hho1Δ hmo1Δ* mutant cells before (A) (Pre) and after (B) (Post) centrifugation of Percoll density gradients loaded with cells harvested from 6.5 mL of day 7 stationary phase cultures.

This result suggested that by day 7 of the stationary phase, the development of Q and NQ populations in the double *hho1Δ hmo1Δ* mutant strain varies from the normal development as seen in the wt Percoll density gradients. It is clear from comparing the two tubes that much less Q cells (lower band) formed in the double *hho1Δ hmo1Δ* mutant strain, compared to the wild type. As a control to this experiment, I next performed this experiment on exponential wt and double *hho1Δ hmo1Δ* mutant cells.

3.3.3 Exponential phase wt and double *hho1Δ hmo1Δ* mutant did not form two cell populations

As a control for the previous experiment, I performed a Percoll gradient centrifugation on exponential wt and double *hho1Δ hmo1Δ* mutant cells. (Fig 3.17).

Exponential Phase Separation

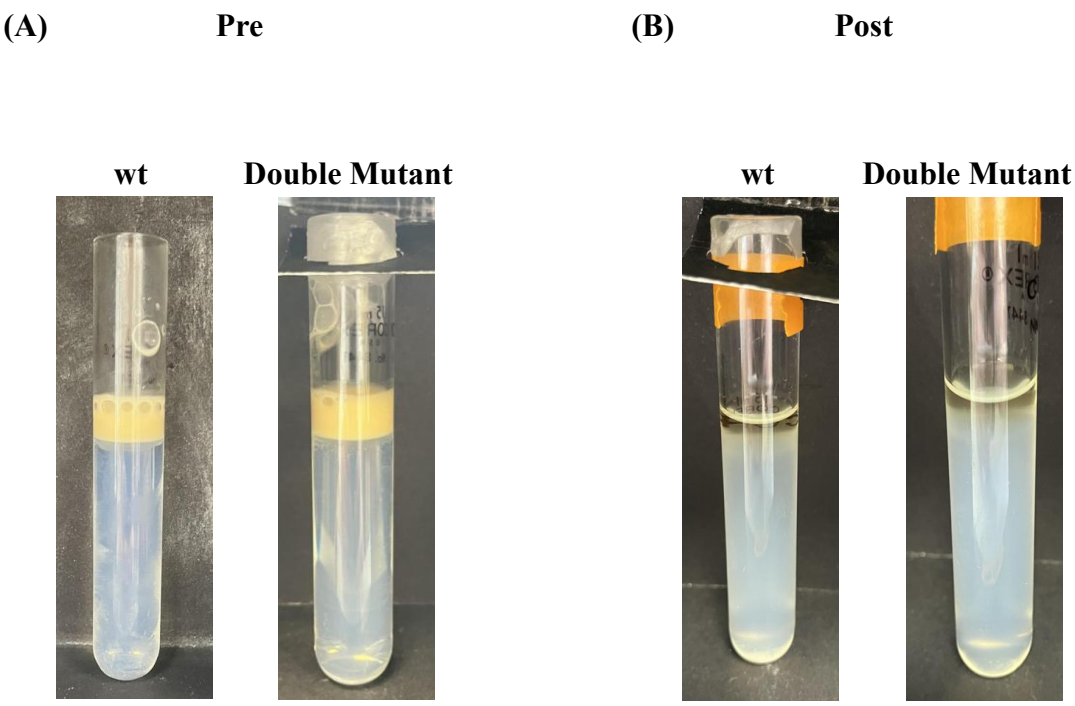

Figure 3.17: Exponential phase cells do not form two populations following Percoll gradient centrifugation. Images of exponential wt and double *hho1Δ hmo1Δ* mutant cells before (A) (Pre) and after (B) (Post) centrifugation of Percoll density gradients loaded with equal cell numbers.

The results showed that following centrifugation, both the wt and the double *hho1Δ hmo1Δ* mutant gradients looked identical and neither strain formed two populations (Fig 3.17). This confirms that the two cell populations formed in wt and the double *hho1Δ hmo1Δ* mutant day 7 stationary phase cells were specific to stationary phase.

3.3.4 The gradients were fractionated to isolate the two populations.

I next fractionated the two separate populations of wt and the double *hho1Δ hmo1Δ* mutants' day 7 stationary phase cells formed after the centrifugation (Fig 3.16) and counted the total number of cells in each of the upper and lower fractions. The result of the cell counts in each fraction were expressed as a percentage of the total number of cells in both the upper and lower fractions to show the proportion of cells found in the upper

(NQ) and lower (Q) cell fractions in the wt and double *hho1Δ hmo1Δ* mutant cultures (Fig 3.18).

A - Post Fractionation

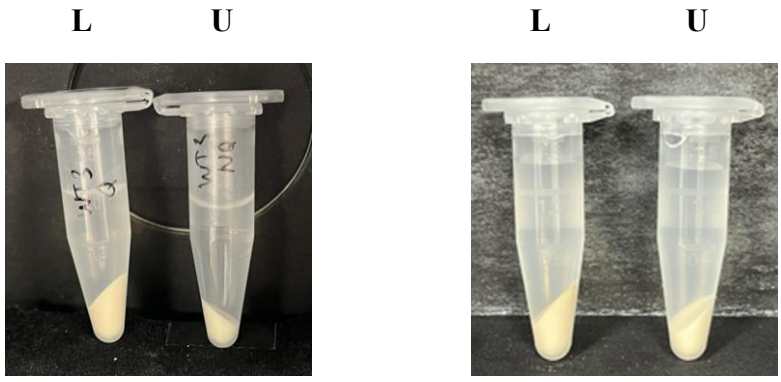

B

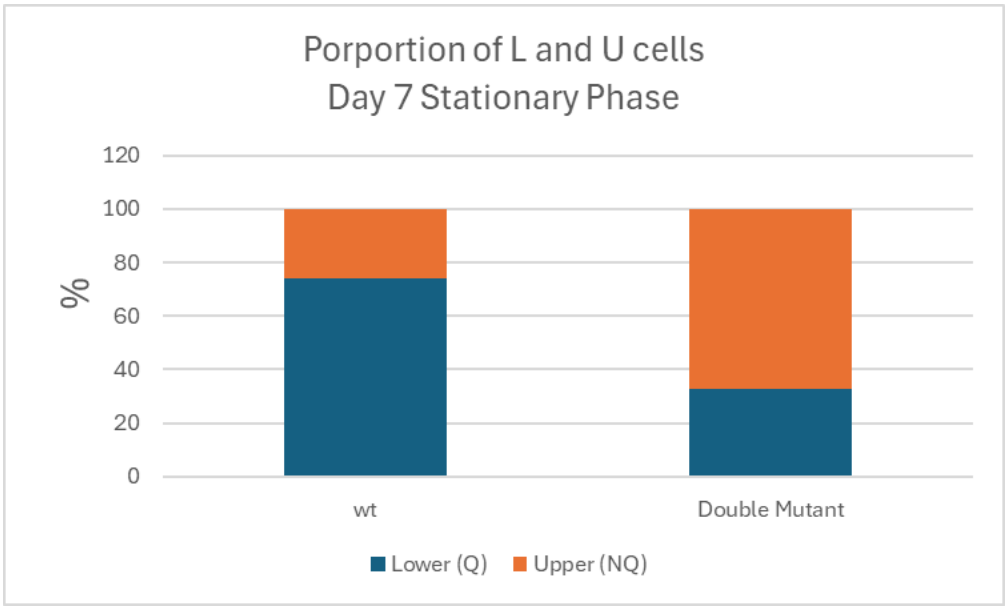

Figure 3.18: The gradients were fractionated to isolate and quantify the two populations formed in the stationary phase wt and double mutant cultures. A- Cells were harvested from the fractionated gradients. L- Lower Quiescent cells, U- Upper non-quiescent cells. **B-** Total cell counts for the upper fraction (NQ) and lower fraction (Q) were calculated using a haemocytometer. The cell counts in each fraction were expressed as a percentage of the total cell numbers from each fraction. The data shown is representative of this experiment performed in triplicate.

The results showed that in wt, much lower (Q) cells formed (74%) compared to upper (NQ) cells (26%). In comparison, in the double *hho1Δ hmo1Δ* mutant there was much less Q cells formed (33%) and a much greater amount of NQ cells (67%), compared to wt. Therefore, we can conclude after 7 days in stationary phase, the double *hho1Δ hmo1Δ* mutant formed far fewer lower Q cells compared to wt cultures. This indicates that Hho1p or Hmo1p, or perhaps both, are required for the normal development of Q and NQ cell formation during stationary phase. This intriguing result raises the question if it is defects in global gene transcription in the double *hho1Δ hmo1Δ* mutant during development of the stationary phase that causes this problem. Identifying the genes under the transcriptional regulation of Hho1p and Hmo1p in exponential phase and in purified day 7 Q cells formed during stationary phase will give an insight into these potential defects by comparing the global RNA transcriptome data of the double *hho1Δ hmo1Δ* mutant with wt transcriptome data.

3.3.5 Preparation and quality assessment of exponential and quiescent RNA from the double *hho1Δ hmo1Δ* mutant for RNA sequencing

I therefore next prepared RNA from six biological replicates of the double *hho1Δ hmo1Δ* mutant strain in exponential phase and from purified quiescent (Q) cells in day 7 of the stationary phase. RNA integrity was then assessed using an Agilent Bioanalyzer. Representative electropherograms showed well defined 18s and 28S rRNA peaks with minimal degradation (Fig 3.19). All samples met the quality requirements for RNA sequencing apart from 1 biological replicate of purified quiescent cells in day 7 of the stationary phase.

Therefore, 6 biological replicates of the double *hho1Δ hmo1Δ* mutant strain in exponential phase were submitted for sequencing along with 5 biological replicates of the double *hho1Δ hmo1Δ* mutant strain from purified quiescent day 7 cells that were also submitted for sequencing. The RNA samples were sent for sequencing, but sequencing results were not received prior to thesis submission. Ultimately, the RNA sequencing data from the exponential phase and quiescent double mutant can then be analysed and compared to existing RNA sequencing data obtained from wt and the *hho1Δ* and *hmo1Δ* single deletion mutants at the same cell growth stages.

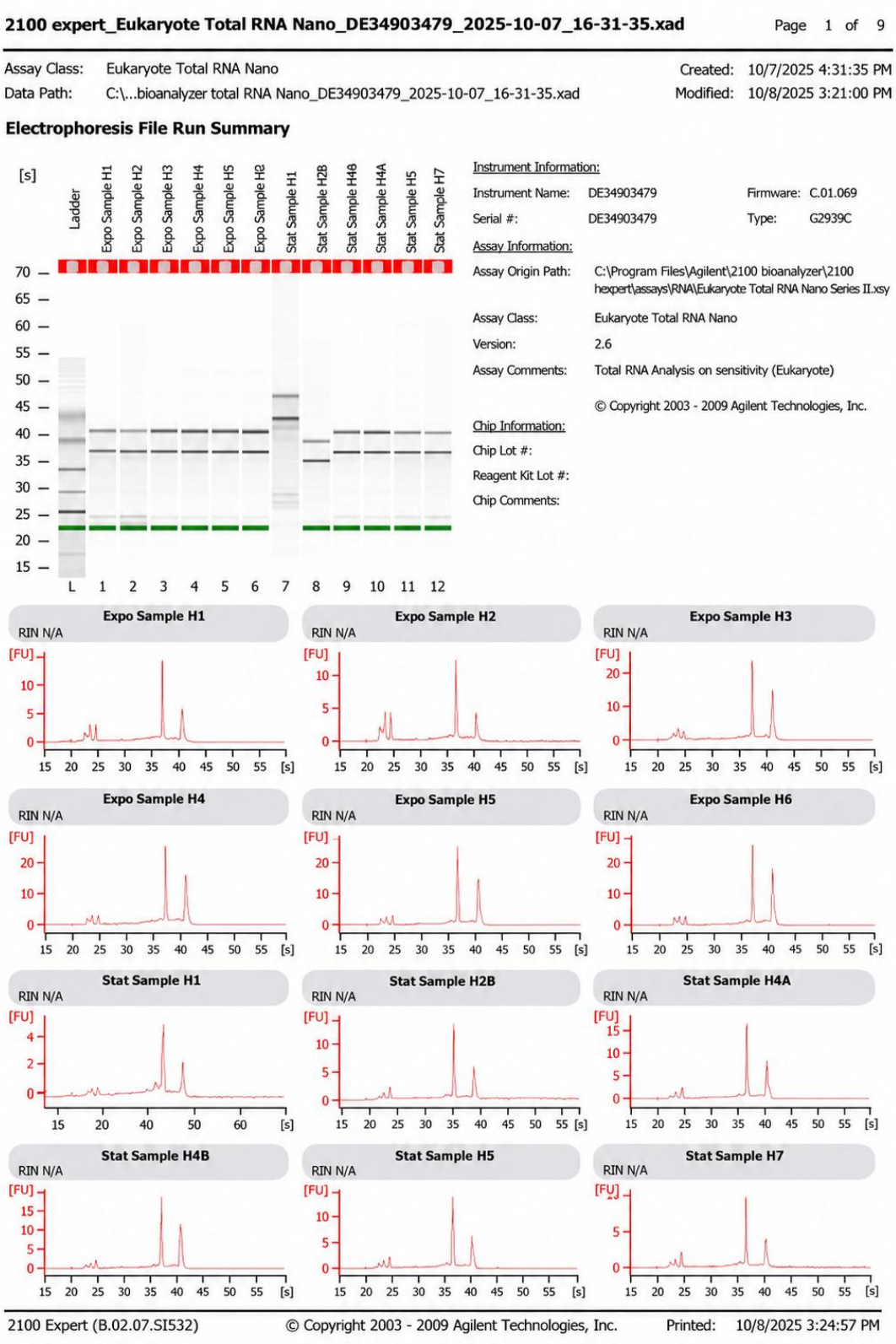

Figure 3.19: Quality assessment of RNA isolated from exponential and purified quiescent day 7 stationary phase double *hho1Δ hmo1Δ* mutant cells.

Representative Agilent Bioanalyzer electropherograms showing intact rRNA peaks and minimal RNA degradation.

3.4 ChIP-seq data analysis

3.4.1 Introduction

Chromatin Immunoprecipitation (ChIP) is a very useful method to identify specific DNA-protein interactions along the genome. Combining ChIP and DNA sequencing technology by using ChIP-Seq means that it is now possible to determine the genome-wide enrichment of a specific protein of interest (Lefrançois et al., 2014). There are several advantages of this method over the traditional ChIP qPCR methods, these include the ability to scan for regions of protein binding over the entire genome and the ability to identify previously unknown regions of protein enrichment, or peaks of protein binding (Fig 3.20).

In this chapter, the location of Hho1p and Hmo1p have been mapped across the entire yeast genome during exponential phase, at the diauxic shift, and in separated day 7 quiescent (Q) cells using ChIP-seq that was previously generated (Al-Najjar, 2024), but had not been analysed. One of the main reasons for this was to identify where proteins bind in actively growing cells and then to see if the proteins redistribute during quiescent cell development. The prediction would be that the proteins will occupy different sites at the different stages of growth.

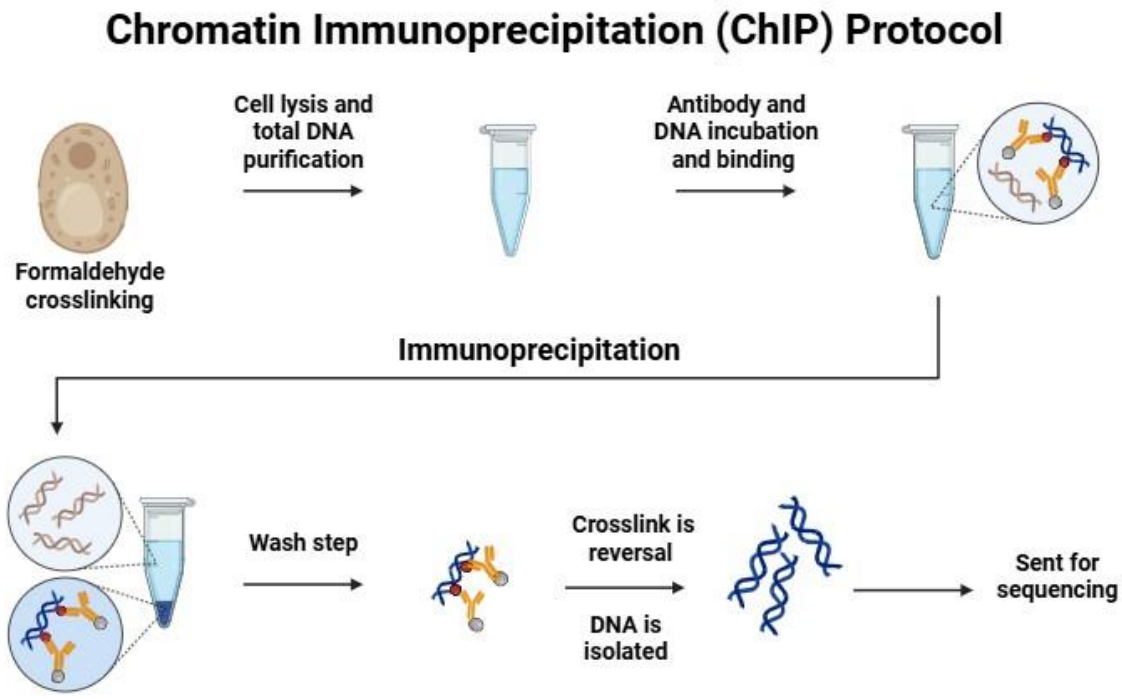

Figure 3.20: Schematic representation to illustrate the ChIP-Seq protocol. The genomic DNA is treated with formaldehyde to cross-link proteins to the DNA. Following the lysis of the cells, the DNA is fragmented using sonication to give DNA fragments approximately 500 bp in length. The Input (IN) sample is removed and the antibody specific to the protein of interest is added to the IP sample. The protein bound fragments are purified from the IP sample. DNA is purified from both the IN and IP samples, which involves reversing the cross-links and degrading any proteins. The purified DNA is then sequenced. Following sequencing the reads are mapped to the reference genome and the regions of enrichment of the protein of interest are identified.

3.4.2 Analysis of Hho1p and Hmo1p occupancy in exponential phase cells.

Using the ChIP-Seq data I received from Dr Reham Hussain Al-Najjar (Al-Najjar, 2024), the occupancy of both Hho1p and Hmo1p in exponential phase cells was analysed. The findings of Hmo1p revealed a total of 855 binding sites compared to 777 binding sites for Hho1p in exponentially growing cells (Table 3.1).

Further investigation into the occupancy sites of Hmo1p showed that it was associated with 812 genes, whereas Hho1p was linked to 698 genes, showing its lower overall occupancy. These gene numbers represent where each protein was found either associated

on a gene coding region (ORF) or was found within a region 1 kb up or downstream of that gene.

Peaks of Hho1p and Hmo1p Occupancy and Genes Associated during Exponential Phase

Protein	Total Peaks	Genes Associated
Hho1p	**777**	**698**
Hmo1p	**855**	**812**

Table 3.1: Peaks of Hho1p and Hmo1p Occupancy and Genes Associated during Exponential Phase. 1- First column is total number of occupancy sites (peaks), **2-** Genes mapped to an ORF.

3.4.3 Analysis of Hho1p and Hmo1p occupancy at genes in exponential phase cells.

I next analysed the sites of occupancy of Hho1p and Hmo1p at the genes that had been associated with Hho1p and Hmo1p in exponential phase cells to determine if the proteins were found at the promoters, ORF, or downstream regions of associated genes (Fig 3.21) (Table 3.2).

Hho1p and Hmo1p were associated with genes predominantly at their promoter regions. Hho1p had a total of 561 sites mapped to the promoters of the 698 genes it had been associated with. In contrast, only 32 sites of Hho1p occupancy mapped to the distal region of its associated genes. Hmo1p had a total of 757 sites mapped to the promoters of the 812 genes it had been associated with. In contrast, only 33 sites of Hmo1p occupancy mapped to the distal region of its associated genes. Another difference noticed was that there were 105 sites of Hho1p occupancy mapped to the ORF, meanwhile only 22 sites of Hmo1p occupancy mapped to the ORF. This showed that the vast majority of both Hho1p and Hmo1p were found at the promoter regions of target genes in exponential phase compared to the distal and ORF regions.

Figure 3.21: Schematic representation of the sites of gene occupancy. The Promoter, ORF or Downstream (Distal) of the associated ORF. TSS is the Transcription Start Site, indicated by the arrow. Stop represents the stop codon.

Distribution of Hmo1p and Hho1p occupancy sites across promoter, ORF and distal regions of associated genes

Protein	Genes Associated	Promoter	ORF	Distal
Hho1p	**698**	**561**	**105**	**32**
Hmo1p	**812**	**757**	**22**	**33**

Table 3.2: Distribution of Hmo1p and Hho1p occupancy sites across promoter, ORF and distal regions of associated genes. 1- First column is total number of genes associated, **2-** Occupancy sites at Promoter region, **3-** Occupancy sites at ORF region, **4-** Occupancy sites at the Distal region.

After analysing the sites of occupancy of Hho1p and Hmo1p at the genes that had been associated with Hmo1p and Hho1p to determine where either protein was found, I next analysed the Hho1p and Hmo1p occupancy around the transcription start site and illustrated this with a heatmap (Fig 3.22). In each case, the ChIP-seq immunoprecipitated (IP) data I received for Hho1p and Hmo1p was quantified with the corresponding input control. The transcription start site was centered in the heat map with a ±1.5 kb window either side. The heat map showcases direct comparison between the IP and input profiles and displays where Hho1p and Hmo1p occupancy is enriched around the transcription start site in exponential phase cells. The Hho1p heatmap demonstrates that Hho1p has evenly disturbed peak profiles upstream and downstream of the TSS, while having a very low occupancy at the TSS (Fig 3.22). The Hmo1p heatmap demonstrates that Hmo1p has

a high occupancy profile upstream of the TSS, peaking at approximately 400 bp upstream of the TSS (Fig 3.22). This concludes that the two proteins differ in their occupancy profiles at genes relative to the TSS in exponential phase cells.

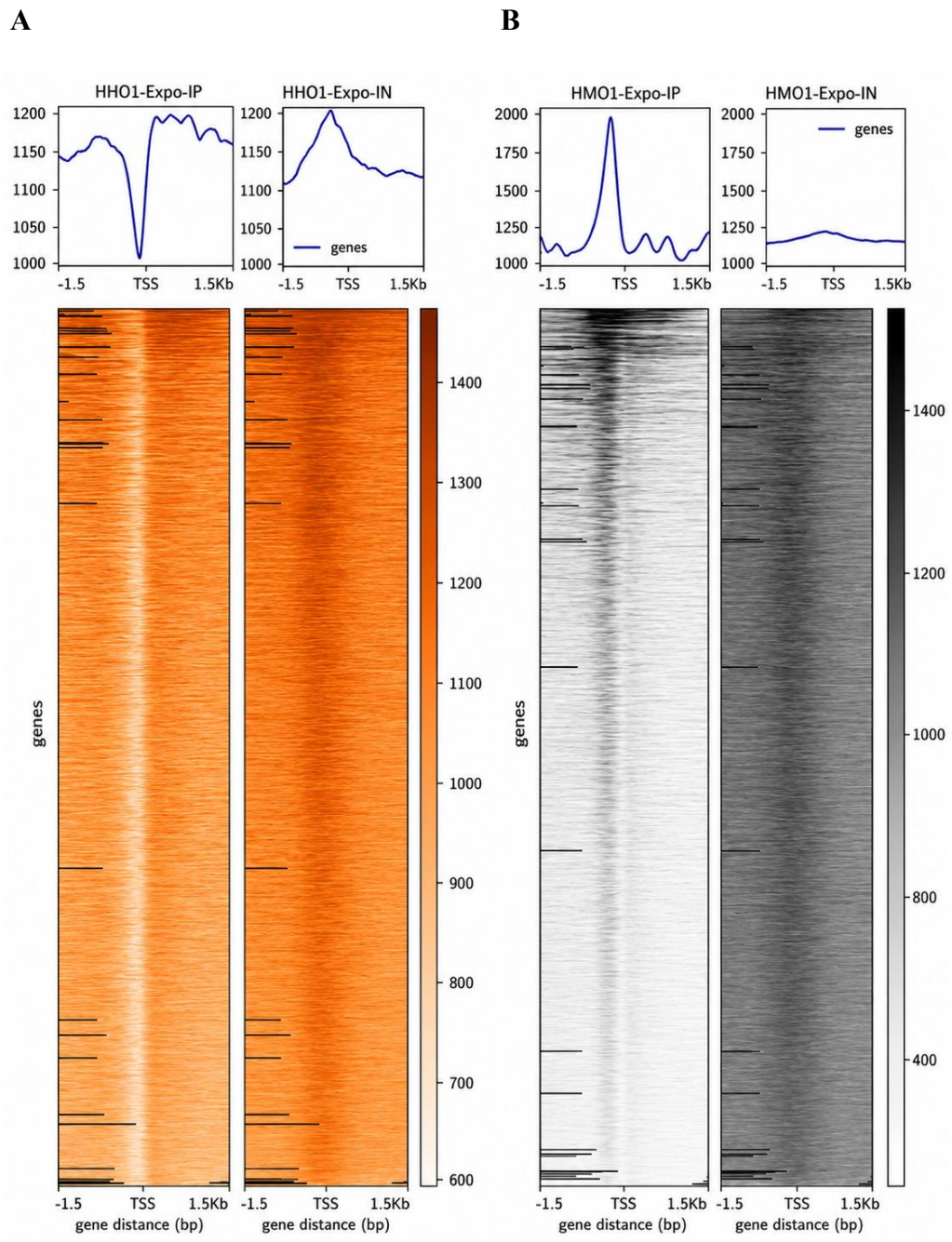

Figure 3.22: TSS-centered heatmap of Hho1p and Hmo1p during exponential phase, ChIP Signal (IP vs Input, ±1.5 kb). Heatmap illustrating Hho1p and Hmo1p occupancy around transcription start sites (TSS). ChIP-seq signal from Hho1p and Hmo1p immunoprecipitated (IP) samples and corresponding input controls was quantified within a ±1.5 kb window centered on the TSS of all annotated genes. Signal intensities were normalized and displayed on a common scale to allow direct comparison between IP and input profiles. Genes are ordered by overall Hho1p and Hmo1p enrichment across the region (highest to lowest), enabling visualization of genome-wide variation in Hmo1p and Hho1p binding patterns.

Next, I examined the number of Hho1p and Hmo1p sites located in promoters, exons, genic regions, intergenic regions, downstream regions, intron and distal regions (Fig 3.23). This data further highlights that Hho1p and Hmo1p show distinct localisation in exponential phase cells. Indeed, Hho1p was found predominantly at promoter regions (Fig 3.23), whilst Hmo1p was equally enriched at promoter and intergenic regions (Fig 3.23). Indeed, Hmo1p has approximately twice as many sites at promoter and intergenic regions compared to Hho1p.

Understanding where DNA-binding proteins are distributed across the genome is essential for determining their regulatory role.

A **Hho1p**

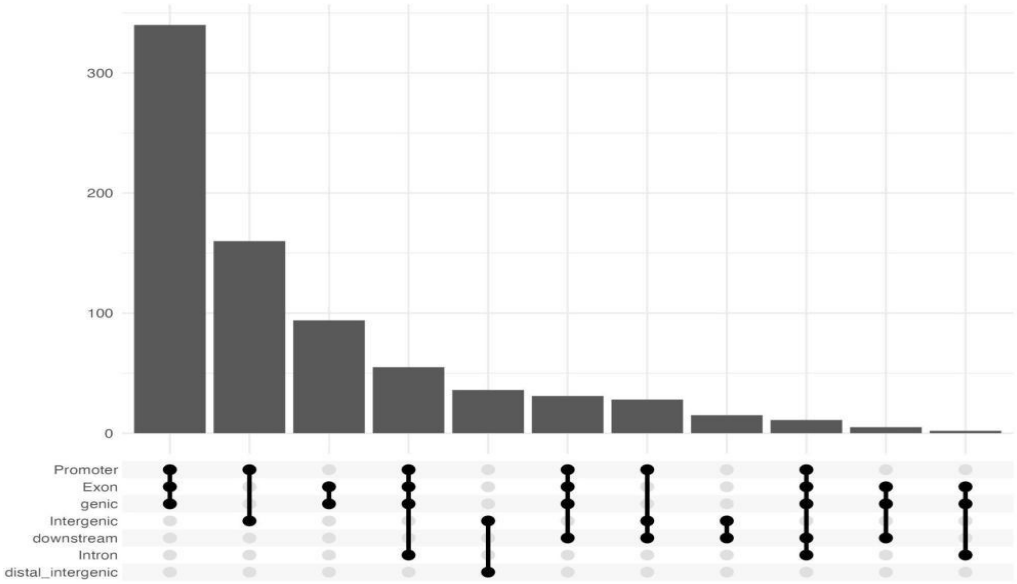

B **Hmo1p**

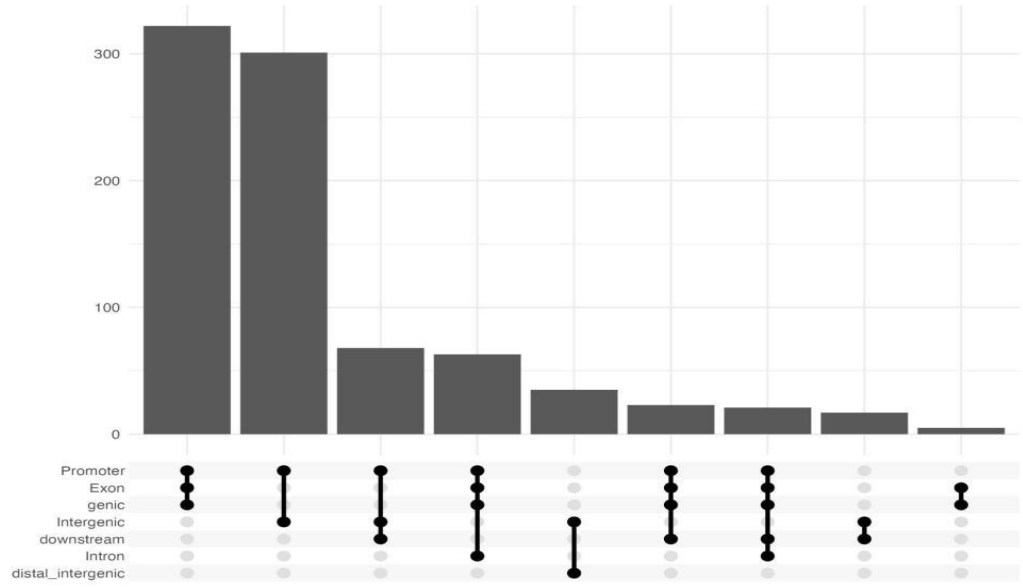

Figure 3.23: Genomic distribution of Hho1p and Hmo1p peaks in cells in exponential phase. A- Bar chart illustrating the distribution of Hho1p associated genes across genomic features. **B-** Bar chart illustrating the distribution of Hmo1p associated genes across genomic features. Bars indicate the proportion of genes or binding sites located in promoters, exons, genic regions, intergenic regions, downstream regions, intron and distal regions, highlighting the preferential localization of Hho1p and Hmo1p occupancy in exponential phase cells.

To further understand where Hho1p and Hmo1p reside in the genome, I performed a pie chart analysis to work out the percentage of Hho1p and Hmo1p occupancy in regions such as promoters, exons, downstream and distal intergenic regions (Fig 3.24). This analysis showcased that most of the sites for both proteins resided in the promoter regions of target genes in exponential phase cells.

A

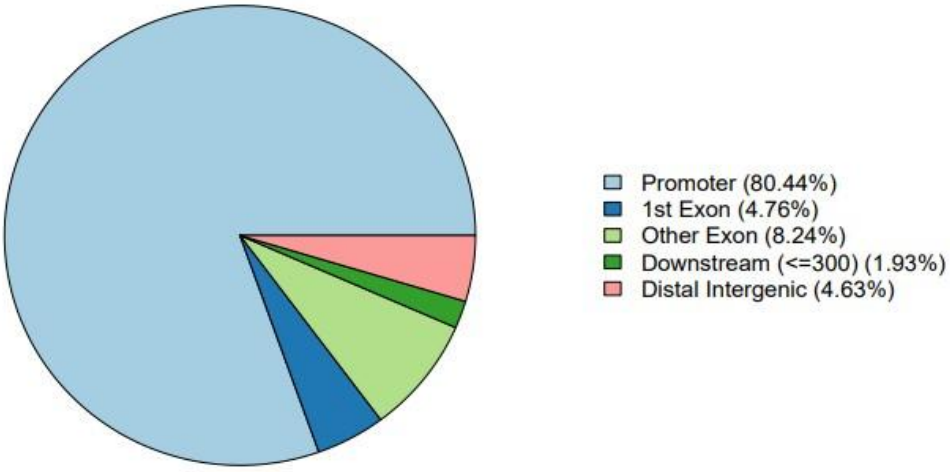

B

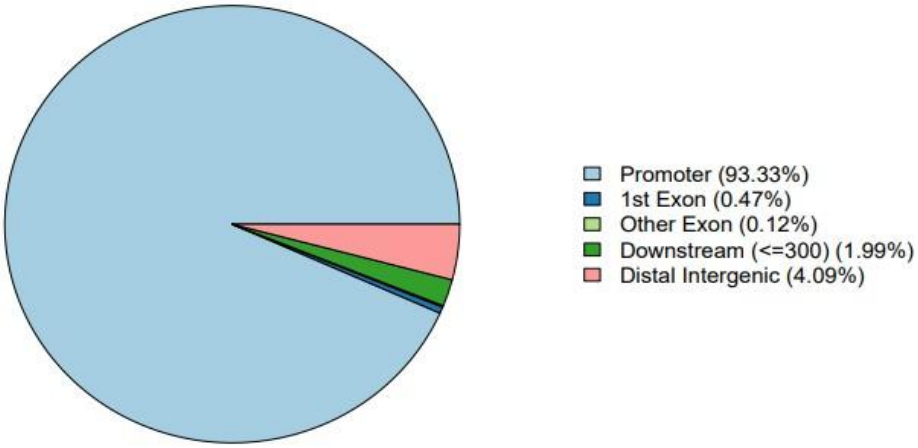

Figure 3.24: Percentage of Hho1p and Hmo1p occupancy across genomic regions in cells in exponential phase. A- Pie chart showing the proportion of Hho1p associated genes located in different genomic regions, including promoter, first exon, other exon, downstream region and distal intergenic region. **B-** Pie chart showing the proportion of Hmo1p associated genes located in different genomic regions, including promoter, first exon, other exon, downstream region and distal intergenic region. Each slice represents the percentage of genes in a specific category, highlighting the preferential localization of Hho1p or Hmo1p across the genome.

Finally, I analysed the overlap in occupancy between Hho1p and Hmo1p in exponential phase (Fig 3.25). This analysis revealed that there were 465 sites showing occupancy by both Hho1p and Hmo1p in exponential phase cells. This high overlap in the occupancy between Hho1p and Hmo1p suggests the two proteins act on similar genomic targets and thus potentially have similar regulatory roles. By comparing the overlap in occupancy in exponential phase cells shown here to a similar analysis of Hho1p and Hmo1p occupancy in diauxic cells and day 7 quiescent cells, it should offer insight into whether these proteins show co-operation or regulate more independently of each other as they make their way through the yeast life cycle.

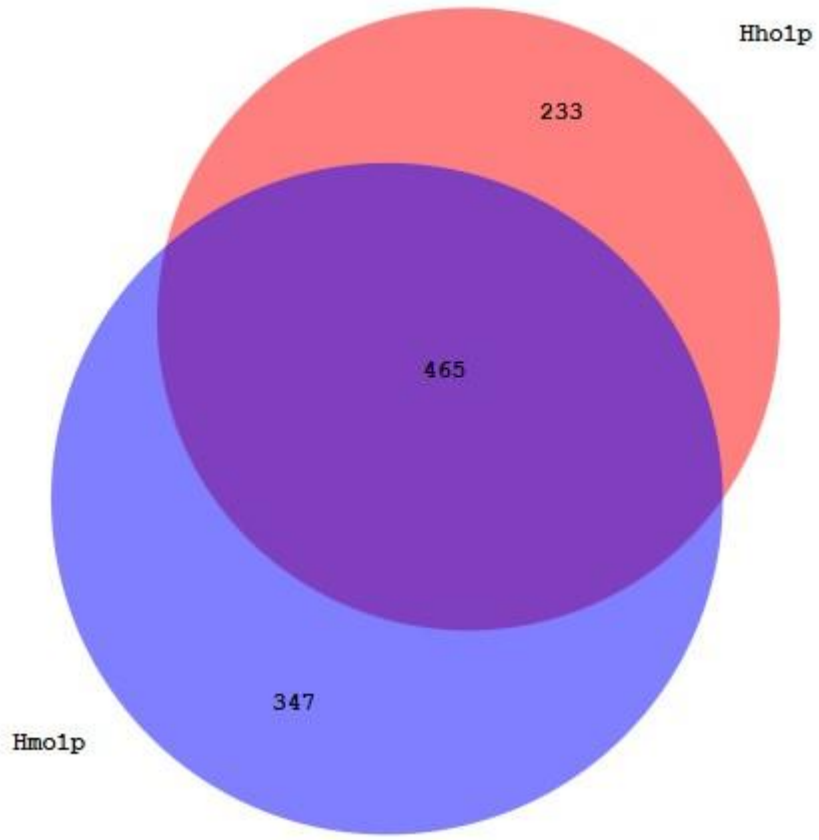

Figure 3.25: Overlap in gene occupancy between Hho1p and Hmo1p in exponential phase. Venn Diagram to show 465 genes shared between Hho1p and Hmo1p in exponential phase cells.

3.4.4 Analysis of Hho1p and Hmo1p occupancy in diauxic cells.

Using the ChIP-seq data I received from Dr Reham Hussain Al-Najjar (Al-Najjar, 2024), the occupancy of both Hho1p and Hmo1p in diauxic cells was analysed. The findings of Hho1p revealed a total of 897 binding sites compared to 459 binding sites for Hmo1p in diauxic cells (Table 3.3).

Further investigation into the occupancy sites of Hho1p showed that it was associated with 827 genes, whereas Hmo1p was linked to 422 genes, showing its lower overall occupancy. These gene numbers represent where each protein was found either associated on an ORF or was found within a region 1 kb up or downstream of that gene.

Peaks of Hho1p and Hmo1p occupancy and genes associated in diauxic cells

Protein	Total Peaks	Genes Associated
Hho1p	**897**	**827**
Hmo1p	**459**	**422**

Table 3.3: Peaks of Hho1p and Hmo1p occupancy and genes associated in diauxic cells. 1- First column is total number of occupancy sites (peaks), **2-** Genes mapped to ORF.

3.4.5 Analysis of Hho1p and Hmo1p occupancy at genes in diauxic cells.

I next analysed the sites of occupancy of Hho1p and Hmo1p at the genes that had been associated with Hho1p and Hmo1p in diauxic cells to determine if the proteins were found at the promoters, ORF or downstream regions of associated genes (Table 3.4).

Hho1p and Hmo1p were associated with genes predominantly at their promoter regions. Hho1p had a total of 736 sites mapped to the promoters of the 827 genes it had been associated with. In contrast, only 12 sites of Hho1p occupancy mapped to the distal region of its associated genes. Hho1p had a total of 79 sites mapped to the ORF region. Hmo1p had a total of 377 sites mapped to the promoters of the 422 genes it had been associated with. In contrast, only 6 sites of Hmo1p occupancy mapped to the distal region of its associated genes. Hmo1p had a total of 39 sites mapped to the ORF region. This

showed that the majority of Hho1p and Hmo1p were found at the promoter regions of target genes in diauxic cells compared to the distal and ORF regions.

Distribution of Hho1p and Hmo1p occupancy sites across promoter, ORF and distal regions of associated genes

Protein	Genes Associated	Promoter	ORF	Distal
Hho1p	**827**	**736**	**79**	**12**
Hmo1p	**422**	**377**	**39**	**6**

Table 3.4: Distribution of Hho1p and Hmo1p occupancy sites across promoter, ORF and distal regions of associated genes. 1- First column is total number of genes associated, **2-** Occupancy sites at promoter region, **3-** Occupancy sites at the ORF region, **4-** Occupancy sites at the distal region.

After analysing the sites of occupancy of Hho1p and Hmo1p at the genes that had been associated with Hho1p and Hmo1p to determine where either protein was found, I next analysed the Hho1p and Hmo1p occupancy around the transcription start site and illustrated this with a heatmap (Fig 3.26). In each case the ChIP-seq immunoprecipitated data I received for Hho1p and Hmo1p was quantified with the corresponding input control. The transcription start site was centered in the heat map with a ± 1.5 kb window either side. The heat map showcases direct comparison between the IP and the input profiles and displays where Hho1p and Hmo1p occupancy is enriched around the transcription start site in diauxic cells. The Hho1p heatmap demonstrates that Hho1p has a very high occupancy just after the TSS, approximately 300 bp downstream of the TSS. It also showcases that Hho1p has a very low occupancy at the TSS (Fig 3.26). The Hmo1p heatmap demonstrates that Hmo1p has a peak of occupancy 350 bp upstream of the TSS and a relatively evenly distributed peak profile downstream of the TSS (Fig 3.26).

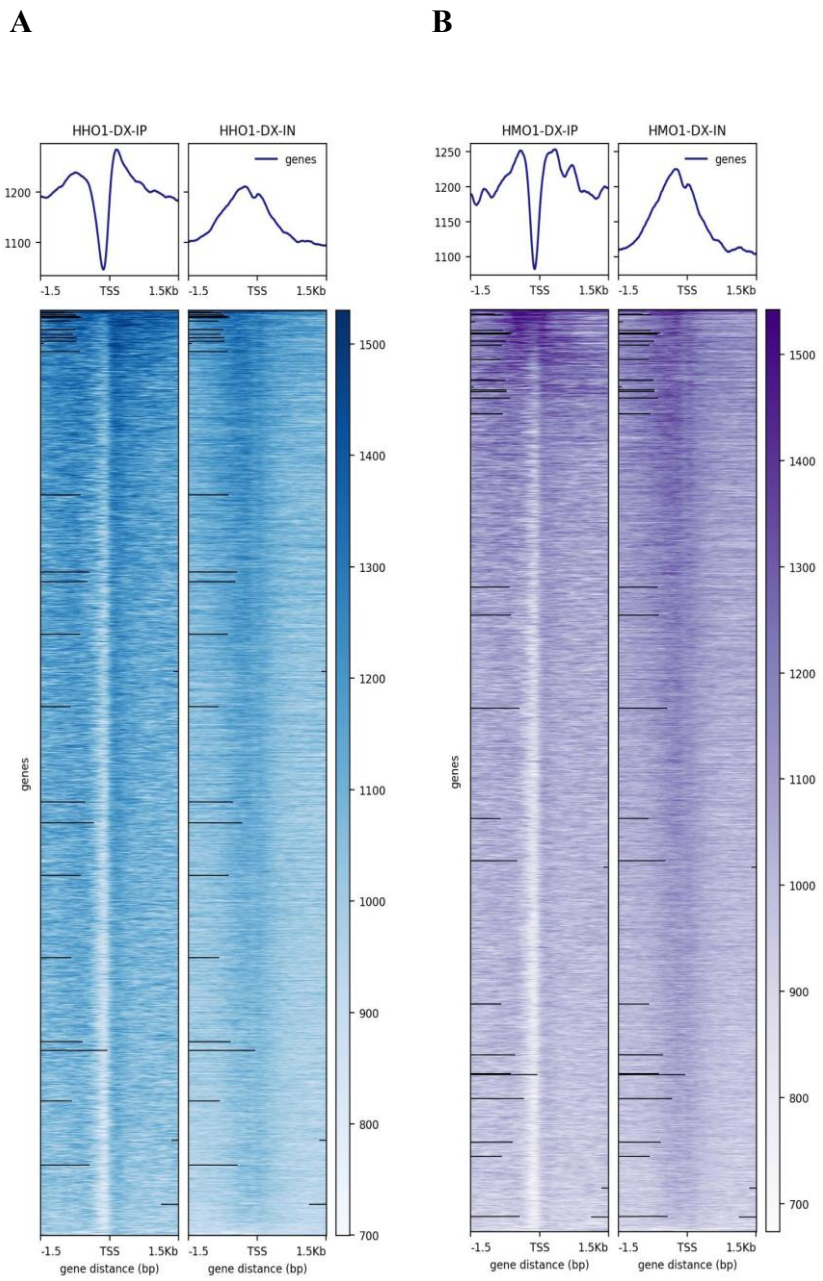

Figure 3.26: TSS-centered heatmap of Hmo1p and Hho1p in diauxic cells, ChIP Signal (IP vs Input, ±1.5 kb). Heatmap illustrating Hmo1p and Hho1p occupancy in diauxic cells around transcription start sites (TSS). ChIP-seq signal from Hmo1p and Hho1p immunoprecipitated (IP) samples and corresponding input controls was quantified within a ±1.5 kb window centered on the TSS of all annotated genes. Signal intensities were normalized and displayed on a common scale to allow direct comparison between IP and input profiles. Genes are ordered by overall Hmo1p and Hho1p enrichment across the region (highest to lowest), enabling visualization of genome-wide variation in Hmo1p and Hho1p binding patterns.

Next, I examined the number of Hho1p and Hmo1p sites located in promoters, exons, genic regions, intergenic regions, downstream regions, intron and distal regions (Fig 3.27). This data further highlighted that Hho1p and Hmo1p show distinct localisation in the promoter regions of target genes in diauxic cells. Visualisation of this occupancy data as a pie chart indicating the % of the sites of occupancy for Hho1p and Hmo1p in diauxic cells showed an almost identical binding profile for both proteins in diauxic cells (Fig 3.28).

A **Hho1p**

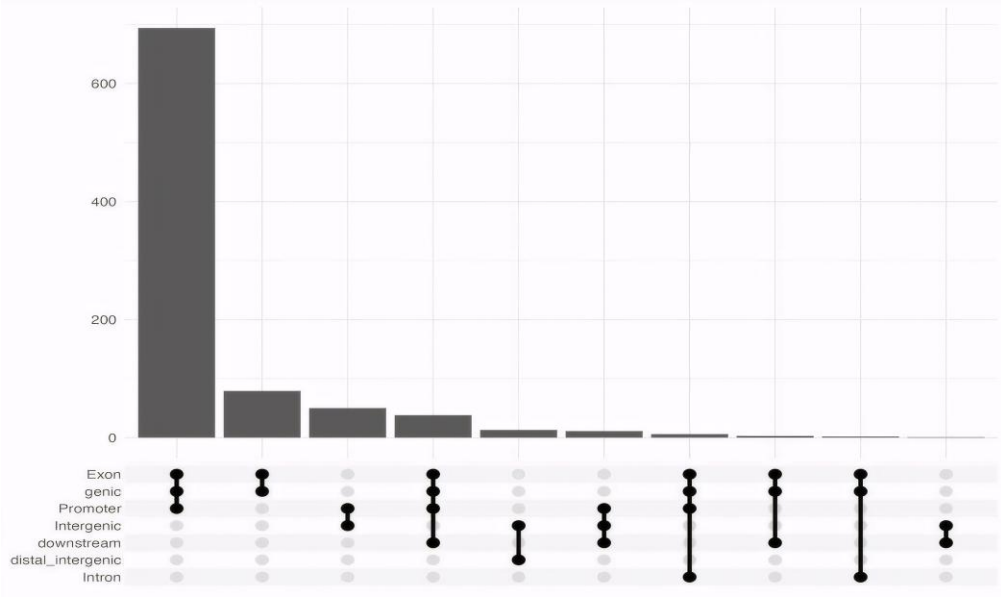

B **Hmo1p**

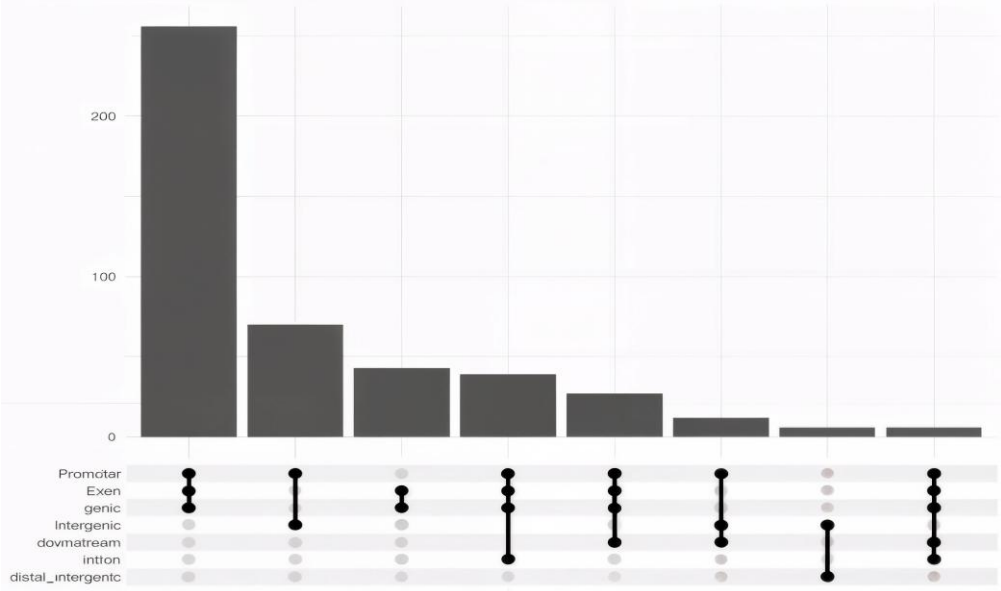

Figure 3.27: Genomic distribution of Hho1p and Hmo1p peaks in cells at diauxie. A- Bar chart illustrating the distribution of Hho1p associated genes across genomic features. **B-** Bar chart illustrating the distribution of Hmo1p associated genes across genomic features. Bars indicate the proportion of genes or binding sites located in promoters, exons, genic regions, intergenic regions, downstream regions, intron and distal regions, highlighting the preferential localization of Hho1p and Hmo1p occupancy in diauxic cells.

A

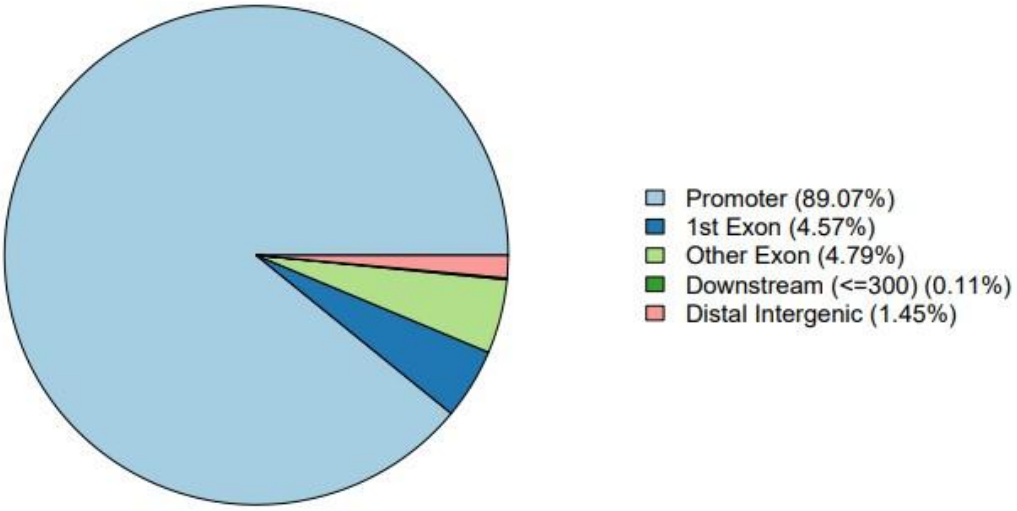

B

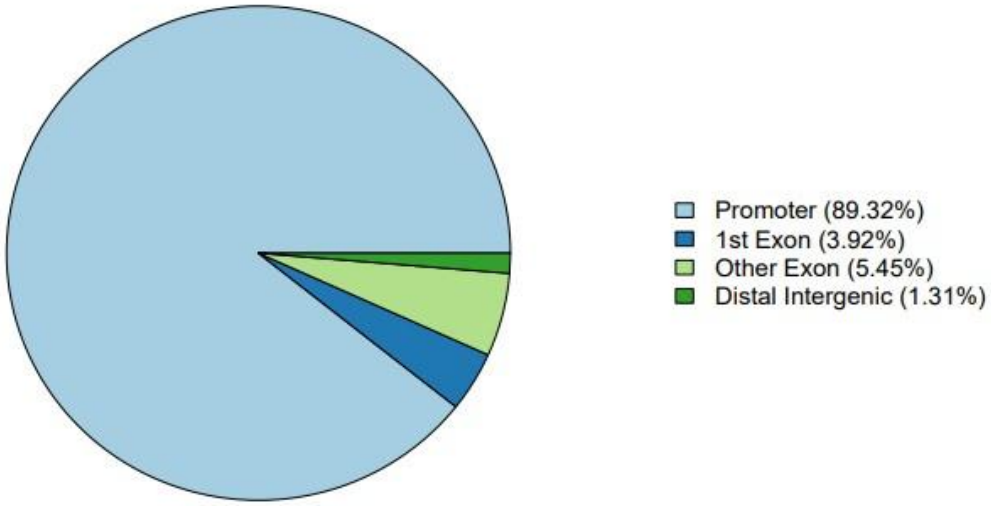

Figure 3.28: Percentage of Hho1p and Hmo1p occupancy across genomic regions in cells at diauxie. A- Pie chart showing the proportion of Hho1p associated genes located in different genomic regions, including promoter, first exon, other exon, downstream region and distal intergenic region. **B-** Pie chart showing the proportion of Hmo1p associated genes located in different genomic regions, including promoter, first exon, other exon, downstream region and distal intergenic region. Each slice represents the percentage of genes in a specific category, highlighting the preferential localization of Hho1p or Hmo1p across the genome.

Finally, I analysed the overlap in occupancy between Hho1p and Hmo1p in diauxic cells. Examining the overlap in the gene occupancy between Hho1p and Hmo1p provides insight into whether the proteins act on similar genomic targets or not. The Venn diagram in Figure 3.29 showed that the number of shared sites of occupancy was 248 in diauxic cells. This is a drop in shared sites of occupancy between Hho1p and Hmo1p compared to exponential cells which had 465 overlapping genes (Fig 3.29).

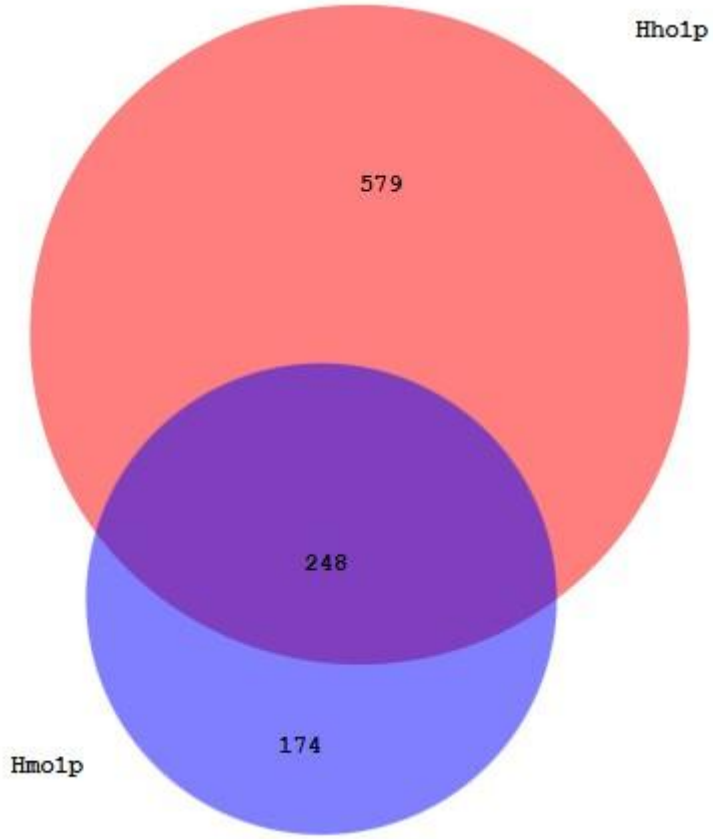

Figure 3.29: Overlap in gene occupancy between Hho1p and Hmo1p in diauxic cells. Venn Diagram to show 248 genes shared between Hho1p and Hmo1p in diauxic cells.

3.4.6 Analysis of Hho1p and Hmo1p occupancy in day 7 quiescent cells.

Using the ChIP-seq data I received from Dr Reham Hussain Al-Najjar (Al-Najjar, 2024), the occupancy of both Hho1p and Hmo1p in day 7 quiescent cells was analysed. The findings of Hho1p revealed 1397 binding sites compared to 659 binding sites for Hmo1p in day 7 quiescent cells (Table 3.5).

Further investigation into the occupancy sites of Hho1p showed it was associated with 1296 genes, whereas Hmo1p was linked to 647 genes, showing its lower overall occupancy. These gene numbers represent where each protein was found either associated on an ORF or was found within a region 1 kb up or downstream of that gene.

Peaks of Hho1p and Hmo1p occupancy and genes associated in day 7 quiescent cells

Protein	Peaks	Genes Associated
Hho1p	**1397**	**1296**
Hmo1p	**659**	**647**

Table 3.5: Peaks of Hho1p and Hmo1p occupancy and genes associated in day 7 quiescent cells. 1- First column is total number of occupancy sites (peaks), **2-** Genes mapped to an ORF.

3.4.7 Analysis of Hho1p and Hmo1p occupancy at genes in day 7 quiescent cells.

I next analysed the distribution of sites at genes that had been associated with Hho1p and Hmo1p in day 7 quiescent cells to determine if the proteins were found at the promoters, ORF, downstream regions of associated genes (Table 3.6).

Hho1p and Hmo1p were associated with genes predominately found at their promoter regions. Hho1p had a total of 1176 sites mapped to the promoters of the 1296 genes it had been associated with. In contrast, only 20 sites of Hho1p occupancy mapped to the distal region of its associated genes. Hho1p had a total of 100 sites mapped to the ORF. Hmo1p had a total of 630 sites mapped to the promoters of the 647 genes it had been associated with. In contrast, only 3 sites of Hmo1p occupancy mapped to the distal region of its associated genes. Hmo1p had a total of 14 sites mapped to the ORF. Comparing both Hho1p and Hmo1p distribution of sites it is evident that there is a larger distribution of sites mapped to the ORF of the genes associated with Hho1p compared to Hmo1p relative to their total number of genes associated.

Distribution of Hho1p and Hmo1p occupancy sites across promoter, ORF and distal regions of associated genes

Protein	Genes Associated	Promoter	ORF	Distal
Hho1p	**1296**	**1176**	**100**	**20**
Hmo1p	**647**	**630**	**14**	**3**

Table 3.6: Distribution of Hho1p and Hmo1p occupancy sites across promoter, ORF and distal regions of associated genes. 1- First column is total number of genes associated, **2-** Occupancy sites at promoter region, **3-** Occupancy sites at the ORF region, **4-** Occupancy sites at the distal region.

After analysing the sites of occupancy of Hho1p and Hmo1p at the genes that had been associated with Hho1p and Hmo1p to determine where either protein was found, I next analysed the Hho1p and Hmo1p occupancy around the transcription start site (TSS) and illustrated this with a heatmap (Fig 3.30). The heat map showcases direct comparison between the IP and input profiles and displays where Hho1p and Hmo1p occupancy is enriched around the TSS in day 7 quiescent cells. The Hho1p heatmap demonstrates that Hho1p has a peak of enrichment at approximately 300 bp downstream of the TSS and low enrichment at approximately 100 bp upstream of the TSS (Fig 3.30). The Hmo1p heatmap demonstrates that Hmo1p has a peak of enrichment approximately 375 bp upstream of the TSS (Fig 3.30). This showcases that the two proteins differ in their occupancy profiles relative to the TSS in day 7 quiescent cells.

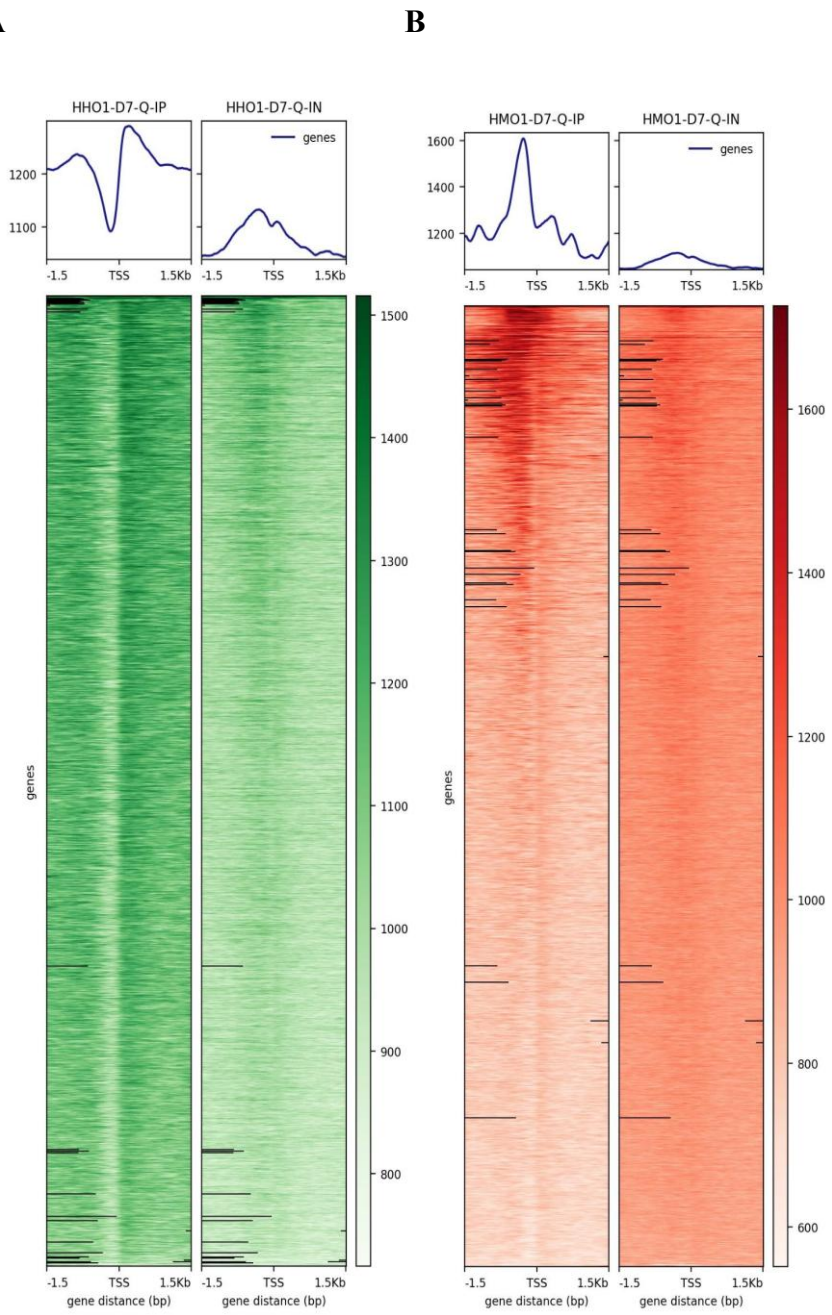

Figure 3.30: TSS-centered heatmap of Hho1p and Hmo1p in day 7 quiescent cells, ChIP Signal (IP vs Input, ±1.5 kb). Heatmap illustrating Hmo1p and Hho1p occupancy in Day 7 quiescent cells around transcription start sites (TSS). ChIP-seq signal from Hmo1p and Hho1p immunoprecipitated (IP) samples and corresponding input controls was quantified within a ±1.5 kb window centered on the TSS of all annotated genes. Signal intensities were normalized and displayed on a common scale to allow direct comparison between IP and input profiles. Genes are ordered by overall Hmo1p and Hho1p enrichment across the region (highest to lowest), enabling visualization of genome-wide variation in Hmo1p and Hho1p binding patterns.

Next, I further examined the number of Hho1p and Hmo1p sites located in promoters, exons, genic regions, intergenic regions, downstream regions, intron and distal regions (Fig 3.31). This data further highlights that Hho1p and Hmo1p show distinct localisation in day 7 quiescent cells. The vast majority of Hho1p was found at promoter and genic regions (Fig 3.31A), like Hho1p occupancy in diauxic cells. This region far outweighed all other regions. Most Hmo1p was found at promoter regions and also had a high association with intergenic regions (Fig 3.31B). This result is like what was seen when examining the genomic distribution of Hmo1p associated peaks in exponential phase cells.

A **Hho1p**

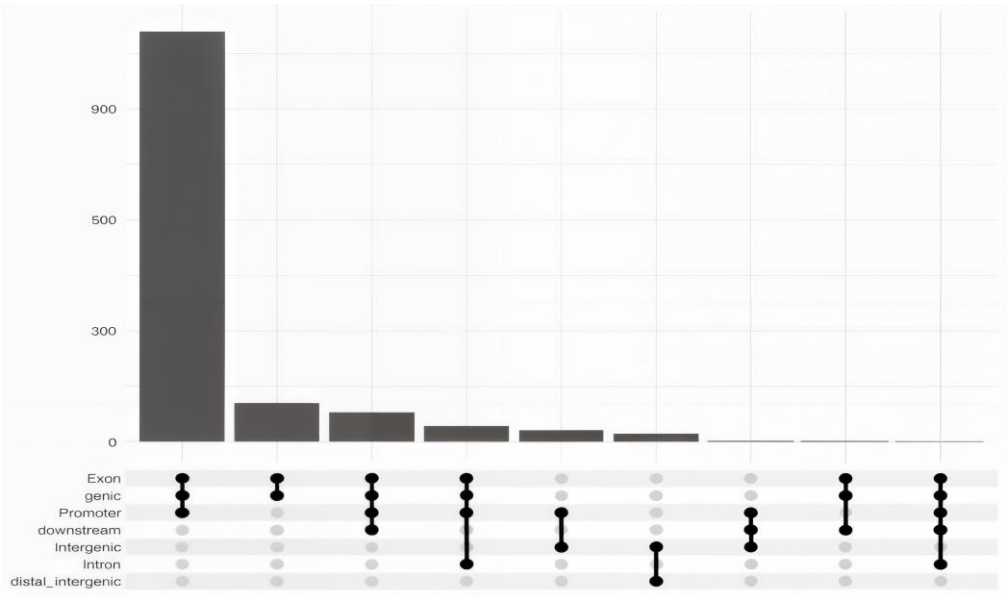

B **Hmo1p**

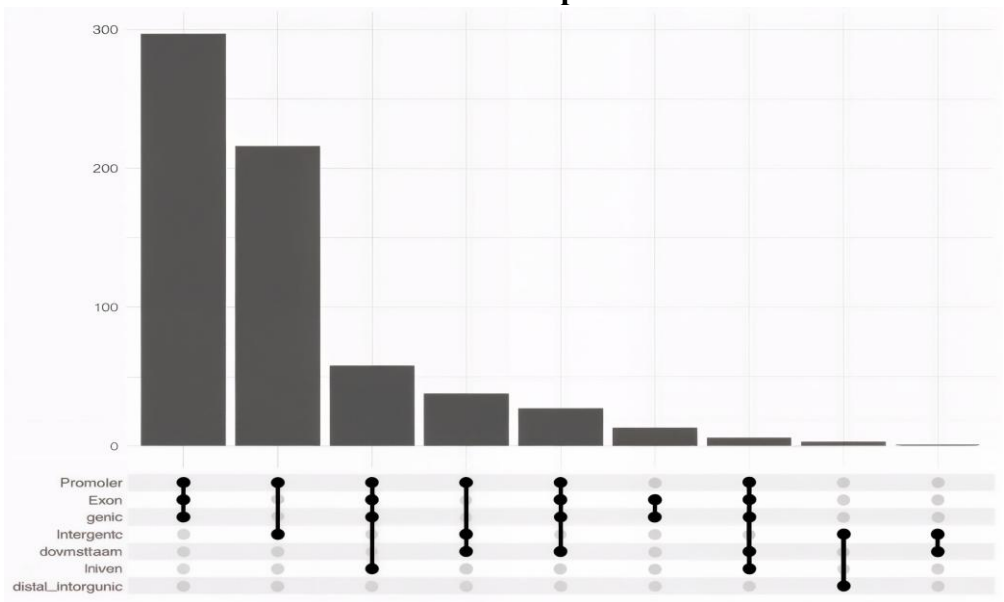

Figure 3.31: Genomic distribution of Hho1p and Hmo1p peaks in day 7 quiescent cells. A- Bar chart illustrating the distribution of Hho1p-associated genes across genomic features. **B-** Bar chart illustrating the distribution of Hmo1p-associated genes across genomic features. Bars indicate the proportion of genes or binding sites located in promoters, exons, genic regions, intergenic regions, downstream regions, intron and distal regions, highlighting the preferential localization of Hho1p and Hmo1p occupancy in day 7 quiescent cells.

Following on from (Fig 3.31), to further understand where Hho1p and Hmo1p reside in the genome, I performed a pie chart analysis to calculate the percentage of Hho1p and Hmo1p occupancy in regions such as promoters, exons, downstream and distal intergenic regions (Fig 3.32). This analysis showcased that most of the sites for both proteins resided in the promoter regions of target genes in day 7 quiescent cells, with Hho1p having a higher percentage of sites in the 1st exon region compared to Hmo1p.

A

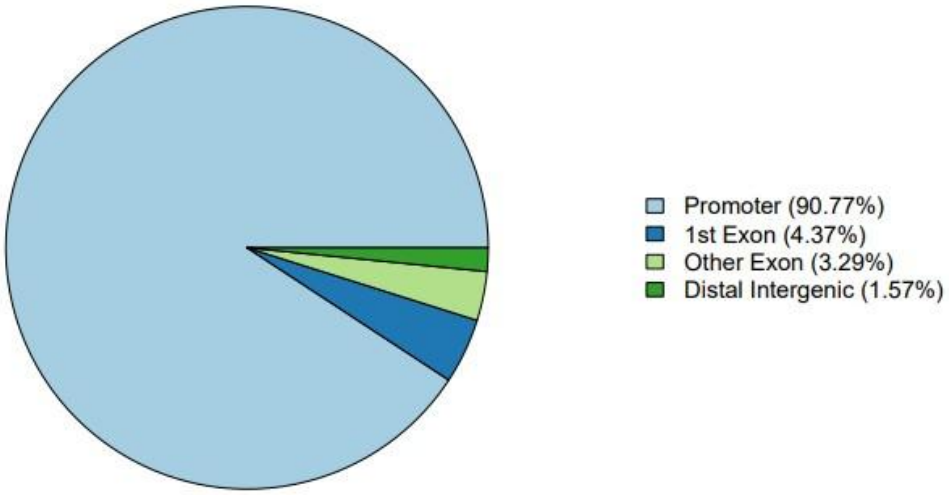

B

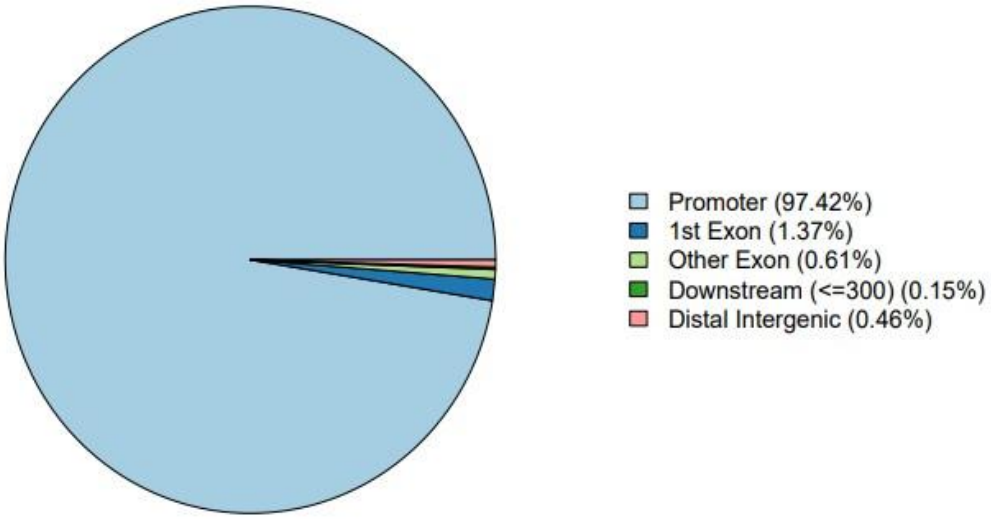

Figure 3.32: Percentage of Hho1p and Hmo1p occupancy across genomic regions in day 7 quiescent cells. A- Pie chart showing the proportion of Hho1p-associated genes located in different genomic regions, including promoter, first exon, other exon, downstream region and distal intergenic region. **B-** Pie chart showing the proportion of Hho1p-associated genes located in different genomic regions, including promoter, first exon, other exon, downstream region and distal intergenic region. Each slice represents the percentage of genes in a specific category, highlighting the preferential localization of Hho1p across the genome.

Finally, I analysed the overlap of occupancy between Hho1p and Hmo1p in day 7 quiescent cells. The Venn diagram in Figure 3.33 shows that there were 147 genes that shared occupancy with Hho1p and Hmo1p in day 7 quiescent cells (Fig 3.33). In exponential cells there was a total of 465 co-occupied genes. This dropped to 248 genes occupied by both Hho1p and Hmo1p in diauxic cells and only 147 genes shared in day 7 quiescent cells. This showcased that the number of genes co-occupied by both Hho1p and Hmo1p drop as the cells progresses from proliferation to quiescence.

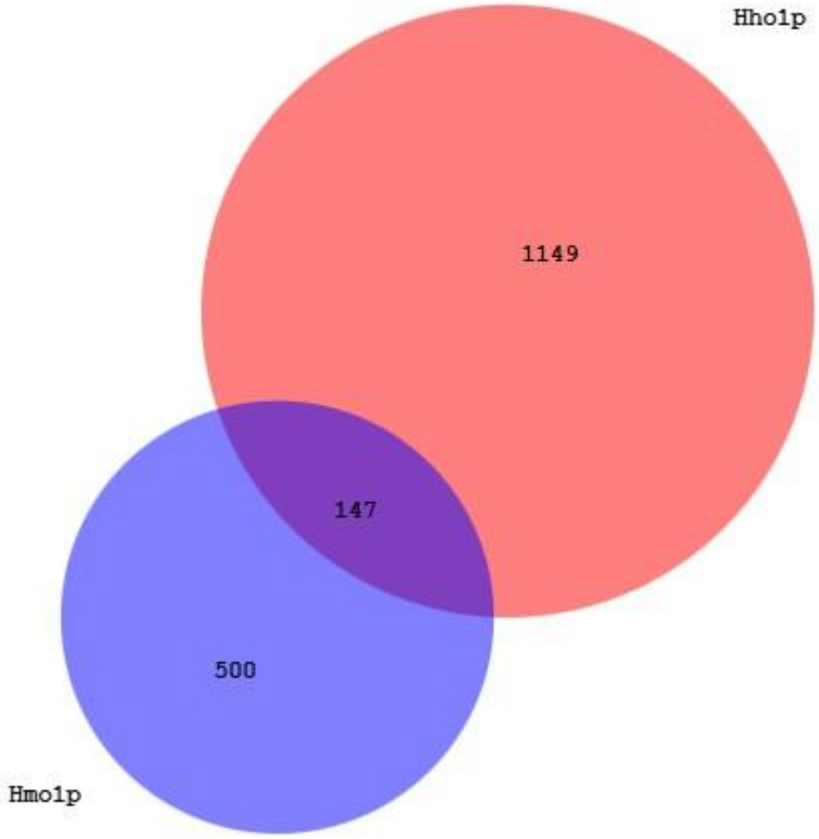

Figure 3.33: Overlap in gene occupancy between Hho1p and Hmo1p in day 7 quiescent cells. Venn Diagram to show 147 genes shared between Hho1p and Hmo1p in day 7 quiescent cells.

4. Discussion

4.1 Discussion

In the yeast *Saccharomyces cerevisiae*, the *HHO1* gene has been proposed to encode the yeast linker histone H1. Hmo1p, a high mobility group protein is suggested to have overlapping roles with Hho1p (Brush, 2015). The research in this thesis investigated the possible interplay between Hho1p and Hmo1p during stationary phase. This involved investigating the phenotypic, physiological and transcriptional features of a *hho1Δ* single gene deletion mutant, a *hmo1Δ* single gene deletion mutant and the *hho1Δ hmo1Δ* double mutant to determine more accurately whether Hho1p or Hmo1p can be considered the true linker histone H1 of yeast and determine any possible interactions between both Hho1p and Hmo1p in stationary phase.

4.2 Gene deletion confirmation

The deletions of *HHO1* and *HMO1* genes in their respective single gene deletion mutants were attained by means of homologous recombination with the coding regions substituted by the *KAN* gene, which provides resistance to kanamycin. Western blot analysis and PCR analysis confirmed the correct and successful deletions of these genes in their mutant strain (Byrant et al., 2012). The confirmation of these two single gene deletion mutants was a vital starting point in this research as the main focus of this research was to construct a double *hho1Δ hmo1Δ* mutant which could be used to investigate a possible interplay between both Hho1p and Hmo1p. The confirmation provided a validated genetic foundation and allowed the construction of the double mutant to begin. Verification of the single gene deletion mutant strains ensured that any observed phenotypic or molecular effects could be confidently attributed to the loss of the target gene.

Initial attempts to delete *HHO1* in the *hmo1Δ* mutant background failed. I hypothesized that the *HHO1* gene deletion attempt in the *hmo1Δ* mutant background was not confirmed potentially due to there being only a partial deletion of the *HHO1* gene. A partial deletion of the gene means that the intended replacement of the *HHO1* coding sequence did not fully remove the entire open reading frame (ORF). This may have occurred due to incomplete recombination, where only one homology arm recombined or recombination occurred internally, leaving part of the ORF intact. Alternatively, the *HHO1* gene was not able to be confirmed as deleted in the *hmo1Δ* mutant because of a tandem duplication or

extra copies of the *HHO1* gene being present in this strain background. If extra copies of the *HHO1* gene were present, deletion of one copy of the gene leaves other copies still expressing Hho1p which would explain how I was unable to confirm the deletion by western blot analysis.

As I was unable to construct the double *hho1Δ hmo1Δ* mutant using this method, I switched my approach to delete the *HMO1* gene in the *hho1Δ* mutant strain and confirmed the deletion by PCR analysis. The *HMO1* deletion cassette was constructed using the PRS406 vector carrying the URA selectable marker. The transformants from the transformation were screened by PCR to verify the correct integration at the *HMO1* gene. The PCR confirmation confirmed that the double *hho1Δ hmo1Δ* mutant had been successfully constructed. The double *hho1Δ hmo1Δ* mutant strain was constructed and genetically confirmed and showcased that the simultaneous deletion of both *HHO1* and *HMO1* is viable under the conditions tested. This revealed an important outcome of this research, that neither gene is individually or jointly essential for basic cellular survival. Constructing the double *hho1Δ hmo1Δ* mutant strain provided a vital tool for this research for investigating a possible interplay between Hho1p and Hmo1p during stationary phase in *Saccharomyces cerevisiae*. The potential genetic interaction between *HHO1* and *HMO1* was further examined following the double *hho1Δ hmo1Δ* mutant construction and carrying out phenotypic and characterisation assays on the mutant strain and comparing the results to the two single gene deletion mutants and wt.

4.3 Growth and viability during exponential growth phase analysis

During the exponential growth phase in glucose containing media, the *hmo1Δ* mutant and the *hho1Δ hmo1Δ* double mutant strain exhibited a slower growth in the exponential phase when measuring $OD_{600\,nm}$ readings compared to the wt. The *hho1Δ* mutant did not exhibit this growth defect and grow similar to the wt. In the doubling time experiment it was observed that the double *hho1Δ hmo1Δ* mutant strain had a statistically significantly slower doubling time compared to the wt, with a p value of less than (0.05). Neither of the single gene deletion mutants *hho1Δ* or *hmo1Δ* mutant showcased a significantly slower doubling time compared to wt. This result confirms what was shown in the growth curve experiment (Fig 3.8), that the double *hho1Δ hmo1Δ* mutant strain has a reduced growth rate compared to the wt strain. This would indicate that the double *hho1Δ hmo1Δ* mutant could also have a lower metabolic activity rate. This would suggest that the double *hho1Δ*

hmo1Δ mutant cells are metabolically less active or perhaps less efficient at using the available nutrient resources available to them to grow and replicate. These exponential growth phase results indicate that Hho1p and Hmo1p may act in co-operation with each other during the exponential phase as the two single mutant strains did not have any doubling time defects but there is clear evidence of a doubling defect in the double *hho1Δ hmo1Δ* mutant. Hmo1p may play a more important role than Hho1p in the doubling time of *Saccharomyces cerevisiae,* as it is clear from the growth curve data (Fig 3.8) that the *hmo1Δ* mutant strain did not reach similar $OD_{600\,nm}$ levels compared to wt and the *hho1Δ* mutant strain.

These findings were further supported by significantly different reduced cell density in all three mutant strains compared to wt after 24 hours of growth. The double *hho1Δ hmo1Δ* mutant and the *hmo1Δ* mutant strain had extremely significantly reduced cell density after 24 hours of growth compared to the wt. The *hho1Δ* mutant strain also had significantly reduced cell density after 24 hours compared to the wt but not as severe as both the double *hho1Δ hmo1Δ* mutant and the *hmo1Δ* mutant strain. This further supports that Hmo1p plays an important role in exponential phase growth, and while Hho1p may not be essential for exponential phase growth, it plays an important role in supporting high density growth.

It was also found that none of the mutant strains lost viability at 24 hours into the growth phase compared to wt. This showed that neither Hho1p nor Hmo1p plays a significant role in maintaining cellular viability in the exponential phase of growth. The differences in growth characteristics noted between the *hho1Δ* mutant, the *hmo1Δ* mutant and the double *hho1Δ hmo1Δ* mutant during the exponential phase signifies the roles played by both Hho1p and Hmo1p and also showcases the co-operation between the two proteins, as the double *hho1Δ hmo1Δ* mutant showed the greatest growth defects of all mutants compared to the wt in the exponential phase. The slower growth and significantly reduced cell density in the *hmo1Δ* mutant suggests that the Hmo1p protein plays a very important role in cellular metabolism and proliferation. These growth defects carry over into the double *hho1Δ hmo1Δ* mutant also.

4.4 Stationary growth phase

In the stationary phase the three mutant strains did not show any viability defects, likewise to what was seen after 24 hours of growth viability test. The *hho1Δ* mutant, the *hmo1Δ* mutant and the double *hho1Δ hmo1Δ* mutant displayed no significant viability defect when compared to the wt. The stationary phase is a period of nutrient constraint and cellular quiescence where cells undergo metabolic remodelling to survive sustained periods of nutrient deprivation. This suggests that Hho1p and Hmo1p may not be vital for cell survival in the stationary phase. It also suggests that both Hho1p and Hmo1p are not crucial for metabolic shifts needed in the stationary phase for survival.

4.5 Cell morphology in exponential and stationary phase

Microscopic analysis of the *hho1Δ* mutant, the *hmo1Δ* mutant and the double *hho1Δ hmo1Δ* mutant strain compared to the wt strain yielded some very intriguing results. The *hmo1Δ* mutant and the double *hho1Δ hmo1Δ* mutant displayed an elongated cell morphology during the exponential phase. This phenotype was not seen in the *hho1Δ* mutant or wt strain. This result reveals that Hmo1p is vital in maintaining typical cellular shape throughout the active cell division in the exponential phase. This is showcased by the *hmo1Δ* mutant and the double *hho1Δ hmo1Δ* mutant having an atypical cell shape in the exponential phase, compared to the wt. This abnormal cell phenotype was less apparent in *hmo1Δ* mutant in the stationary phase but still visible. The double *hho1Δ hmo1Δ* mutant did not have an elongated cell shape in the stationary phase. The *hmo1Δ* mutant in the stationary phase also appeared to have larger cells compared to the wt. The absence of any morphological changes in the *hho1Δ* mutant cell morphology in both exponential and stationary phase suggests that the role of Hho1p is not linked to directly impacting cell shape in exponential or stationary phase. Several cellular functions are closely linked to cellular morphology such as cell differentiation and cell response to external stimuli. The elongated cell shape caused by the deletion of the *HMO1* gene might suggest a defect in cell cycle regulation or cell wall synthesis. The absence of Hmo1p may lead to the mis-regulation of the genes involved in these vital processes, which therefore leads to the abnormal, elongated cell morphology in the *hmo1Δ* mutant and the double *hho1Δ hmo1Δ* mutant.

4.6 Stress responses

The *hho1Δ* mutant, the *hmo1Δ* mutant and the double *hho1Δ hmo1Δ* mutant were exposed to different external stresses. These stresses included low and high temperatures varying from 15 °C to 42 °C and different concentrations of caffeine. The mutant strains were exposed to these external stressors in both the exponential and stationary phase. The different levels of stress highlight the different roles that Hho1p and Hmo1p play in mechanisms of stress response and resistance. In the exponential phase, none of the mutant strains showed any sensitivity to the temperature stresses compared to the wt. Conversely, in the stationary phase, sensitivity and resistance was shown compared to the wt. The *hmo1Δ* mutant revealed a slight sensitivity in the plate incubated at 20 °C, compared to the wt strain. The double *hho1Δ hmo1Δ* mutant strain showed resistance compared to the wt in the plates incubated at 37 °C and 42 °C. This variety in responses to different temperature stresses suggest different roles that Hho1p and Hmo1p play in temperature stress response mechanisms. This result indicates that Hmo1p contributes to mechanisms that play a defensive role during low temperature stress in the stationary phase. Also, more intriguingly it showcases that the double *hho1Δ hmo1Δ* mutant displays resistance to high temperatures in the stationary phase compared to the wt and that the deletion of both genes resulted in a more resistant strain under high temperature stress. It also points to Hmo1p playing a more important role in temperature stress response in the stationary phase compared to exponential phase.

These results suggest that there is a possible interplay between Hho1p and Hmo1p during stationary phase, as when both *HHO1* and *HMO1* were deleted from the double mutant it showcased a more superior resistance to the higher temperature stresses in stationary phase. It suggests that Hho1p and Hmo1p may be interacting together to inhibit resistance to higher temperature stresses in the stationary phase. Following on from the temperature stress response tests, the mutant strains were tested for their sensitivity and resistance to different concentrations of caffeine. Caffeine has pleiotropic effects on yeast, but it primarily assesses yeast resistance to cell wall stress via the Mpk1p-mediated cell wall integrity pathway (Levin, 2005). There was no major sensitivity or resistance noted in any of the caffeine concentrations for the *hho1Δ, hmo1Δ* and double *hho1Δ hmo1Δ* mutant compared to wt in exponential and stationary phase. There was slight evidence of some sensitivity to the 10 mM caffeine concentration plate in the double *hho1Δ hmo1Δ* mutant in stationary phase compared to wt. This suggests a potential interaction between Hho1p

and Hmo1p during the stationary phase that contributes to a defensive role against cell wall stresses. The enhanced sensitivity of the double mutant relative to wt and the two single gene deletion mutants supports the hypothesis of potential interaction between *HHO1* and *HMO1*. This also suggests that Hho1p and Hmo1p may have cooperative roles during the stationary phase which are critical for stress adaptation and survival.

4.7 Quiescent cell development

The results showed that the Percoll density gradient was able to separate quiescent and non-quiescent cells from a stationary phase population. Separation was carried out successfully in both the wt and the double *hho1Δ hmo1Δ* mutant during day 7 of the stationary phase. Separation of both strains yielded some important results for this thesis. The strains were fractionated into two separate populations, quiescent and non-quiescent cell populations. The percentage of total cells that were quiescent and non-quiescent showcased a large variance between the double *hho1Δ hmo1Δ* mutant and wt. The double *hho1Δ hmo1Δ* mutant had 33% quiescent cells of its total cells, compared to that of 74% for the wt strain. This revealed a large difference in the amount of quiescent and non-quiescent cells in the two populations. This indicates that quiescent cell formation was decreased in the double *hho1Δ hmo1Δ* mutant. The reduction in quiescent cell formation observed in the double mutant supports a functional interplay between Hho1p and Hmo1p in regulating quiescence. The double *hho1Δ hmo1Δ* mutant shows aberrant quiescent development during the stationary phase.

Further experiments will need to be performed to examine the viability of the quiescent and non-quiescent cells in the double *hho1Δ hmo1Δ* mutant to understand more the potential interaction between both Hho1p and Hmo1p in regulating quiescence. To understand the role each protein is playing in the quiescent and non-quiescent populations, both single gene deletion mutants *hho1Δ* and *hmo1Δ* should also be tested for viability in the quiescent and non-quiescent populations alongside the double mutant to get a deeper understanding of the role. Further characterization of the fractionated upper and lower cell populations will also be needed to confirm if they are in fact quiescent and non-quiescent cells and not mixed together.

4.8 Preparation and quality assessment of RNA

To further investigate the molecular basis underlying the observed phenotypic differences between the double *hho1Δ hmo1Δ* mutant and wt, high quality RNA was isolated from exponential and purified day 7 quiescent double *hho1Δ hmo1Δ* mutant cells. The RNA was submitted for RNA sequencing, but sequencing results were not received prior to thesis submission. RNA integrity assessment using the Agilent Bioanalyzer and confirmed that the sample met the quality requirement for sequencing analysis. Although the sequencing data was not available within the timeframe of this thesis, the preparation of these samples represents a vital step towards defining the transcriptional changes in the double *hho1Δ hmo1Δ* mutant, which may reveal an interplay between Hho1p and Hmo1p during the stationary phase in *Saccharomyces cerevisiae*.

This RNA sequencing data alongside the phenotypic analysis of the double mutant will be vital for identifying regulatory processes affected in the double *hho1Δ hmo1Δ* mutant. This could give important insights into the processes involved in quiescent cell development and stationary phase adaptation. The double mutant RNA sequencing data will be analysed in the future combined with the existing RNA sequencing data from wt and the two single mutants to identify genes regulated by both Hho1p and Hmo1p.

4.9 Occupancy of Hho1p and Hmo1p in *Saccharomyces cerevisiae*

This thesis also examined ChIP-seq data to analyse the occupancy of chromatin associated proteins Hho1p and Hmo1p across different stages of the growth cycle of *Saccharomyces cerevisiae*. The overlapping of their gene occupancy was of great interest to investigate a possible interplay between Hho1p and Hmo1p during the stationary phase. Their dynamic binding patterns play a vital role in chromatin remodelling and gene regulation. Hho1p exhibits 777 peaks in the exponential phase but sees an increase to 897 peaks in diauxic cells and a large increase to 1397 peaks in day 7 quiescent cells. This highlights its important role in chromatin organization. Hmo1p displays 855 peaks in the exponential phase, a decrease in peaks in diauxic cells to 459 peaks but then increase in day 7 quiescent cells to have 659 peaks. This indicates the adaptability to metabolic conditions of Hmo1p. It is also found that there were 698 genes associated with Hho1p in the exponential phase, this increases

to 827 genes associated in diauxic cells and increases again in day 7 quiescent cells to 1296 genes associated with Hho1p. Conversely, Hmo1p had 812 genes associated in the exponential phase, 422 genes associated in diauxic cells and 647 cells in day 7 quiescent cells.

This thesis was based on investigating a possible interplay between Hho1p and Hmo1p during stationary phase so investigating the genes that overlapped with both proteins could suggest interactions between both proteins. In the exponential phase, there was 465 genes overlapping with both proteins. This lowered to 248 genes overlapping in diauxic cells and then further lowered to 147 genes in day 7 quiescent cells. This shared occupancy is consistent with a coordinated role in chromatin organisation under stationary phase conditions. This shared occupancy also indicates a potential transcription associated regulation between Hho1p and Hmo1p. The observed co-occupancy provides a mechanistic framework for future transcriptomic analysis. Since there is more gene overlapping between Hho1p and Hmo1p in the exponential phase compared to the day 7 quiescent cells, this suggests that the functional relationship between the two proteins may also be important during active proliferation. The reduced overlap in day 7 quiescent cells may be due to a redistribution of Hho1p and Hmo1p across the genome as cells transition into a low transcriptional state.

The ChIP-seq analysis also indicated that the majority of the genes associated with Hho1p and Hmo1p were located at promoter regions. This widespread promoter enrichment throughout different stages of the yeast growth cycle suggests that both Hho1p and Hmo1p are broadly associated with transcriptional regulatory regions across the genome and not restricted to gene bodies. The preferential localisation of Hho1p and Hmo1p at promoters is consistent with a role in regulating transcription-associated chromatin. Promoter occupancy enrichment would also support the interpretation of both Hho1p and Hmo1p contribute to chromatin organisation or transcriptional competence at promoter regions.

4.10 Conclusion

In conclusion, this research improves our knowledge of the functional interplay between Hho1p and Hmo1p during the exponential and stationary phase of

Saccharomyces cerevisiae. This study set out to investigate a possible interplay between Hho1p and Hmo1p during the stationary phase in *Saccharomyces cerevisiae.* Evidence of different phenotypic effects was observed across growth phases, suggesting that the functional co-operative relationship between Hho1p and Hmo1p is influenced by cellular physiological state. Although this research does not establish a direct biochemical relationship between Hho1p and Hmo1p, the data suggests that there are interactions between both proteins in both the exponential and stationary phase. Amongst the strains tested, the double *hho1Δ hmo1Δ* mutant had a significantly slower doubling time, significantly lower 24-hour cell density and produced less than half the percentage of quiescent cells in day 7 stationary phase compared to wt. Additionally, the data also suggests that Hmo1p is the more likely candidate as yeast linker H1.

Future research on this work should include analysing the double mutant RNA sequencing data and comparing it to the existing RNA sequencing data from wt and the two single mutants to identify genes regulated by both Hho1p and Hmo1p. Additionally, further experiments will need to be performed to examine the viability of the quiescent and non-quiescent cells in the double *hho1Δ hmo1Δ* mutant to understand more the potential interaction between both Hho1p and Hmo1p in regulating quiescence. Furthermore, to understand the role of each protein is playing in quiescent and non-quiescent cell populations, both single gene deletion mutants *hho1Δ* and *hmo1Δ* should also be tested for viability in the quiescent and non-quiescent populations alongside the double mutant to get a deeper understanding of the role. Further characterization of the fractionated upper and lower cell populations will also be needed to confirm if they are in fact quiescent and non-quiescent cells and not mixed together. In summary, this research provides evidence that suggests there is a possible functional interplay between Hho1p and Hmo1p during the exponential and stationary phase in *Saccharomyces cerevisiae.*

References

Allan, J., P. Hartman, C. Crane-Robinson and F. Aviles (1980). The structure of histone H1 and its location in chromatin. Nature 288: 675-679.

Al-Najjar, R., 2024. Investigating a role for linker histone H1 in quiescent cells of Saccharomyces cerevisiae. (Doctoral dissertation, Trinity College Dublin. School of Genetics and Microbiology).

Allen, C., S. Büttner, A. D. Aragon, J. A. Thomas, O. Meirelles, J. E. Jaetao, D. Benn, S. W. Ruby, M. Veenhuis and F. Madeo (2006). Isolation of quiescent and nonquiescent cells from yeast stationary-phase cultures. The Journal of cell biology 174: 89-100.

Amigo, R., C. Farkas, C. Gidi, M. I. Hepp, N. Cartes, E. Tarifeño, J. L. Workman and J. L. Gutiérrez (2022). The linker histone Hho1 modulates the activity of ATP-dependent chromatin remodeling complexes. Biochimica et Biophysica Acta (BBA)-Gene Regulatory Mechanisms 1865: 194781.

An, W., K. van Holde and J. Zlatanova (1998). The non-histone chromatin protein HMG1 protects linker DNA on the side opposite to that protected by linker histones. Journal of Biological Chemistry 273: 26289-26291.

Baker Brachmann, C., A. Davies, G. J. Cost, E. Caputo, J. Li, P. Hieter and J. D. Boeke (1998). Designer deletion strains derived from Saccharomyces cerevisiae S288C: a useful set of strains and plasmids for PCR-mediated gene disruption and other applications. Yeast 14: 115-132.

Baker, M. (2011) Making sense of chromatin states. Nat Methods 8: 717-722

Bauerle, K. T., E. Kamau and A. Grove (2006). Interactions between N-and C-terminal domains of the Saccharomyces cerevisiae high-mobility group protein HMO1 are required for DNA bending. Biochemistry 45: 3635-3645.

Baxevanis, A. D. and D. Landsman (1998). Histone Sequence Database: new histone fold family members. Nucleic acids research 26: 372-375.

Bednar, J., A. Hamiche and S. Dimitrov (2016). H1–nucleosome interactions and their functional implications. Biochimica et Biophysica Acta (BBA)-Gene Regulatory Mechanisms 1859: 436-443.

Bermejo, R., T. Capra, V. Gonzalez-Huici, D. Fachinetti, A. Cocito, G. Natoli, Y. Katou, H. Mori, K. Kurokawa and K. Shirahige (2009). Genome-organizing factors Top2 and Hmo1 prevent chromosome fragility at sites of S phase transcription. Cell 138: 870-884.

Brush, G. S. (2015). Evidence that histone H1 is dispensable for proper meiotic recombination in budding yeast. BMC research notes 8: 275.

Bryant, J. M., J. Govin, L. Zhang, G. Donahue, B. F. Pugh and S. L. Berger (2012). The linker histone plays a dual role during gametogenesis in Saccharomyces cerevisiae. Molecular and cellular biology 32: 2771-2783.

Choder, M. (1991). A general topoisomerase I-dependent transcriptional repression in the stationary phase in yeast. Genes & development 5: 2315-2326.

Collart, M. A. and S. Oliviero (1993). Preparation of yeast RNA. Current protocols in molecular biology 23: 13-12.

Davidson, G. S., R. M. Joe, S. Roy, O. Meirelles, C. P. Allen, M. R. Wilson, P. H. Tapia, E. E. Manzanilla, A. E. Dodson and S. Chakraborty (2011). The proteomics of quiescent and nonquiescent cell differentiation in yeast stationary-phase cultures. Molecular biology of the cell 22: 988-998.

De Virgilio, C. (2012). The essence of yeast quiescence. FEMS microbiology reviews 36: 306-339.

Gadal, O., S. Labarre, C. Boschiero and P. Thuriaux (2002). Hmo1, an HMG-box protein, belongs to the yeast ribosomal DNA transcription system. The EMBO journal: 5498-5507.

Gallagher, S., S. E. Winston, S. A. Fuller and J. G. Hurrell (2011). Immunoblotting and immunodetection. Current protocols in cell biology 52: 6-2.

Ghaemmaghami, S., W.-K. Huh, K. Bower, R. W. Howson, A. Belle, N. Dephoure, E. K. O'Shea and J. S. Weissman (2003). Global analysis of protein expression in yeast. Nature 425: 737-741.

Gietz, R. D. and R. H. Schiestl (2007). Quick and easy yeast transformation using the LiAc/SS carrier DNA/PEG method. Nature protocols 2: 35-37.

Grunstein, M. and S. M. Gasser (2013). Epigenetics in Saccharomyces cerevisiae. Cold Spring Harbor perspectives in biology 5: a017491.

Herman, P. K. (2002). Stationary phase in yeast. Current opinion in microbiology 5: 602-607.

Kamau, E., K. T. Bauerle and A. Grove (2004). The Saccharomyces cerevisiae high mobility group box protein HMO1 contains two functional DNA binding domains. Journal of Biological Chemistry 279: 55234-55240.

KASINSKY, H. E., J. D. LEWIS, J. B. DACKS and J. USLÓ (2001). Origin of H1 linker histones. The FASEB journal 15: 34-42.

Landsman, D. (1996). Histone H1 in Saccharomyces cerevisiae: a double mystery solved? Trends in biochemical sciences 21: 287-288.

Laporte, D., L. Jimenez, L. Gouleme and I. Sagot (2018). Yeast quiescence exit swiftness is influenced by cell volume and chronological age. Microbial Cell 5: 104.

Lee, K.-B. and J. O. Thomas (2000). The effect of the acidic tail on the DNA-binding properties of the HMG1, 2 class of proteins: insights from tail switching and tail removal. Journal of molecular biology 304: 135-149.

Lefrançois, P., J. E. Gallagher and M. Snyder (2014). Global analysis of transcription factor-binding sites in yeast using ChIP-Seq. Yeast Genetics: Methods and Protocols: 231-235.

Lever, M. A., J. P. Th'ng, X. Sun and M. J. Hendzel (2000). Rapid exchange of histone H1. 1 on chromatin in living human cells. Nature 408: 873-876.

Levin, D. E. (2005). Cell wall integrity signaling in Saccharomyces cerevisiae. Microbiology and molecular biology reviews 69: 262-291.

Luger, K., A. W. Mäder, R. K. Richmond, D. F. Sargent and T. J. Richmond (1997). Crystal structure of the nucleosome core particle at 2.8 Å resolution. Nature 389: 251-260.

Miloshev, G., D. Staneva, K. Uzunova, B. Vasileva, M. Draganova-Filipova, P. Zagorchev and M. Georgieva (2019). Linker histones and chromatin remodelling complexes maintain genome stability and control cellular ageing. Mechanisms of Ageing and Development 177: 55-65.

Noll, M. and R. D. Kornberg (1977). Action of micrococcal nuclease on chromatin and the location of histone H1. Journal of molecular biology 109: 393-404.

Panday, A. and A. Grove (2017). Yeast HMO1: linker histone reinvented. Microbiology and Molecular Biology Reviews 81: 10-1128.

Patterton, H. G., C. C. Landel, D. Landsman, C. L. Peterson and R. T. Simpson (1998). The biochemical and phenotypic characterization of Hho1p, the putative linker histone H1 of Saccharomyces cerevisiae. Journal of Biological Chemistry 273: 7268-7276.

Ray, S. and A. Grove (2009). The yeast high mobility group protein HMO2, a subunit of the chromatin-remodeling complex INO80, binds DNA ends. Nucleic acids research 37: 6389-6399.

Schäfer, G., C. R. McEvoy and H.-G. Patterton (2008). The Saccharomyces cerevisiae linker histone Hho1p is essential for chromatin compaction in stationary phase and is displaced by transcription. Proceedings of the National Academy of Sciences 105: 14838-14843.

Stedman, E. and E. Stedman (1951). The basic proteins of cell nuclei. Philosophical Transactions of the Royal Society of London. Series B, Biological Sciences 235: 565-595.

Suda, T., F. Arai and A. Hirao (2005). Hematopoietic stem cells and their niche. Trends in immunology 26: 426-433.

Sučhilienė, S. and A. Gineitis (1978). Histones from Saccharomyces cerevisiae. Experimental cell research 114: 454-458.

Svenkrtova, A., L. Belicova, A. Volejnikova, K. Sigler, S. M. Jazwinski and A. Pichova (2016). Stratification of yeast cells during chronological aging by size points to the role of trehalose in cell vitality. Biogerontology 17: 395-408.

Szymanski, E. P. and O. Kerscher (2013). Budding yeast protein extraction and purification for the study of function, interactions, and post-translational modifications. Journal of visualized experiments: JoVE 80.

Thoma, F., T. Koller and A. Klug (1979). Involvement of histone H1 in the organization of the nucleosome and of the salt-dependent superstructures of chromatin. The Journal of cell biology 83: 403-427.

Thomas, J. O. and K. Stott (2012). H1 and HMGB1: modulators of chromatin structure. Biochemical Society Transactions 40: 341-346.

Ueda, T., H. Chou, T. Kawase, H. Shirakawa and M. Yoshida (2004). Acidic C-tail of HMGB1 is required for its target binding to nucleosome linker DNA and transcription stimulation. Biochemistry 43: 9901-9908.

Ushinsky, S., H. Bussey, A. Ahmed, Y. Wang, J. Friesen, B. Williams and R. Storms (1997). Histone H1 in Saccharomyces cerevisiae. Yeast 13: 151-161.

Uzunova, K., M. Georgieva and G. Miloshev (2013). Saccharomyces cerevisiae linker histone—Hho1p maintains chromatin loop organization during ageing. Oxidative medicine and cellular longevity 1: 437146.

Vinayachandran, V., R. Reja, M. J. Rossi, B. Park, L. Rieber, C. Mittal, S. Mahony and B. F. Pugh (2018). Widespread and precise reprogramming of yeast protein–genome interactions in response to heat shock. Genome research 28: 357-366.

Wach, A., A. Brachat, C. Alberti-Segui, C. Rebischung and P. Philippsen (1997). Heterologous HIS3 marker and GFP reporter modules for PCR-targeting in Saccharomyces cerevisiae. Yeast 13: 1065-1075.

Woodcock, C. L., A. I. Skoultchi and Y. Fan (2006). Role of linker histone in chromatin structure and function: H1 stoichiometry and nucleosome repeat length. Chromosome Research 14: 17-25.